



**Commission on Crystallographic Computing  
International Union of Crystallography**

<http://www.iucr.org/iucr-top/comm/ccom/>

**Newsletter No. 8, November 2007**

**This issue:**

**'Crystallographic Computing at Oak Ridge  
National Laboratory: 1954 to 1968' by  
William Busing; and other articles**

<http://www.iucr.org/iucr-top/comm/ccom/newsletters/>

**Table of Contents**

(This issue's editor: Lachlan Cranswick)

(Warning – unless you want to kill 109 pages worth of forest – DO NOT press the “print” button. For hardcopies – you may like to only print out the articles of personal interest.)

<a href="#">Editor's Comments</a>	2	Following historical software reports courtesy of ORNL as a separate addendum PDF file to this issue
<a href="#">IUCr Commission on Crystallographic Computing</a>	3	
<a href="#">IUCr Computing Commission related sessions scheduled at the IUCr 2008 Congress in Osaka, Japan</a>	4	
<b>Articles:</b>		
<a href="#">Crystallographic Computing at Oak Ridge National Laboratory: 1954 to 1968</a> <i>William R. Busing</i>	5	A crystallographic least squares refinement program for the IBM 704, ORNL-CF-59-4-37, Oak Ridge, TN : Oak Ridge National Laboratory, 1959. <i>W. R. Busing and H. A. Levy</i>
<a href="#">Early Stereoscopic Drawings generated by ORTEP-I for two crystallographic meetings: 1965 and 1966</a> <i>Carroll K. Johnson</i>	13	A crystallographic function and error program for the IBM 704, ORNL-CF-59-12-3, Oak Ridge, TN : Oak Ridge National Laboratory, 1959. <i>W. R. Busing and H. A. Levy</i>
Stereoscopic Drawings prepared for the joint ACA and MSA meeting, Gatlinburg, Tennessee, USA, June 27 - July 2, 1965.	14	OR ABS : a FORTRAN program for calculating single crystal absorption corrections, ORNL-TM-229, Oak Ridge, TN : Oak Ridge National Laboratory, 1962. <i>D. J. Wehe, W. R. Busing and H. A. Levy</i>
Stereoscopic Drawings of Myoglobin, Vitamin B-12 coenzyme, and poly-L-alanine. Prepared for the Second Biophysical Congress, Vienna, Austria, September 5-9, 1966.	36	OR GLS : a general fortran least squares program, ORNL-TM-271, Oak Ridge, TN : Oak Ridge National Laboratory, 1962. <i>W. R. Busing and H. A. Levy</i>
<a href="#">What you can expect from Jana2006</a> <i>Václav Petříček and Michal Dušek</i>	48	OR FLS, A Fortran crystallographic least-squares program, ORNL-TM-305, Oak Ridge, TN : Oak Ridge National Laboratory, 1962. <i>W. R. Busing, K. O. Martin, and H. A. Levy</i>
<a href="#">Report from the GSAS-II Workshop: May 10-11, 2007</a> <i>Brian H. Toby and Robert B. Von Dreele</i>	57	OR FFE, a FORTRAN crystallographic function and error program, ORNL-TM-306, Oak Ridge, TN : Oak Ridge National Laboratory, 1964. <i>W. R. Busing, K. O. Martin, and H. A. Levy</i>
<a href="#">cctbx news</a> <i>Luc J. Bourhis, Ralf W. Grosse-Kunstleve and Paul D. Adams</i>	74	OR TEP : A Fortran thermal-ellipsoid plot program for crystal structure illustrations, ORNL-3794, Oak Ridge, TN : Oak Ridge National Laboratory, 1965. <i>Carroll K. Johnson</i>
<a href="#">Rietveld refinement of structural distortion-mode amplitudes</a> <i>Branton J. Campbell, John S. O. Evans, Francesca Perselli and Harold T. Stokes</i>	81	OR TEP-II : a FORTRAN Thermal-Ellipsoid Plot Program for crystal structure illustration, ORNL-5138, Oak Ridge, TN : Oak Ridge National Laboratory, 1976. <i>Carroll K. Johnson</i>
<a href="#">MAX3D - Visualization of Reciprocal Space Volumes</a> <i>Jim Britten and Weiguang Guan</i>	96	
<a href="#">Call for Contributions to the Next CompComm Newsletter</a>	109	

---

## From the Editor of Newsletter No. 8

In the computing monograph of the 1950 crystallographic computing school, Ray Pepinsky stated "*records of what has been considered and what has been accomplished are essential to the proper development of this or any other field.*"<sup>[1]</sup> To crystallographic software developers, it can be worthwhile to peruse the ideas and implementations behind existing and previous software source code and manuals. This is reflected somewhat in Armel Le Bail's Crystallography Source Code Museum<sup>[2]</sup>, which has been found a popular and useful resource. However much historical crystallographic source code and the context of their development is not readily in view, and the ideas and philosophy behind them risk being obscured or lost.

With this in mind, the primary theme of this newsletter's edition is a history of the Busing and Levy based crystallographic programming of the 1950's to 1960's at Oak Ridge National Laboratory (ORNL) via an article by William Busing. The ORFLS refinement program of William Busing, Kay Martin & Henri Levy<sup>[3]</sup> was deemed a citation classic<sup>[4]</sup>. A range of software was developed by Busing, Levy and co-workers as described in the Busing. Another famous and influential software program developed at Oak Ridge was the ORTEP program originally developed by Carroll Johnson at Oak Ridge, and now maintained by Michael N. Burnett. Relevant ORNL reports of the 1950's to 1970's (with source-code) have also been included in this newsletter as an addendum PDF article courtesy of Oak Ridge National Laboratory.

Lachlan Cranswick ([Lachlan.cranswick@nrc.gc.ca](mailto:Lachlan.cranswick@nrc.gc.ca))

[1] Pepinsky, R., (1952b). *Computing Methods and the Phase Problem in X-ray Crystal Analysis*, edited by R. Pepinsky, Foreward, State College, PA, USA: Department of Physics, The Pennsylvania State College.

[2] Le Bail, A., (2002). *Crystallography Source Code Museum*, <http://www.cristal.org/museum/>.

[3] Busing, W. R., Martin, K. O. & Levy, H. A. (1962). *ORFLS, a Fortran Crystallographic Least-Squares Program*, Report ORNL-TM-305. Oak Ridge National Laboratory, Oak Ridge, Tennessee.

[4] Busing, W. R. (1982). *Current Contents*, **13**, 20.

**Chairman: Professor Dr. Anthony L. Spek**

Director of National Single Crystal Service Facility,  
Utrecht University,  
H.R. Kruytgebouw, N-801,  
Padualaan 8, 3584 CH Utrecht,  
the Netherlands.  
Tel: +31-30-2532538  
Fax: +31-30-2533940  
E-mail: [a.l.spek@chem.uu.nl](mailto:a.l.spek@chem.uu.nl)  
WWW: <http://www.cryst.chem.uu.nl/spea.html>  
WWW: <http://www.cryst.chem.uu.nl/platon/>

**Lachlan M. D. Cranswick**

Canadian Neutron Beam Centre (CNBC),  
National Research Council of Canada (NRC),  
Building 459, Station 18, Chalk River Laboratories,  
Chalk River, Ontario, Canada, K0J 1J0  
Tel: (613) 584-8811 ext: 3719  
Fax: (613) 584-4040  
E-mail: [lachlan.cranswick@nrc.gc.ca](mailto:lachlan.cranswick@nrc.gc.ca)  
WWW: [http://neutron.nrc-cnrc.gc.ca/peep\\_e.html#cranswick](http://neutron.nrc-cnrc.gc.ca/peep_e.html#cranswick)

**Dr Ralf W. Grosse-Kunstleve**

Lawrence Berkeley National Laboratory  
One Cyclotron Road, BLDG 64R0121,  
Berkeley, California, 94720-8118, USA.  
Tel: (510) 486-5929  
Fax: (510) 486-5909  
E-mail: [RWGrosse-Kunstleve@lbl.gov](mailto:RWGrosse-Kunstleve@lbl.gov)  
WWW: <http://cctbx.sourceforge.net/>  
WWW: <http://www.phenix-online.org/>  
WWW: <http://cci.lbl.gov/~rwgk/>

**Professor Alessandro Gualtieri**

Università di Modena e Reggio Emilia,  
Dipartimento di Scienze della Terra,  
Via S.Eufemia, 19,  
41100 Modena, Italy  
Tel: +39-059-2055810  
Fax: +39-059-2055887  
E-mail: [alex@unimore.it](mailto:alex@unimore.it)  
WWW: <http://www.terra.unimo.it/en/personaledettaglio.php?user=alex>

**Professor Luhua Lai**

Institute of Physical Chemistry,  
Peking University,  
Beijing 100871, China.  
Fax: +86-10-62751725.  
E-mail: [lh lai@pku.edu.cn](mailto:lh lai@pku.edu.cn)  
WWW: <http://mdl.ipc.pku.edu.cn/>

**Dr Airlie McCoy**

Structural Medicine,  
Cambridge Institute for Medical Research (CIMR)  
Wellcome Trust/MRC Building,  
Addenbrooke's Hospital,  
Hills Road, Cambridge CB2 2XY, UK  
Tel: +44 (0) 1223 217124  
Fax: +44 (0) 1223 217017  
E-mail: [ajm201@cam.ac.uk](mailto:ajm201@cam.ac.uk)  
WWW: <http://www.haem.cam.ac.uk/>  
WWW: <http://www-structmed.cimr.cam.ac.uk/>

**Professor Atsushi Nakagawa**

Research Center for Structural and Functional Proteomics,  
Institute for Protein Research, Osaka University,  
3-2 Yamadaoka, Suita, Osaka, 565-0871, Japan  
Tel: +81-(0)6-6879-4313  
Fax: +81-(0)6-6879-4313  
E-mail: [atsushi@protein.osaka-u.ac.jp](mailto:atsushi@protein.osaka-u.ac.jp)  
WWW: <http://www.protein.osaka-u.ac.jp/rcsfp/supracryst/>

**Dr. Simon Parsons**

School of Chemistry  
Joseph Black Building,  
West Mains Road,  
Edinburgh, Scotland, EH9 3JJ, UK  
Tel: +44 131 650 5804  
Fax: +44 131 650 4743  
E-mail: [s.parsons@ed.ac.uk](mailto:s.parsons@ed.ac.uk)  
WWW: <http://www.crystal.chem.ed.ac.uk/>

**Dr Harry Powell**

MRC Laboratory of Molecular Biology,  
Hills Road, Cambridge, CB2 2QH, UK.  
Tel: +44 (0) 1223 248011  
Fax: +44 (0) 1223 213556  
E-mail: [harry@mrc-lmb.cam.ac.uk](mailto:harry@mrc-lmb.cam.ac.uk)  
WWW: <http://www.mrc-lmb.cam.ac.uk/harry/>

**Consultants**

**Professor I. David Brown**

Brockhouse Institute for Materials Research,  
McMaster University,  
Hamilton, Ontario, Canada  
Tel: 1-(905)-525-9140 ext 24710  
Fax: 1-(905)-521-2773  
E-mail: [idbrown@mcmaster.ca](mailto:idbrown@mcmaster.ca)  
WWW:  
[http://www.physics.mcmaster.ca/display.php4?page=sw://lists/Minibio\\_2004.php4?ID=4](http://www.physics.mcmaster.ca/display.php4?page=sw://lists/Minibio_2004.php4?ID=4)

**Professor Eleanor Dodson**

York Structural Biology Laboratory,  
Department Of Chemistry,  
University of York, Heslington, York, UK, YO10 5YW  
Tel: +44 (1904) 328253  
Fax: +44 1904 328266  
E-mail: [e.dodson@ysbl.york.ac.uk](mailto:e.dodson@ysbl.york.ac.uk)  
WWW: <http://www.ytbl.york.ac.uk/people/6.htm>

**Dr David Watkin**

Chemical Crystallography,  
Oxford University,  
9 Parks Road,  
Oxford, OX1 3PD, UK.  
Tel: +44 (0) 1865 272600  
Fax: +44 (0) 1865 272699  
E-mail: [david.watkin@chemistry.oxford.ac.uk](mailto:david.watkin@chemistry.oxford.ac.uk)  
WWW: <http://www.chem.ox.ac.uk/researchguide/djwatkin.html>

---

## IUCr Computing Commission related sessions scheduled at the IUCr 2008 Congress in Osaka, Japan

### Keynote Speaker:

- Gábor Oszlányi, Hungarian Academy of Sciences
- Title: Charge Flipping (A lecture in honor of the two developers of the Charge-Flipping Algorithm)
- KN 21, Aug-27, 2008, pm (17:30-18:30)
- Chair: Lynne McCusker, Switzerland

### Symposia:

#### New algorithms for single crystal and powder diffraction

- MS 3, Aug-24 2008: am 9:55-12:00
- Chair: Fujio Izumi, fujioizumi@mac.com
- Co-chair: Richard Cooper, richardiancooper@gmail.com

#### Decision making and algorithms for automation of data acquisition

- MS 10, Aug-24 2008: pm 14:45-17:20
- Chair: Simon Teat, sjteat@lbl.gov
- Co-chair: James F. Britten, britten@mcmaster.ca

#### Crystallographic algorithm libraries (in honor of P. Jane Brown)

- MS 21, Aug-25 2008: am 9:55-12:00
- Chair: Jon Wright, wright@esrf.fr
- Co-chair: Lukas Palatinus, lukas.palatinus@epfl.ch

#### Decision making and algorithms for automation in Macromolecular Structure Solution

- MS 42, Aug-26 2008: pm 14:45-17:20
- Chair: Harry Powell, harry@mrc-lmb.cam.ac.uk
- Co-chair: Rob Hooft, rob.hooft@bruker-axs.nl

#### New algorithms for magnetic crystallography and understanding magnetic structures

- MS 61, Aug-28 2008: am 9:55-12:00
- Chair: Sean Cadogan, cadogan@physics.umanitoba.ca
- Co-chair: Maxim Avdeev, maxim.avdeev@ansto.gov.au

#### Algorithmic developments for solving and refining periodic and aperiodic structures

- MS 88, Aug-30 2008: am 9:55-12:00
- Chair: Hai-fu Fan, fan@aphy.iphy.ac.cn
- Co-chair: Martin Lutz, m.lutz@chem.uu.nl

#### Programming for CIF and related Filestructures

- MS 96, Aug-30 2008: pm 13:45-16:20
- Chair: I. David Brown, idbrown@mcmaster.ca
- Co-chair: Ilia Guzei, iguzei@chem.wisc.edu

---

# Crystallographic Computing at Oak Ridge National Laboratory 1954 to 1968

## William R. Busing

ORNL Chemistry Division (retired), 317 Louisiana Avenue, Oak Ridge, Tennessee, 37830, USA.

E-mail: [wrb200@aol.com](mailto:wrb200@aol.com)

## The ORACLE (Oak Ridge Automatic Computer and Logical Engine)

I arrived at Oak Ridge National Laboratory (ORNL) in September, 1954, and joined the neutron-crystallography group headed by Henri A. Levy. My previous work had been in Raman and infrared spectroscopy and I was interested in structures, but I had very little knowledge of crystallography. I was certainly aware of the pioneering work that had been done by Henri together with Selmer W. Peterson, who was on sabbatical for the year. I started out by trying to grow millimeter-sized crystals of various hydroxides.

I knew that Henri had been learning to program for the ORACLE (Oak Ridge Automatic Computer and Logical Engine), and when I expressed some interest in this, he offered to teach me all about it while I waited for crystals to grow. According to Henri, the first step in writing a program is to make a flow chart, a procedure that I have found useful in all my subsequent work. We started out by writing a simple program to calculate Bragg angles and put out an ordered list.

Shown in Figure 1 is the ORACLE, a vacuum-tube computer that occupied a large room. It had been built at Argonne National Laboratory by ORNL personnel and installed here during the previous year. Its cathode-ray-tube (CRT) memory consisted of 1024 40-bit words. Each word can be described as ten hexadecimal characters, using the symbols 0 to 9 and A to F. A word could be treated as one fixed-point number or as two five-character commands. Each command used two characters for the command and three for an address ranging from 000 to 3FF.



**Fig. 1:.** An engineer at the console of the Oak Ridge Automatic Computer and Logical Engine. (Photograph courtesy of ORNL)

Fixed-point additions and subtractions were done in a 41-bit accumulator, or A register, and multiplications and divisions used a 40-bit Q, or quotient register. Numbers in these registers could be shifted left or right, using either one or both registers. There were no index registers or indirect

addressing. To step through a loop, we would set a counter initially and then increment it and test it on each pass through the loop. To step through an array, we would set an initial address in a command. Then after each pass we would pick it up, increment it, and put it back.

Input and output were done with five-hole teletype tape. Four hole positions were used for the characters 0 to F and the fifth was a parity check. Input tapes were prepared by typing on teletype machines, and output tapes were printed on these same machines.

Programs were prepared in hexadecimal and temporary storage locations were assigned. If pi or other constants were needed, they would be manually converted to hexadecimal and included in the program. Then the program would be manually typed onto tape so that it could be loaded into the ORACLE, starting at a specified location. Input and output subroutines were available so that decimal data could be read by a program and output could be converted to decimal, punched, and later printed off line.

At the console of the ORACLE was a cathode-ray tube that displayed the 32 x 32 grid representing one bit of the 40-bit words in the memory. One could follow the course of a program by watching where the spots brightened momentarily. A speaker also produced an audio signal as the commands were executed, and one could get to know what a particular program sounded like. Our Bragg-angle program was finally ready for its initial tests just before the December holidays. The program was loaded and started, but shortly thereafter the speaker started emitting a continuous tone and one area of the memory lit up brightly indicating that the program was in an unending loop. We followed the usual procedure of punching out and printing a dump of the memory contents. Overnight I found what I hoped was the single bug, and the next day I went back to get another shot at the ORACLE. But it was Christmas Eve, the mathematics party was in full swing, and the ORACLE was playing Christmas carols! I had to wait till after the holidays to get my first list of ordered Bragg angles.

## **Absorption-correction software for the ORACLE**

The first crystals that I was able to grow were calcium hydroxide. The heavy-atom positions were known from the early x-ray work of Bernal and Megaw (1935), who also postulated the hydrogen positions. In previous neutron diffraction studies by Levy and Peterson the practice had been to grind the samples to a cylindrical shape, so that tabulated absorption corrections could be applied. This had been done by putting the oriented crystal on a sandblasting lathe and grinding the edges off. But calcium hydroxide is a layer structure that cleaves like mica, and the sandblaster immediately caused the crystals to open up like the pages of a book. This led Henri and me to consider whether we could use the ORACLE to calculate the absorption correction for a crystal whose shape had been carefully measured.

In the first version of this absorption program, we integrated the correction over a few hundred equally spaced scattering points within the crystal volume. Later a consultation with mathematicians showed us that we could get better accuracy by selecting the points and weighting the contributions according to the rules of Gaussian integration. This program (Busing & Levy, 1957) and a later Fortran version (Wehe, Busing, & Levy, 1962) were used for all our neutron-diffraction studies after that.

Structure-factor data for fifty-three *h0l* reflections from calcium hydroxide were measured at two temperatures (Busing & Levy, 1957), and Henri suggested that we should make a Fourier projection. He had commissioned the ORNL Math Panel to prepare a Fourier program for us, but our first tries at using that program showed that it would be very tedious to use. This led us to prepare a new two-dimensional Fourier program more suitable for crystallographic purposes. This program initially calculated a look-up table with all the values of the sines and cosines that would be needed. Most of the rest of the memory was allocated to the map that would be produced. The indices and structure factor were read from paper tape one reflection at a time, and its contribution was added to each point of the map. After all the reflections had been included, an output tape was punched so the map would be printed in a suitable format to be contoured by hand.

## **Least-squares software written for the ORACLE**

To get more precise coordinates and interatomic distances, Henri suggested that we could use the method of least squares. My knowledge of least-squares refinement was based on Margenau and Murphy (1943). I was not even aware of the pioneering crystallographic least-squares refinement work of Hughes (1941). The parameters for calcium hydroxide included two coordinates, six anisotropic temperature-factor coefficients, and a scale factor, for a total of nine parameters. The ORACLE program that we wrote was probably designed for this particular problem. The appropriate derivatives were used to set up the full matrix, and a subroutine was available to solve the nine simultaneous equations. The four cycles of least-squares adjustments needed for convergence took about twenty minutes of ORACLE time.

In order to calculate the standard errors of the distances and angles, we needed the variance-covariance matrix that could be derived from the inverse of the least-squares matrix; but no matrix inverter was available for the ORACLE at that time. Instead, we inverted the matrix by solving nine simultaneous equations a total of nine times, using as the nine column vectors (1,0,0,0,0,0,0,0,0), (0,1,0,0,0,0,0,0,0), etc. The nine solution vectors then formed the columns of the inverse matrix.

At about this time Henri and I realized the desirability of writing a generalized least-squares program that could be used to adjust the parameters defining any arbitrary function. The function would be provided by the user, who would need only to write a subroutine to evaluate the function based on the parameters and the values of one or more independent variables for which experimental values had been obtained. For example, we refined the lattice parameters of diaspore (Busing & Levy, 1958) using observations of the Bragg angles from an x-ray powder pattern. Here the independent variables were the indices, along with an indicator as to whether the wavelength for an  $\alpha_1$ , an  $\alpha_2$ , or unresolved line should be used.

A unique feature of this general least-squares program was that the user had the option of calculating the required derivatives of the function with respect to the parameters or letting the program calculate derivatives numerically. In the latter case the user would just provide a list of increments to be added to one parameter at a time. The function was recalculated with the incremented parameter, and the derivative was taken as the ratio of the change in the function to the parameter increment. This program and its successors (Busing & Levy, 1962) were so easy to use that other groups at ORNL and elsewhere used it routinely to analyze thermodynamic data, spectral patterns, and other complicated functions.

## **Crystallographic least-squares refinement on the IBM 704**

About 1958 an IBM 704 computer became available at the gaseous diffusion plant in Oak Ridge. Although this required a drive of about seven miles, the advantages over the ORACLE were considerable. These included a memory of 8,192 36-bit words, hardware floating-point arithmetic, index registers, removable magnetic tapes, and punched card input and output. An assembler was available to facilitate writing programs that would be automatically converted to binary form.

Henri and I decided to write a least-squares program that could be used for the refinement of any crystal structure based on x-ray or neutron-diffraction data. Whenever we couldn't decide how to do something we left it as an option for the user. Thus the program could refine a structure based on either  $F$  or  $F^2$ . An overall temperature factor or individual isotropic or anisotropic temperature factors could be used. Symmetry cards were included to allow for the refinement of any centrosymmetric or noncentrosymmetric structure. Atom multipliers were provided to correctly weight atoms in special positions or to treat disordered structures. Anomalous scattering factors could be included. Different scale factors could be applied to data from different samples. Henri and I wrote a program to invert a symmetric matrix in the space required to store only its unique upper-triangular elements (Busing & Levy, 1962). Although this program was later shown to be rather inefficient, it allowed for the adjustment of up to 120 parameters in the 8,192-word memory. When Carroll Johnson joined our group in 1962, he

and Henri wrote an improved matrix inverter that made use of the Choleski method of factoring a symmetric matrix.

We wanted to distribute this program to anyone who requested it. However, with instructions punched one per card, the source program consisted of over 4,000 cards. We considered that this would be too expensive to copy and ship. Instead, we distributed copies of the binary card decks that were produced by the assembler. A handbook was available that gave detailed instructions on how to use the program (Busing & Levy, 1959).

In 1961 Kay Martin of the ORNL Math Panel joined our group to help with computer programming. Her first job was to convert the structure-factor least-squares program to Fortran (Busing, Martin, & Levy, 1962). This made it easier for us to distribute the source program either on punched cards or via magnetic tape. When the ORACLE was replaced by the Control Data 1604 and later by the IBM 360, the Fortran program was easily adapted to the new computers.

Availability of the Fortran source code also allowed others to make changes in the program. Jim Ibers and Walter Hamilton of Brookhaven National Laboratory improved the form for input of the symmetry information. Methods of correcting for extinction were introduced. Carroll Johnson added the ability to refine more complicated forms of thermal motion. No further printed reports were written, but the instructions included with the distributed program were kept up to date. The latest version lists nine persons as contributing authors. In 1982 *Current Contents* listed the 1962 report as a *Citation Classic* that had been cited more than 3000 times (Busing, 1982).

The primary purpose of most crystallographic investigations is to obtain detailed information about the chemical structures of the molecules or ions involved. After the lattice parameters, atomic coordinates, and temperature factor coefficients have been obtained, it is desirable to calculate bond distances, bond angles, torsion angles, and other quantities, some of which depend on the observed thermal motion. It certainly is useful to obtain the standard errors of the calculated quantities, and these can be calculated in a straightforward way from the variance-covariance matrix that is proportional to the inverse matrix of the normal equations.

After completing the first version of our crystallographic least-squares program Henri and I proceeded to write a Fortran program to calculate some fifteen different kinds of functions together with their standard errors (Busing & Levy, 1959). The functions calculated included bond distances, bond angles, torsion angles, the difference between two bond distances or angles, the sum of several bond angles, and nine more functions involving thermal motion.

The calculation of standard errors requires the values of the derivative of the function with respect to each parameter involved. A unique feature of this program is that, instead of deriving expressions for these derivatives, we decided to determine them numerically by adding an increment to a parameter, recalculating the function, and computing the derivative as the ratio of the change in the function to the parameter increment. This method produces a correct result, even when certain parameters are constrained by symmetry or for some other reason, provided that the constraint is reapplied each time a parameter is incremented.

Provision was made for the user to write subroutines defining any new functions desired. Available for this purpose were subroutines for picking up atomic coordinates and temperature factor coefficients, manipulating matrices and vectors, and calculating angles. Other mathematical routines could also be used. This program was later modified by Kay Martin to conform to the Fortran version of the least-squares program (Busing, Martin, & Levy, 1964). It has been kept up to date with a few improvements and has been generally distributed on request together with the least-squares program.



## Three-circle neutron diffractometer control using paper tape

Shown in Figure 2 is the three-circle neutron diffractometer that we installed in 1960 at the newly operational Oak Ridge Research Reactor. A crystal monochromator centered in a concrete shield reflected the neutrons to produce a vertical beam. A General Electric diffractometer was mounted on its side to support the appropriately counter-weighted neutron counter. Centered on this instrument was a ring to provide the chi-angle orientation and support the phi-angle drive.



**Fig. 2.:** *The three-circle paper-tape controlled neutron diffractometer at the Oak Ridge Research Reactor. (Photograph courtesy of ORNL)*

This instrument was controlled by electronics that read the desired angles two theta, chi, and phi from paper tape. Motors would drive each shaft until the encoders registered the desired angles. It was arranged that the final adjustment of each angle would always be made slowly in the same direction to avoid backlash problems.

With this then-new type of instrument we no longer needed to orient a crystal sample. We only had to center it and determine its orientation by observing the angles for two or more reflections. ORACLE programs were written to use this angle information to refine the orientation and prepare a tape with the angles for data collection. The methods we used for determining orientation and calculating diffractometer angles have been described (Busing & Levy, 1967).

It was arranged that after the electronics had set the initial angles it would make a theta-two-theta step scan through the reflection, punching the observed counts on an output paper tape. This tape was then carried back to the ORACLE for further data processing to obtain the integrated count and the peak position in two-theta. Assuming that the counter has a large aperture, this peak maximum occurs when the reflecting plane best satisfies the Bragg condition. Deviations from the calculated two-theta were then used to further refine the orientation and lattice parameters.

After the ORACLE was replaced by the Control Data 1604 computer the three-circle data collection programs were rewritten for that machine. The Control Data 160A auxiliary computer was used to convert from magnetic tape to paper tape and vice-versa.

## Four-circle x-ray diffractometer control using a DEC PDP-5

In the fall of 1962 I went to England to spend a year on sabbatical working with Owen S. Mills at the University of Manchester. There the computer engineers were in the process of installing the Ferranti Atlas supercomputer, a state-of-the-art machine that was to run several programs at a time, switching them in and out of memory from an auxiliary storage drum. Owen was having a four-circle x-ray diffractometer built by Hilger-Watts, and he intended to use the Atlas computer to control this instrument. Working in this time-sharing mode, the diffractometer would use only a small fraction of the computer's resources.

I wrote computer programs to calculate instrument angles, drive motors, center reflections, calculate orientation, and collect intensity data. All these programs were written without the presence of the diffractometer that was not delivered until April of 1963. After the diffractometer was interfaced to the computer, we were only permitted to test it on Saturday mornings, times set aside for computer maintenance. After we got started it seemed as though the Atlas would never run for more than about fifteen minutes before it crashed. Then we would spend the rest of the morning arguing with the engineers as to whether the problem was with our software or with the computer hardware. I had to leave Manchester before these problems were solved.

When I returned to Oak Ridge we wanted to install an automatic four-circle x-ray diffractometer, but I was sure that we didn't want to interface it to a large time-sharing computer. Cole, Okaya, & Chambers (1963) had recently described a diffractometer controlled by a dedicated IBM 1620 computer, but that computer, at about \$100,000, was too expensive for our budget. Then we learned of the DEC PDP-5 computer that was available for about \$20,000.

We also knew that Tom Furnas of the Picker X-ray Corporation had recently designed and built a four-circle diffractometer that Picker intended to market for use with paper-tape control. It didn't take long for us to realize that we could easily control this diffractometer with the PDP-5 computer. In 1965 we produced the system shown in Figure 3. (Busing, Ellison, Levy, King, & Roseberry, 1968).

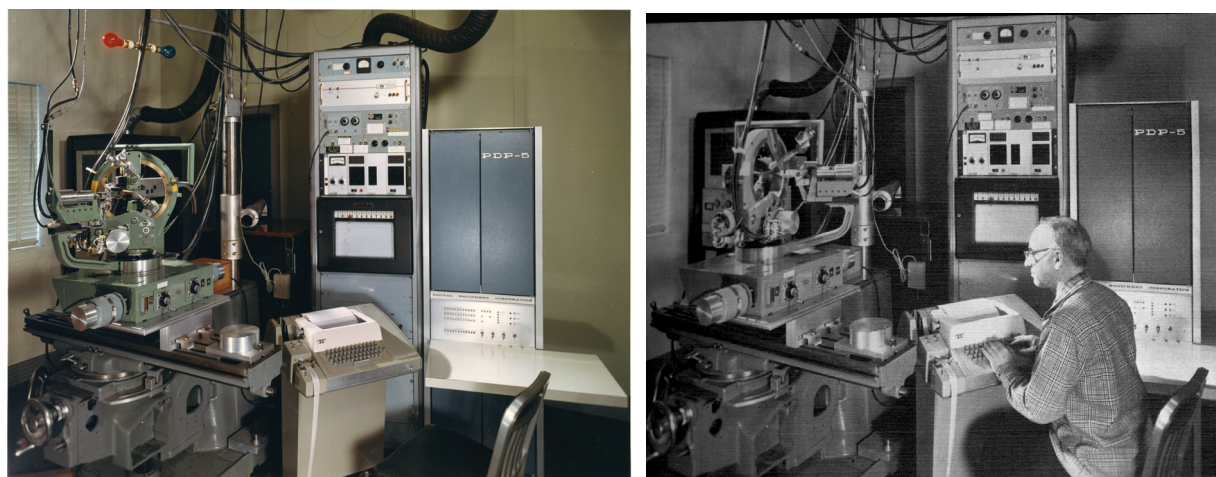


**Fig. 3.:** a) The four-circle Picker x-ray diffractometer and the PDP-5 computer that was programmed to control it and b) Henri Levy at the keyboard of this instrument. (Photographs courtesy of ORNL)

The PDP-5 (a predecessor of the PDP-8) had a core memory of 4096 12-bit words divided into 32 pages of 128 words each. An instruction occupied one word and the type of instruction was defined by the first three bits so there were only eight different kinds of commands. Six of these instructions used seven bits to define an address that could be either on the same page or on page zero, but it could also refer to any

location in the memory by indirect addressing. Hardware arithmetic was limited to addition, but a complete package of subroutines to perform floating point arithmetic was available.

Input or output was accomplished by a teletype interfaced directly to the computer. Input could be typed or loaded from punched-paper tape. Output could be printed or punched on tape.

We decided to use Slo-Syn stepping motors that took one hundred steps to make a revolution. The angles of the Picker diffractometer were geared to change one degree for each turn of a drive shaft. Thus, with a motor on each shaft, the angles two-theta, omega, chi, and phi could be set to the nearest 0.01 degree without the use of encoders. To provide a check on the angles ORNL engineers designed an optical detector to signal the computer at each even degree.

A feature of the PDP-5 that was new to us was the availability of a hardware interrupt. Thus any external action, such as the typing of a teletype key or the closing of a limit switch, could interrupt the program that was operating and jump to a special interrupt program. We knew that the Slo-Syn motors could run smoothly at 300 pulses per second, so we arranged for a crystal-controlled oscillator to interrupt the computer 300 times each second. An interrupt program would check to see which motors should be running and send a single pulse to step that motor forward or backward. Every 30th clock interrupt was treated as a tenth-of-a-second interrupt and used for timing counts or any required delays.

At about the time the PDP-5 was delivered, Sharron King of the ORNL Mathematics Division joined our group to help with the diffractometer programming.. Although an assembler program was available for the PDP-5, we found it useful to create an assembler program, written in Fortran, to run on the CDC 1604 and 160A computers. We put our instructions on punched cards, and the assembler produced a binary tape that could be loaded into the PDP-5.

The subroutines for floating point arithmetic, trigonometric functions, and matrix operations took up about half of the memory. The other half would be loaded with programs for the particular operations we were performing. A setup program would be used to search for reflections, center them, and establish initial lattice parameters and sample orientation. Then a least-squares program could be loaded to refine this information. Finally, a data collection program would measure the reflections systematically, making step scans and punching the results on paper tape. This output tape would be processed further by the CDC computers.

This data collection system remained in operation for almost twenty years. When it was acquired, the PDP-5 was one of the first minicomputers at ORNL. When it was finally decommissioned it was the oldest computer at the laboratory.

This has been the story of one group's experiences in the early uses of computers for crystallography. Everything seemed new and exciting at the time we were working on it. We certainly never envisioned the days when similar things could be done on a laptop computer at unimagined speeds. But that seems to be the way science works.

## References:

Bernal, J. D. & Megaw, H. D. (1935). *Proc. Roy. Soc. (London)* **A151**, 384.

Busing, W. R. & Levy, H. A. (1957). *Acta Cryst.* **10**, 180-182.

Busing, W. R. & Levy, H. A. (1957). *J. Chem. Phys.* **26**, 563-568.

Busing, W. R. & Levy, H. A. (1958). *Acta Cryst.* **11**, 798-803.

- Busing, W. R. & Levy, H. A. (1959). ORNL-CF-59-4-37, *A Crystallographic Least-Squares Refinement Program for the IBM 704*.
- Busing, W. R. & Levy, H. A. (1959). ORNL-CF-59-12-3, *A Crystallographic Function and Error Program for the IBM 704*.
- Busing, W. R. & Levy, H. A. (1962). *Comm. Assoc. Comp. Mach.* **5**, 445-446.
- Busing, W. R. & Levy, H. A. (1962). ORNL-TM-271, *OR GLS, A General Fortran Least Squares Program*.
- Busing, W. R. & Levy, H. A. (1967). *Acta Cryst.* **22**, 457-464
- Busing, W. R., Martin, K. O., & Levy, H. A. (1962). ORNL-TM-305, *OR FLS, A Fortran Crystallographic Least-Squares Program*.
- Busing, W. R., Martin, K. O., & Levy, H. A. (1964). ORNL-TM-306, *OR FFE, A Fortran Crystallographic Function and Error Program*.
- Busing, W. R., Ellison, R. D., Levy, H. A., King, S. P., & Roseberry, R. T. (1968). ORNL-4143, *The Oak Ridge Computer-Controlled X-ray Diffractometer*.
- Busing, W. R. (1982). *Current Contents*, **13**, 20.
- Cole, H., Okaya, Y., & Chambers, F. W. (1963). *Rev. Sci. Inst.* **34**, 872-876.
- Hughes, E. W. (1941). *J. Am. Chem. Soc.* **63**, 1737-1752.
- Margenau, H. & Murphy, G. M. (1943). *The Mathematics of Physics and Chemistry*. New York: Van Nostrand.
- Wehe, D. J., Busing, W. R., & Levy, H. A. (1962). ORNL-TM-229, *OR ABS, A Fortran Program for Calculating Single-Crystal Absorption Corrections*.

---

## Early Stereoscopic Drawings generated by ORTEP-I for two crystallographic meetings: 1965 and 1966

### Carroll K. Johnson

Retiree/Consultant, Chemical and Analytical Sciences Division, Oak Ridge National Laboratory, Building 4500N, MS 6197, Oak Ridge TN, 37831-6197, USA. E-mail: johnsonck@ornl.gov ; WWW: <http://www.ornl.gov/sci/ortep/ckj.html>

### Sets of drawings:

1. Stereoscopic Drawings prepared for the joint American Crystallographic Association and Mineralogical Society of America joint meeting, Gatlinburg, Tennessee, USA, June 27 - July 2, 1965.
2. Stereoscopic Drawings of Myoglobin, Vitamin B-12 coenzyme, and poly-L-alanine. Prepared for the Second Biophysical Congress, Vienna, Austria, September 5-9, 1966.

### Note from Carroll K. Johnson relating to an original request for copies of the ORTEP-I and ORTEP-II manuals: August 8, 2007:

*"Something of greater historical interest is perhaps the handout with ORTEP drawings for the stereo slides I made for crystal structure papers at the 1965 ACA meeting in Gatlinburg TN. We had stereo projectors and Polaroid viewing glasses there and with ORNL the host lab for the meeting, I offered to make one free stereo slide for any participant who would send me coordinate data at least a month before the meeting and almost everyone there took me up on the offer. That was a quite successful debugging (and to my surprise also marketing) exercise for ORTEP."*

Stereoscopic Drawings of Some Crystal Structures Presented  
at the Joint Meeting of the American Crystallographic  
Association and Mineralogical Society of America  
June 27 - July 2, 1965  
Gatlinburg, Tennessee

C. K. Johnson  
Chemistry Division, Oak Ridge National Laboratory

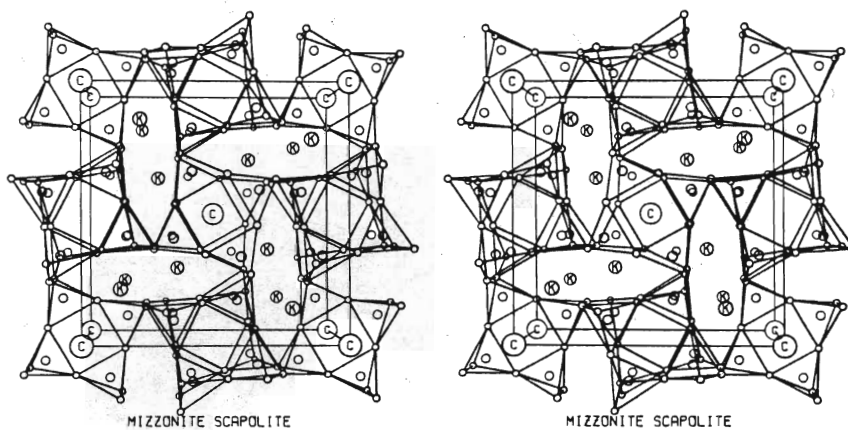
This atlas of stereoscopic drawings was prepared at the Oak Ridge National Laboratory<sup>1</sup> with a programmed<sup>2</sup> incremental x-y plotter. Computing and plotting facilities were provided by the ORNL Mathematics Division. The figure captions are the titles of the corresponding abstracts for the meeting.

ORNL Drawing Numbers 65-6837 Through 65-6873 Consecutively.

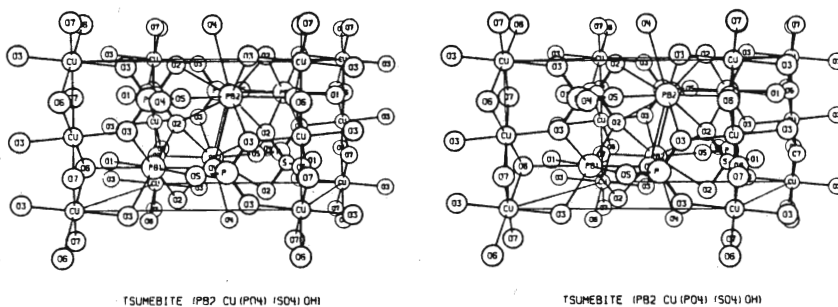
---

<sup>1</sup>Operated by Union Carbide Corporation for the U. S. Atomic Energy Commission.

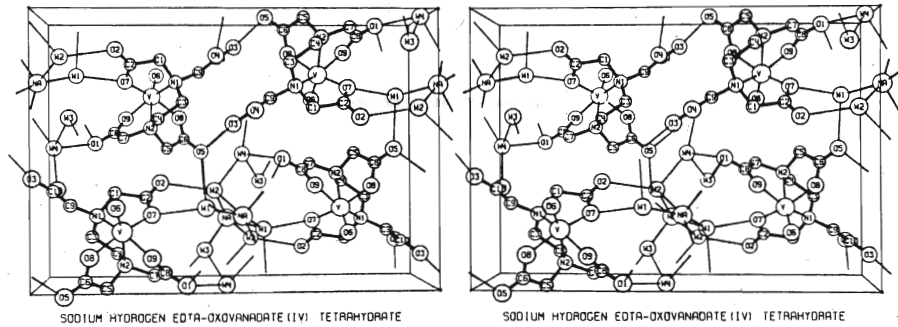
<sup>2</sup>C. K. Johnson, OR TEP: A FORTRAN Thermal Ellipsoid Plot Program for Crystal Structure Illustrations, ORNL-3794 (June, 1965).



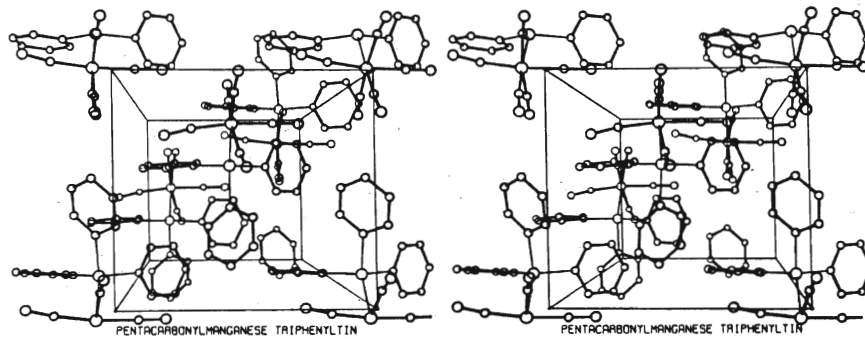
MSA I-2. THE CRYSTAL STRUCTURE OF MIZZONITE, A CALCIUM AND CARBONATE RICH SCAPOLITE, James J. Papike and Neville Stephenson, U. S. Geological Survey.



MSA II-7. THE CRYSTAL STRUCTURE OF TSUMEBITE, Monte C. Nichols, Lawrence Radiation Laboratory, University of California, Livermore.

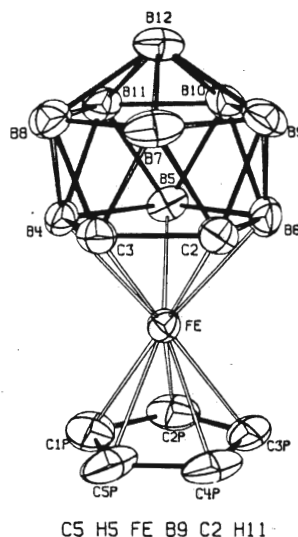
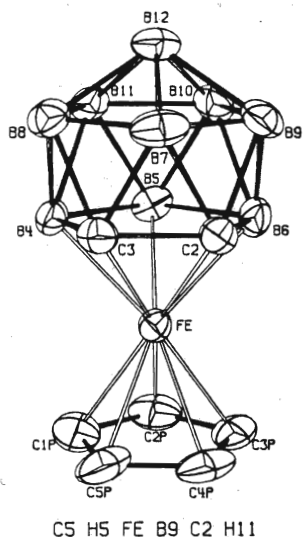


B1 THE STRUCTURE OF CRYSTALLINE MONOSODIUM MONOHYDROGEN  
ETHYLENEDIAMINETETRAACETATOXOVANADATE (IV) TETRAHYDRATE,  
F. A. Muller and J. L. Hoard, Cornell University

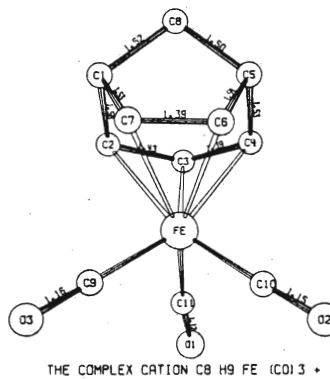
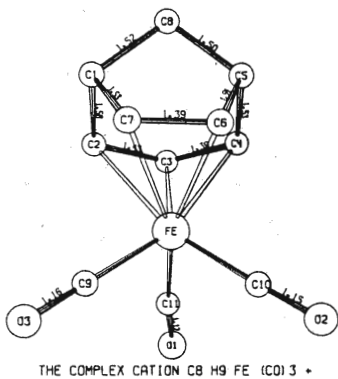


B3 THE CRYSTAL AND MOLECULAR STRUCTURE OF PENTACARBONYL-MANGANESE  
TRIPHENYL TIN, Robert F. Bryan and Hans-Peter Weber, Johns Hopkins  
University

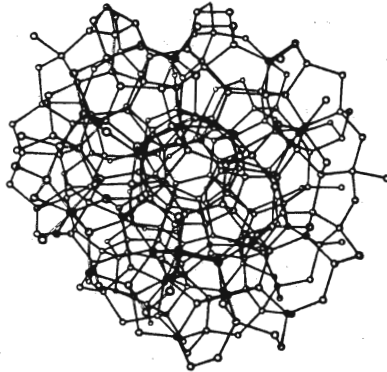




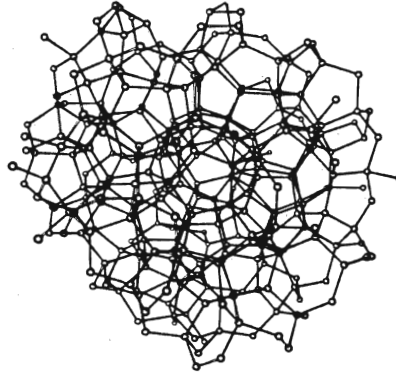
B4 THE CRYSTAL AND MOLECULAR STRUCTURE OF  $C_5H_5FeC_2B_9H_{11}$ , Allan Zalkin, David H. Templeton and Ted E. Hopkins, University of California, Berkeley



B5 THE STRUCTURE OF BICYCLO [3.2.1] OCTADIENYLIRON TRICARBONYL TETRAFLUOROBORATE, T. N. Margulis, L. Schiff and M. Rosenblum, Brandeis University

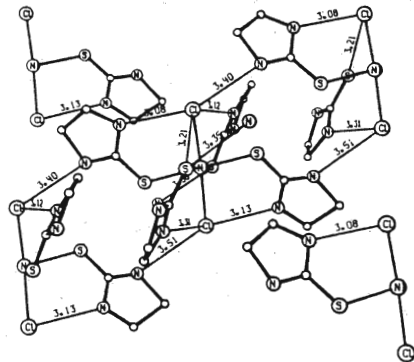


TETRAHEDRAL RANDOM NETWORK OF 300 UNITS

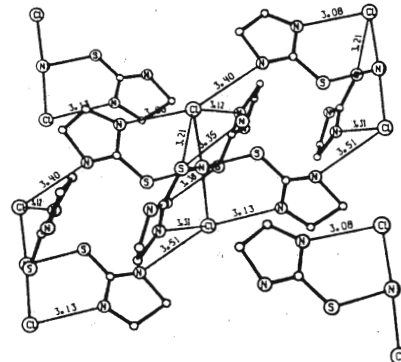


TETRAHEDRAL RANDOM NETWORK OF 300 UNITS

C4 GEOMETRICAL STATISTICS OF A TETRAHEDRAL RANDOM NETWORK MODEL, VITREOUS SILICA, AND LIQUID WATER, Fred Ordway, Melpar, Inc., Falls Church, Va.

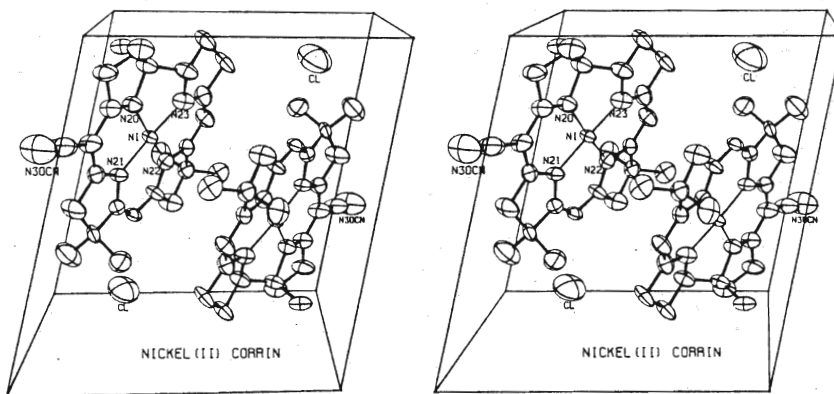


DICHLOROTETRAKIS (ETHYLENETHIOUREA) NICKEL (II)

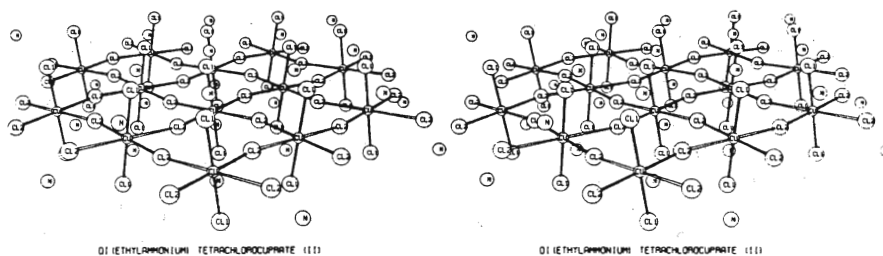


DICHLOROTETRAKIS (ETHYLENETHIOUREA) NICKEL (II)

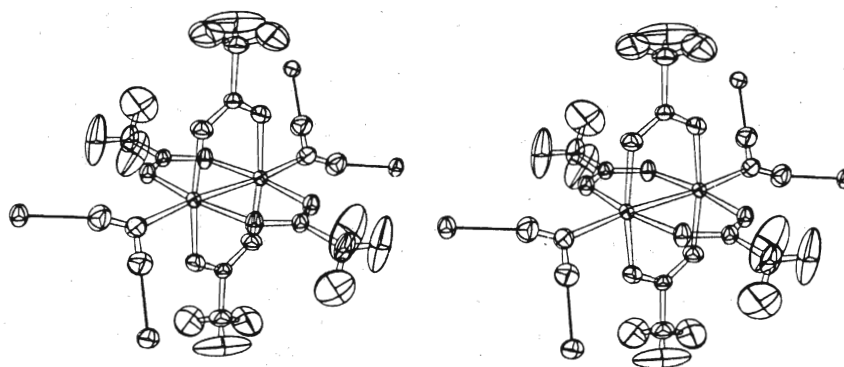
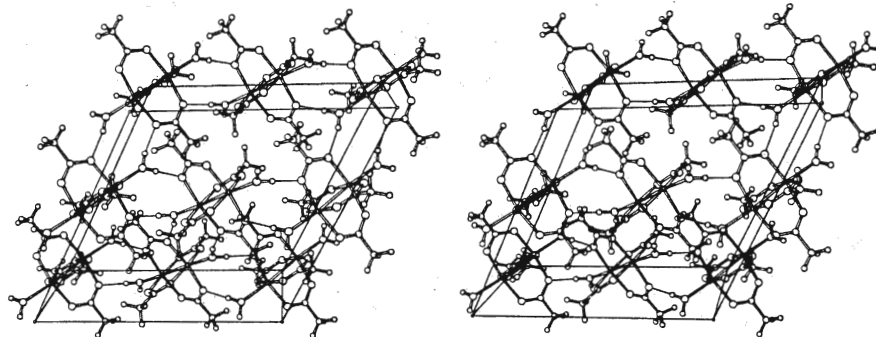
D1 THE STRUCTURES OF TWO ISOMERS OF DICHLOROTETRAKIS-(ETHYLENETHIOUREA)NICKEL(II), Ward T. Robinson, Smith L. Holt, Jr. and G. B. Carpenter, Brown University



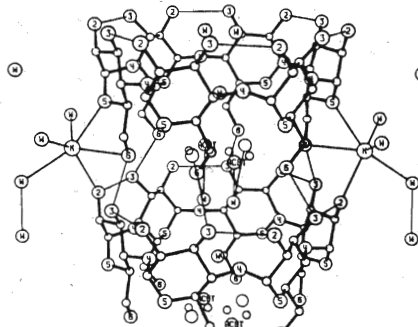
D2 THE CRYSTAL AND MOLECULAR STRUCTURE OF THE NICKEL(II) COMPLEX OF 1,8,8,13,13-PENTAMETHYL-5-CYANO-TRANS-CORRIN, E. F. Meyer and J. D. Dunitz, E.T.H., Zurich



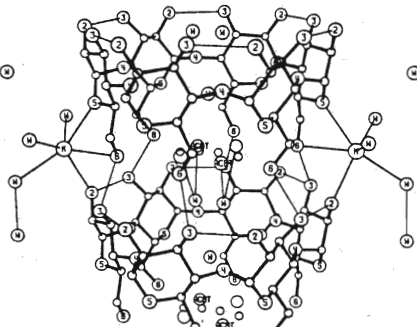
D6 THERMOCHROMISM OF COPPER(II) CHLORIDE COMPLEXES, Paul Steadman, Ona Liles and Roger D. Willett, Washington State University



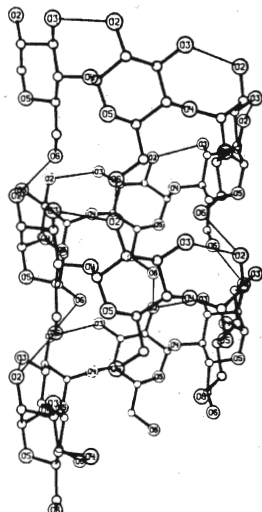
D3 A NEUTRON-DIFFRACTION STUDY OF THE STRUCTURE OF HYDRATED CUPRIC ACETATE,  $\text{Cu}_2(\text{CH}_3\text{COO})_4 \cdot 2\text{H}_2\text{O}$ , R. Chidambaram and G. M. Brown, Oak Ridge National Laboratory



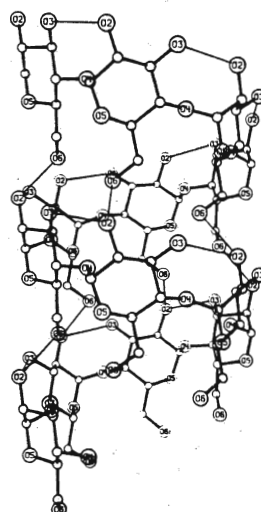
CYCLOHEXAAMYLOSE POTASSIUM ACETATE COMPLEX



CYCLOHEXAAMYLOSE POTASSIUM ACETATE COMPLEX

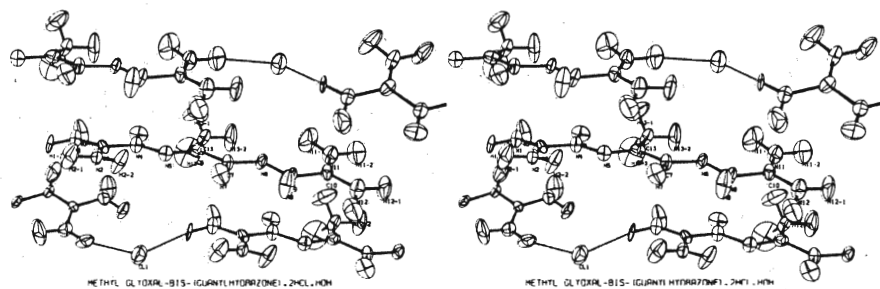


PROPOSED MODEL FOR  $\alpha$ -D-GLUCOPYRANOSE

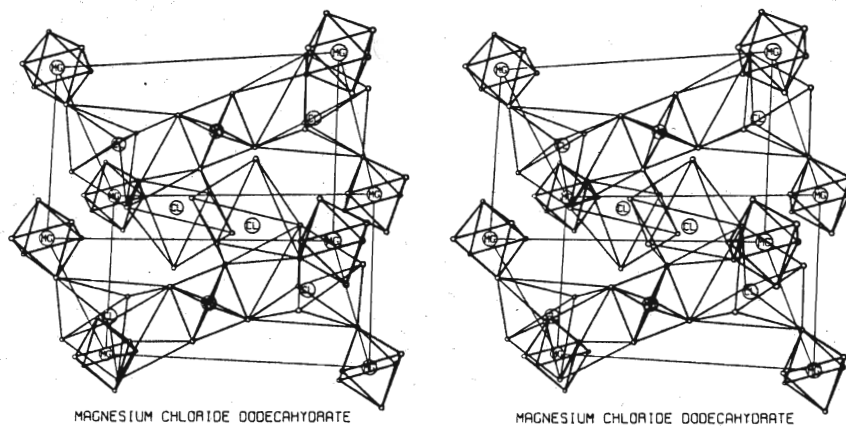


PROPOSED MODEL FOR  $\alpha$ -D-GLUCOPYRANOSE

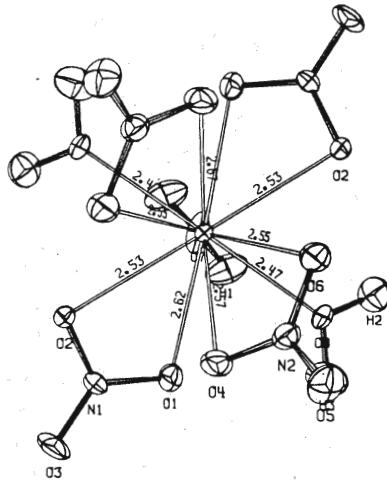
E6 THE CRYSTAL STRUCTURE OF CYCLOHEXAAMYLOSE, Albert Hybl, University of Maryland, School of Medicine



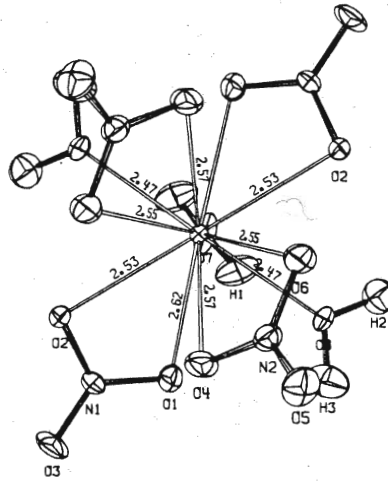
E9 A VERY SHORT INTERPLANAR SPACING IN METHYL GAG: COMPARISON OF THE X-RAY AND NEUTRON STUDIES, Walter C. Hamilton and Sam J. La Place, Brookhaven National Laboratory



F1 THE CRYSTAL STRUCTURE OF MAGNESIUM CHLORIDE DODECAHYDRATE, K. Sasvari and G. A. Jeffrey, University of Pittsburgh

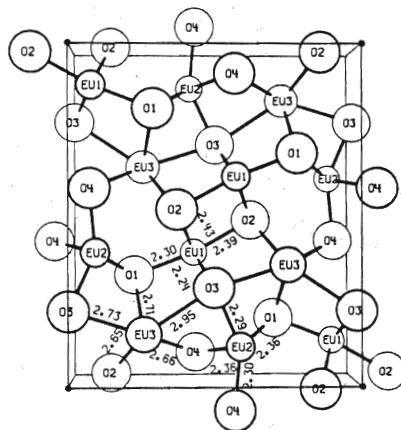


THORIUM NITRATE PENTAHYDRATE

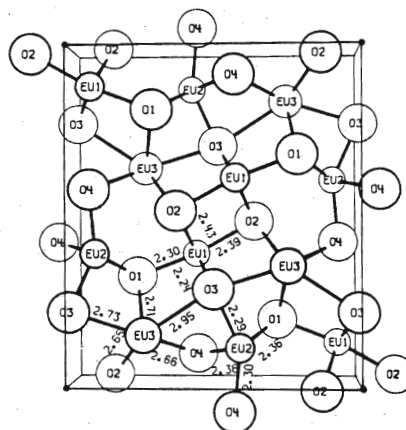


THORIUM NITRATE PENTAHYDRATE

F2 THE CRYSTAL STRUCTURE OF THORIUM NITRATE PENTAHYDRATE BY NEUTRON DIFFRACTION, J. C. Taylor, M. H. Mueller and R. L. Hitterman, Argonne National Laboratory

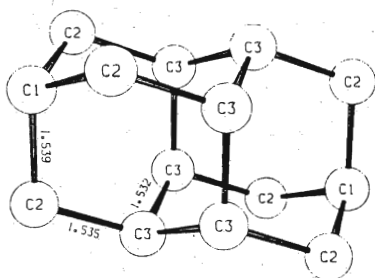


TRIEUROPIUM TETRAOXIDE

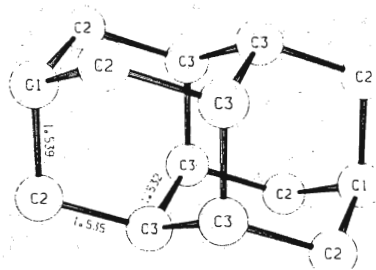


TRIEUROPIUM TETRAOXIDE

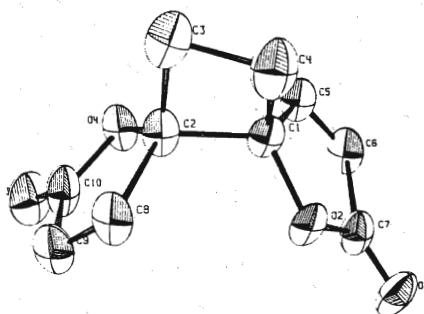
F6 THE CRYSTAL STRUCTURE OF  $\text{Eu}_3\text{O}_4$ , Robert C. Rau, General Electric Company, Cincinnati



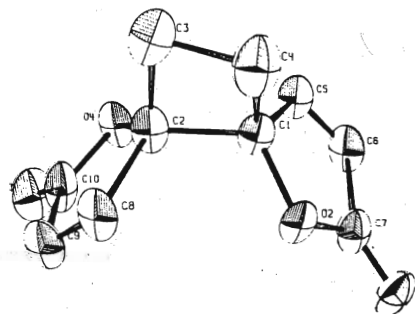
CONGRESSANE



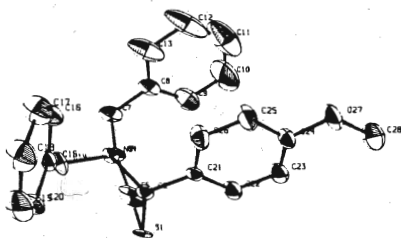
CONGRESSANE



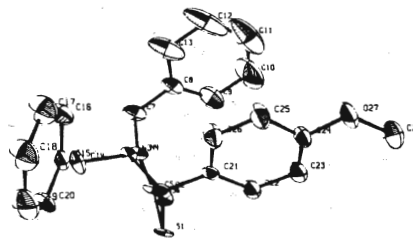
ANEMONIN



ANEMONIN



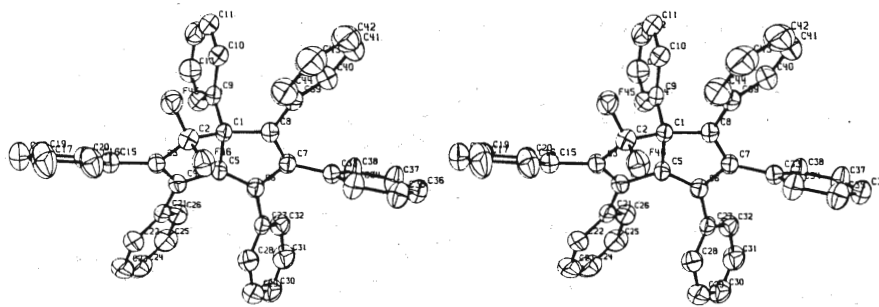
2-p-METHOXYPHENYL-3,4-DIBENZYL-1,3,4-THIAZOLIDINE-5-THIONE



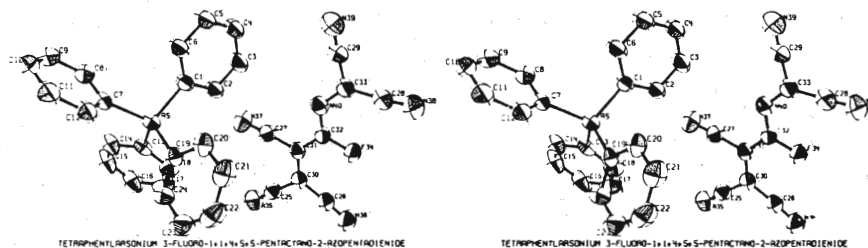
2-p-METHOXYPHENYL-3,4-DIBENZYL-1,3,4-THIAZOLIDINE-5-THIONE

G1 STRUCTURES OF SEVERAL COMPOUNDS OF INTEREST TO THE ORGANIC CHEMIST, I. L. Karle and J. Karle, U. S. Naval Research Lab

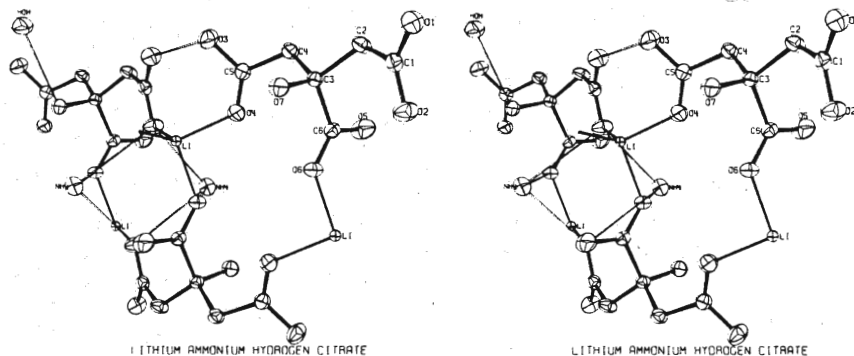




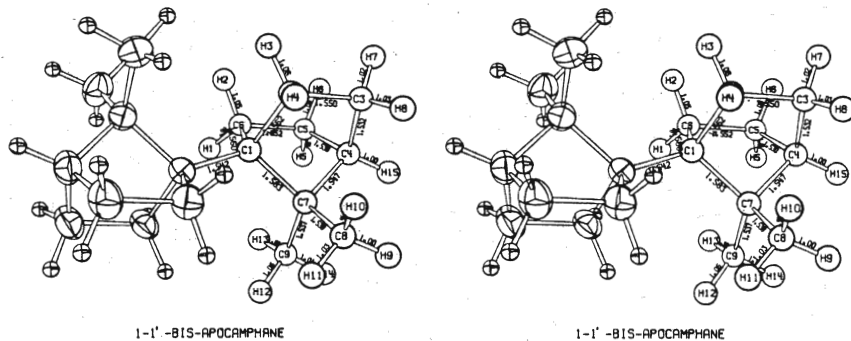
G2 THE STRUCTURE OF A NEW DIMER OF TRIPHENYLFLUOROCYCLOBUTADIENE,  $C_{44}H_{30}F_2$ ; APPLICATION OF THE DIRECT METHOD, Thomas A. Beineke and Edward W. Hughes, California Institute of Technology



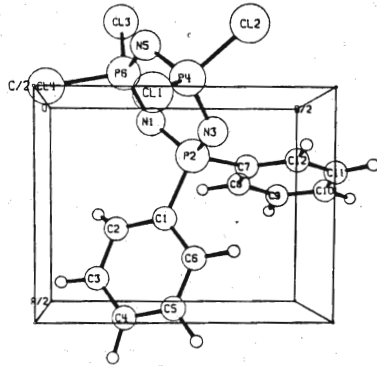
G4 THE CRYSTAL STRUCTURE OF TETRAPHENYLARSONIUM 1,1,4,5,5-PENTACYANO-4-FLUORO-2-AZAPENTADIENIDE: AN EXAMPLE OF CHEMICAL ANALYSIS BY X-RAY DIFFRACTION, Gus J. Palenik, U. S. Naval Ordnance Test Station, China Lake, California



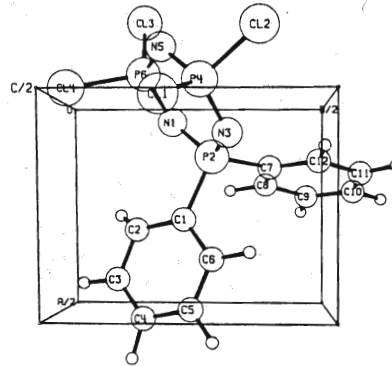
G5 THE CRYSTAL STRUCTURE OF LITHIUM AMMONIUM HYDROGEN CITRATE, E. J. Gabe, J. A. Minkin and J. P. Glusker, The Institute for Cancer Research, Philadelphia



G7 THE CRYSTAL STRUCTURES OF SOME BICYCLOALKANE DIMERS, R. A. Alden, J. Kraut and T. G. Traylor, University of California, San Diego



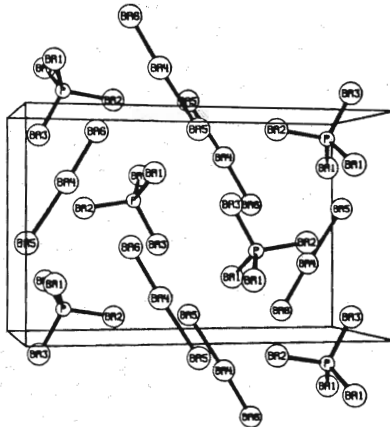
DIPHENYL TETRACHLORO CYCLOTRIPHOSPHAZATRIENE



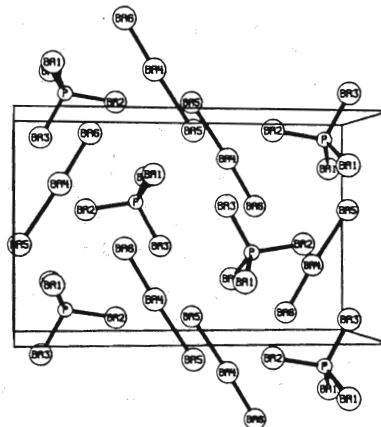
DIPHENYL TETRACHLORO CYCLOTRIPHOSPHAZATRIENE

G10

THE CRYSTAL STRUCTURE OF 2,2-DIPHENYL-4,4,6,6-TETRACHLORO CYCLO-TRIPHOSPHAZATRIENE, N. V. Mani, F. R. Ahmed and W. H. Barnes, National Research Council, Canada



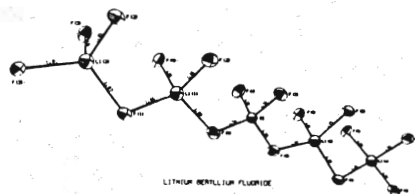
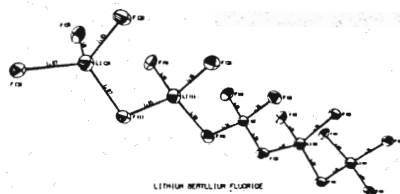
PHOSPHOROUS HEPTABROMIDE



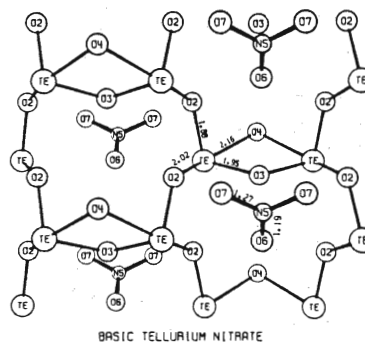
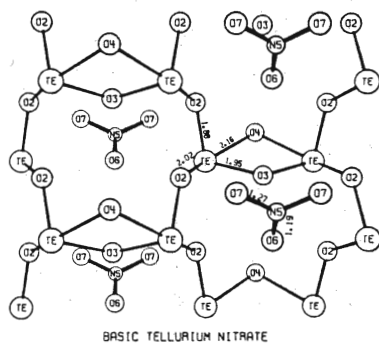
PHOSPHOROUS HEPTABROMIDE

H3

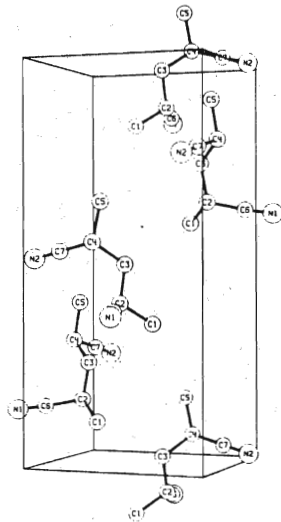
THE CRYSTAL STRUCTURE OF PBr<sub>7</sub>, Gary Breneman and Roger D. Willett, Washington State University



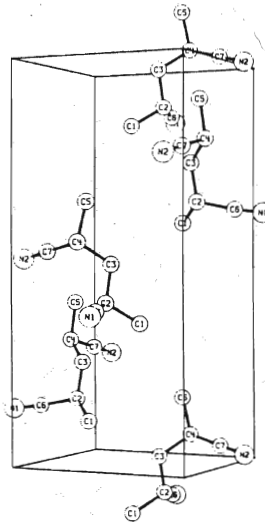
H4 REFINEMENT OF THE STRUCTURE OF  $\text{Li}_2\text{BeF}_4$ , John H. Burns and E. Kent Gordon, Oak Ridge National Laboratory



H7 THE CRYSTAL STRUCTURE OF "BASIC TELLURIUM NITRATE",  $\text{Te}_2\text{O}_4 \cdot \text{HNO}_3$ , Laurence N. Swink and G. B. Carpenter, Brown University

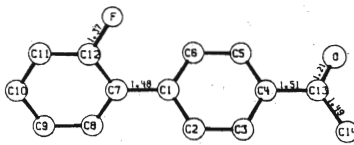


D-ISOMER OF 2,4-DICYANOPENTANE IN P4 SUB 1

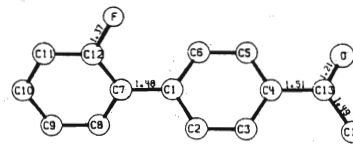


D-ISOMER OF 2,4-DICYANOPENTANE IN P4 SUB 1

- L2 CRYSTAL STRUCTURE OF THE *d*, *l* ISOMER OF 2,4-DICYANOPENTANE (PAN-2), Leroy E. Alexander and Rolf Engmann, Mellon Institute; and Howard G. Clark, Research Triangle Institute, Durham, N. C.

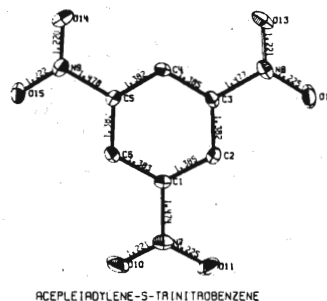
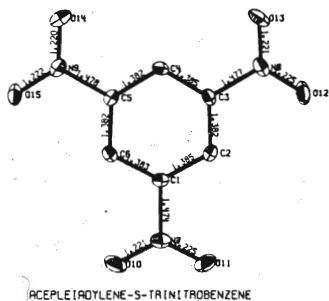
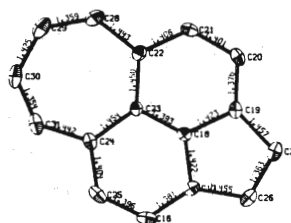
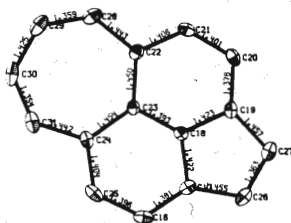
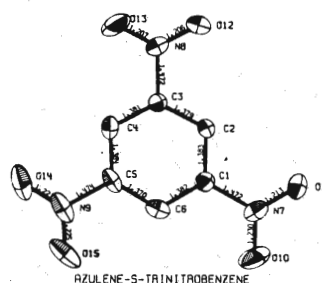
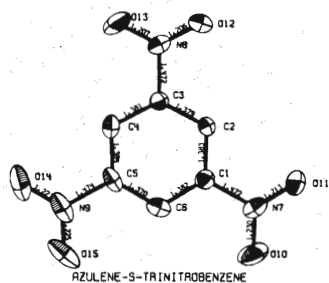
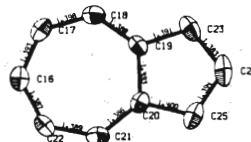
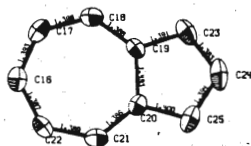


4-ACETYL-2-FLUORO BIPHENYL (REFINEMENT INCOMPLETE)

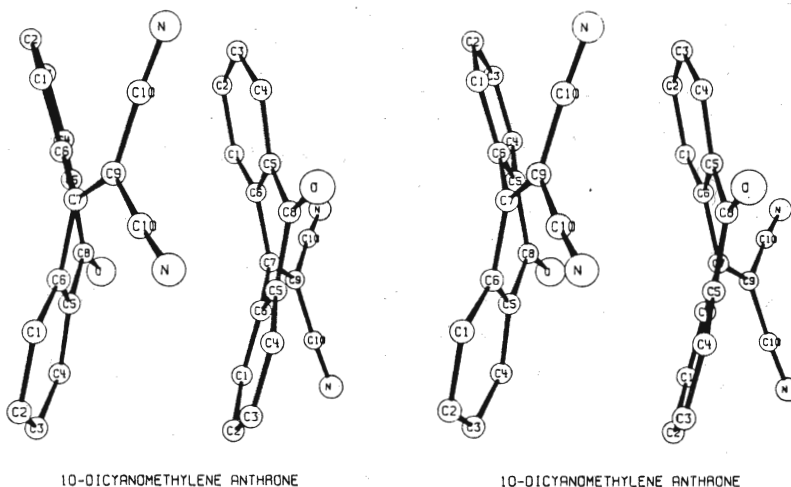


4-ACETYL-2-FLUORO BIPHENYL (REFINEMENT INCOMPLETE)

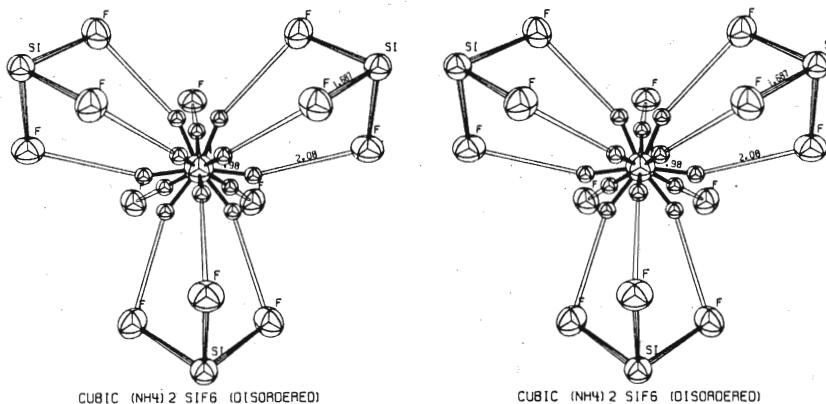
- L5 THE DETERMINATION OF THE STRUCTURE OF 4-ACETYL 2'-FLUORO-BIPHENYL, P. Tollin and D. W. Young, University of St. Andrews, Scotland; and H. Sutherland, University of Hull, England



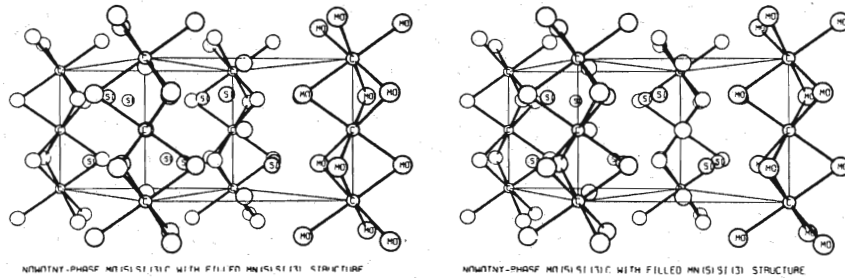
L3 THE CRYSTAL STRUCTURES OF THE 1:1 COMPLEXES OF AZULENE AND ACEPLEIADYLENE WITH *s*-TRINITROBENZENE, A. W. Hanson, National Research Council, Canada



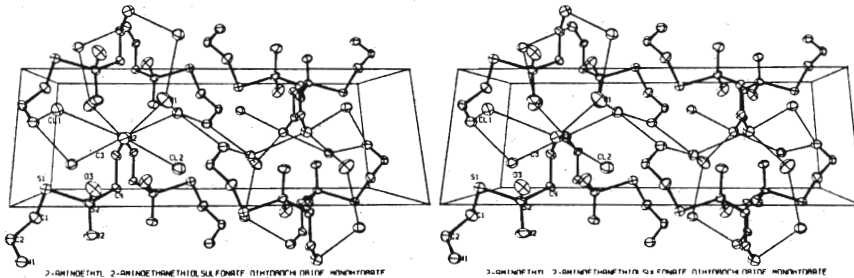
L6 THE CRYSTAL STRUCTURE OF 10-DICYANOMETHYLENE ANTHRONE,  
J. Silverman and N. F. Yannoni, Air Force Cambridge Research  
Laboratories, Bedford, Mass.



M3 HYDROGEN BONDING AND DISORDER IN (NH<sub>4</sub>)<sub>2</sub>SiF<sub>6</sub> AND (NH<sub>4</sub>)<sub>2</sub>SO<sub>4</sub>,  
E. O. Schlemper and W. C. Hamilton, Brookhaven National Laboratory



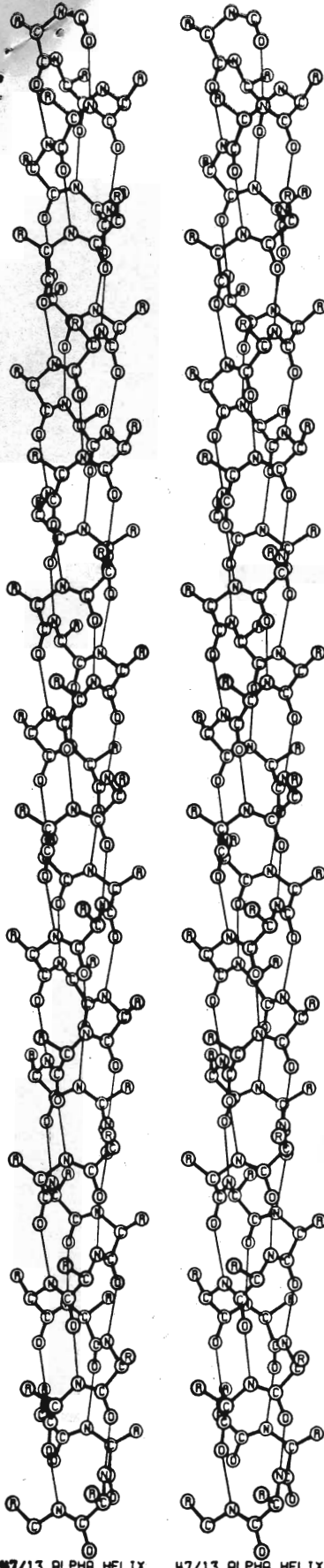
M8 NEUTRON DIFFRACTION STUDY OF THE NOWOTNY-PHASE Mo<sub>5</sub>Si<sub>3</sub>C<sub>1</sub>,  
Erwin Parthe and Wolfgang Jeitschko, University of Pennsylvania;  
and Varadachari Sadagopan, Massachusetts Institute of Technology



O4 THE CRYSTAL STRUCTURE OF 2-AMINOETHYL 2-AMINOETHANETHIOL-  
SULFONATE DIHYDROCHLORIDE MONOHYDRATE, C<sub>4</sub>H<sub>12</sub>O<sub>2</sub>N<sub>2</sub>S<sub>2</sub>·2HCl·H<sub>2</sub>O,  
W. J. Ristey and P. Galen Lenhert, Vanderbilt University

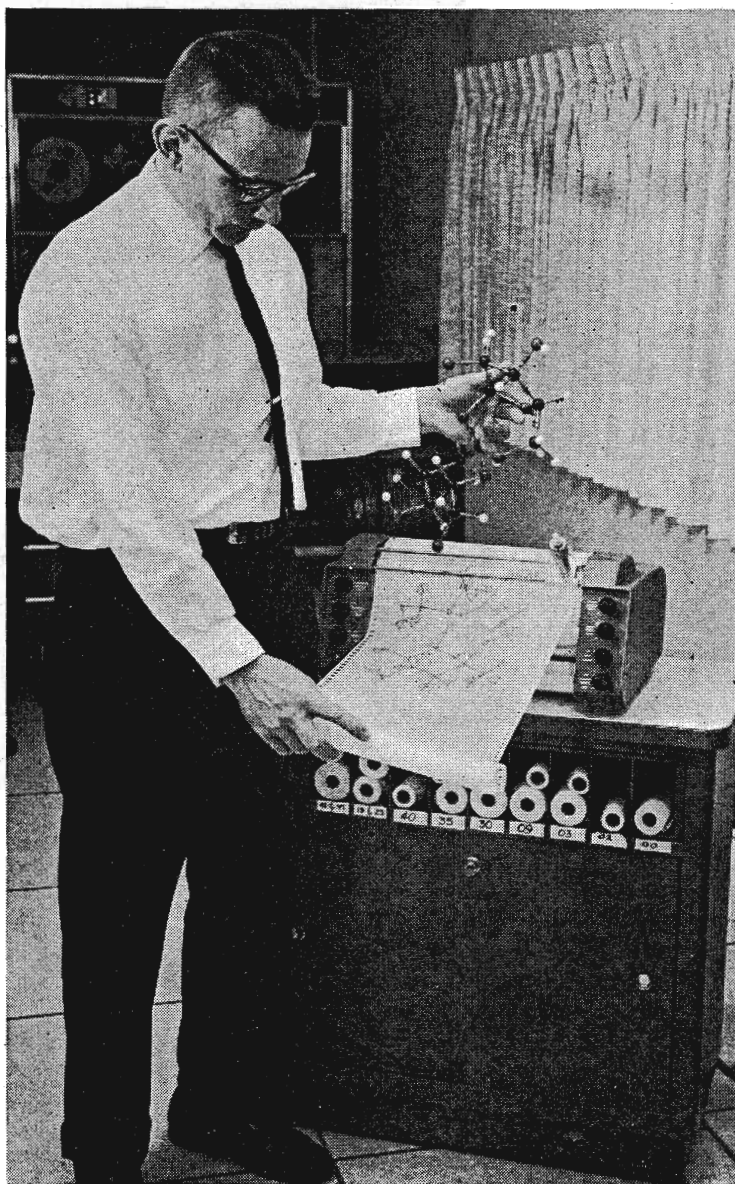


Stereoscopic line drawing of the Pauling and Corey Alpha Helix, with CalComp X-Y plotter which produced the drawing.



47/13 ALPHA HELIX

47/13 ALPHA HELIX



# THE CHEMICAL BULLETIN

A FREE CHEMICAL PRESS IN SUPPORT OF CHEMISTS TO BETTER THEIR STATUS

Return Requested

The Chemical Bulletin  
86 East Randolph St.  
Chicago, Illinois 60601

U. S. POSTAGE  
**PAID**  
Mendota, Illinois  
Permit No. 54

## CRYSTAL STRUCTURE IN THREE-D, BY COMPUTER

*This article, and our cover picture, were first published nearly two years ago in The News of the Oak Ridge National Laboratory. Both Mr. Johnson, who did the work described, and Mr. Bill Felknor, who wrote the article, have graciously given us permission to reproduce it here. We have slightly altered the article to fit our needs.*

A PICTURE is worth a thousand words particularly to an Oak Ridge National Laboratory scientist who has revived an old turn-of-the-century household entertainment device to help visualize complex crystal structures.

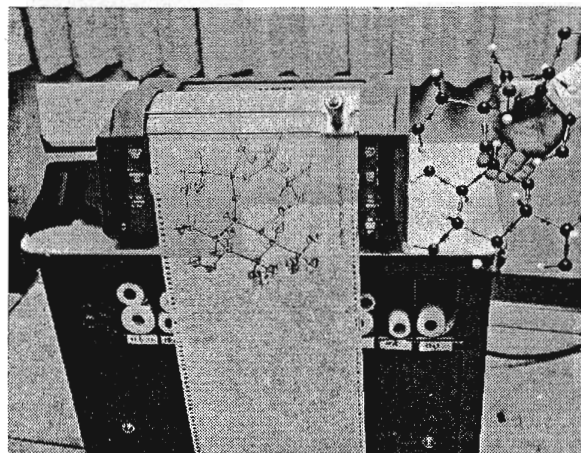
Remember grandma's stereoscope and cabinet of stereoscopic pictures? They were found in nearly every parlor during the early 1900's. C. K. Johnson of ORNL's Chemistry Division has developed a modern computer program to utilize "automated graphic arts" in the drawing of similar stereoscopic (three dimensional) figures. But, instead of seeing Niagara Falls or a circus elephant, the drawings are of highly complex chemical and biological structures.

The precision of the computer and mechanical plotter used makes it feasible to produce accurate stereoscopic line drawings with great detail in just a fraction of the time normally required to hand-draw figures.

The layman might ask, what is a stereo figure? It's a pair of drawings with one member for each eye. The drawings are perspective projections relative to the "view points" of the eyes. The brain fuses the separate figures automatically and the perception of depth results. This permits the true three-dimensional appearance of a crystal structure model to be visualized rapidly by the reader.

Johnson's research project began when he attempted to illustrate a technical paper with a picture of the thermal motion in magnesium citrate. A crude program was prepared to see if this could be better accomplished with a computer. The results were encouraging enough to warrant further research and the present, rather elaborate general computer

program, ORTEP,<sup>1</sup> evolved. It was largely a case of trial and error method to find a graphical technique applicable to automation and numerical techniques suitable for graphics.



In the past, the optimal way of studying the three-dimensional character of a crystal structure has been to build a model (see accompanying picture). Scientists have been using such methods since the study of crystallography began. Another method has been to hand-draw stereoscopic figures. This, however, requires very time consuming draftsmanship. For this reason, extensive use of such graphic aids techniques has not been made to any extent since the 1920's and 1930's when some work along these lines was done by pioneers in X-ray diffraction crystallography.

A first application of stereoscopic drawing to crystal structures was made by the German crystallographer Max von Laue, who in 1926 edited an atlas of stereoscopic crystal structure drawings. This was followed by a second volume in 1936.

Automated graphic arts techniques are particularly well suited to the field of crystallography because the crystal structure models are defined in numerical terms. The parameters which define the model are normally obtained from an X-ray, neutron, or electron diffraction

<sup>1</sup>C.K. Johnson, "ORTEP: A Fortran Thermal-Ellipsoid Plot Program for Crystal Structure Illustrations," ORNL-3794, June, 1965. (Available from the Clearinghouse for Federal Scientific and Technical Information, National Bureau of Standards, U. S. Department of Commerce, Springfield, Virginia 22151. \$4.00.)

study of crystalline material. Structure models are used in fields such as chemistry, solid state physics, biology, mineralogy, and metallurgy.

Several stereo-pair illustrations of crystal structures drawn with Johnson's program have been accepted for publication in scientific literature.<sup>2</sup> It is hoped that the use of such computer-drawn stereoscopic illustrations will help alleviate the bottleneck in information transfer that results from the fact that the three-dimensional character of the crystallographic results must be communicated on the two-dimensional printed page. Stereoscopic viewers costing from 35 cents to \$10 can be used to view the figures in stereo directly from a technical journal.

Another use of stereoscopic figures is in the presentation of crystal structure information to an audience. A special projector and polaroid viewing spectacles are needed for this visual aid technique. In order to explore the potential of this medium in an actual crystallographic conference, the ORNL Chemistry Division, in cooperation with the Mathematics Division, offered to prepare a computer - drawn stereo slide for any crystal structure paper presented at the annual meeting of the American Crystallographic Association in June of 1965.

<sup>2</sup>Atlases of stereoscopic drawings were prepared for publication at the American Crystallographic Association meeting in 1965 and the Second International Biophysics Congress in Vienna in 1966.

### FREE JOURNAL EXCHANGE

Mount Marty College, Yankton, South Dakota, has available all or portions of ANALYTICAL CHEMISTRY, volumes 19, 20, 21, 23, 25, 28, 34; and CHEMICAL ABSTRACTS, volumes 19, 23, 26, and 40-50.

They need ANALYTICAL CHEMISTRY, volumes 12-18, 24, 26, 29, 34, 36-7; CHEMICAL ABSTRACTS, volumes 1-16, 20, and 28-38; and JOURNAL ACS, volumes 42 and 46-63.

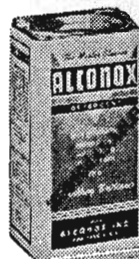
For further information on exchange possibilities write Sister M. Laetitia Kilzer, OSB, at the College.

## CHOOSE THE BEST DETERGENTS for Your needs! ALL BIODEGRADABLE

FOR EVERY CRITICAL CLEANING NEED  
LABORATORY, HOSPITAL OR INDUS

# ALCONOX

### THE MASTER CLEAN



For manual cleaning. Most highest government specifications! In 3 lb. boxes, and 50, 100, 300 lb. drums.

**3 lb. BOX—\$2.12**  
Case of 12 Boxes—\$20.0

# ALCOJET



prevents water-spotting from final rinse, for scientifically-clean glass, metals, plastics, etc., in all chemical washers. In 5 boxes and drums as above.

**5 lb. BOX—\$3.0**  
Case of 6 Boxes—\$15.

# ALCOTAB



For syphon-type pipette test tube washers — one operation! In 100-tablet boxes.

**Box of 100 Tablets—\$5.**

# LIQUI-NOX

THE PERFECT LIQUID DETERGENT!

For manual cleaning. Mild (neutral pH). Non-toxic. Contains no phosphates. Equally effective in hard or soft water. Outstanding blood and fat solvent. In quarts, gallons, & 15 gallon drums.

**PER QUART—\$2.15**  
Case of 12 Quarts—\$19.92  
**PER GALLON—\$7.00**  
Case of 4 Gallons—\$24.00



**MATHESON  
SCIENTIFIC**

1850 Greenleaf Ave.  
Elk Grove Village, Illinois 6000  
Telephone: (312) 439-5880

Write for Bulk Prices,  
Literature and Samples

## STEREOSCOPIC DRAWINGS OF MYOGLOBIN, VITAMIN B-12 COENZYME, AND POLY-L-ALANINE<sup>1</sup>

(Prepared for Presentation at the Second International Biophysics Congress, September 5-9, 1966, Vienna, Austria.)

Carroll K. Johnson, Chemistry Division, Oak Ridge National Laboratory, Oak Ridge, Tennessee, U.S.A.

These stereoscopic pairs of perspective projection drawings were drawn by a CalComp plotter controlled by the computer program OR TEP.<sup>2</sup> A stereoscopic viewer should be used while examining the drawings.

Thanks are expressed to Drs. H. C. Watson and J. C. Kendrew for kindly supplying their unpublished preliminary atomic coordinates for myoglobin<sup>3,4,5</sup> and Drs. P. G. Lenhert and D. C. Hodgkins for kindly supplying their unpublished atomic coordinates for vitamin B-12 coenzyme.<sup>6</sup>

The illustrations are referenced as ORNL drawing numbers 66-8029 through 66-8044 consecutively.

---

<sup>1</sup>Research sponsored by the U.S. Atomic Energy Commission under contract with the Union Carbide Corporation.

<sup>2</sup>C. K. Johnson, *OR TEP: A FORTRAN Thermal Ellipsoid Plot Program for Crystal Structure Illustrations*, ORNL-3794, June, 1965. A modified version of the program was used for Figs. 9 through 14.

<sup>3</sup>J. C. Kendrew, H. C. Watson, B. E. Strandberg, and R. E. Dickerson, *Nature* **190**, 666 (1961).

<sup>4</sup>J. C. Kendrew, *Brookhaven Symp. Biol.* **15**, 215 (1963).

<sup>5</sup>A. B. Edmundson, *Nature* **205**, 883 (1965).

<sup>6</sup>P. G. Lenhert and D. C. Hodgkins, *Nature* **192**, 937 (1962).

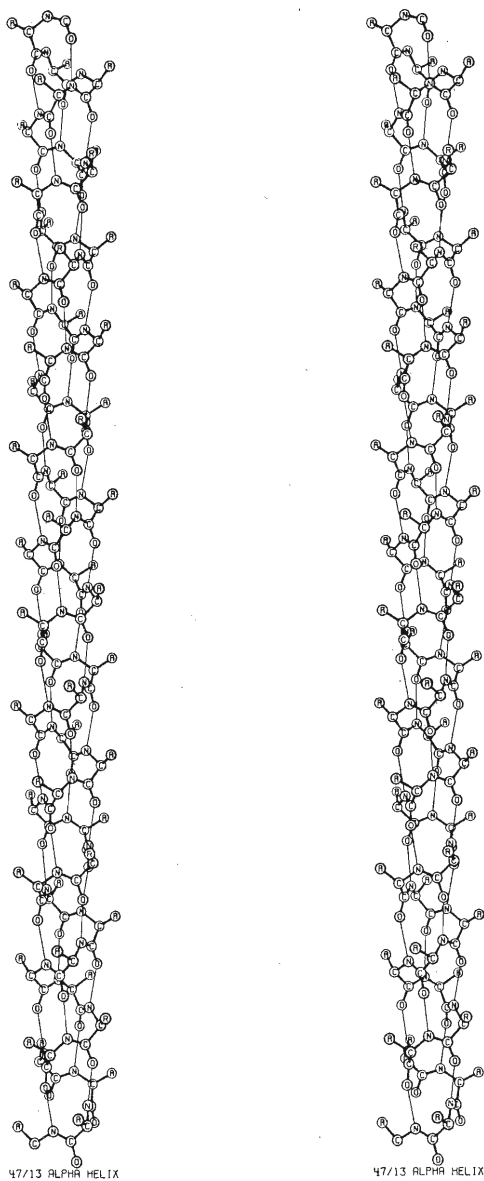


Fig. 1. The  $\frac{47}{13}$  Alpha Helix. The alpha helix shown here is an idealized representation for the alpha form of the synthetic polypeptide poly-L-alanine. There are 47 residues in 13 turns of the helix. Covalent bonds are shown as thick lines, and hydrogen bonds as thin lines. The methyl-group side chains are designated by the symbol R. Hydrogen atoms are not shown. A. Elliott and B. R. Malcolm, *Proc. Roy. Soc. (London), Ser. A*, 249, 31 (1959).

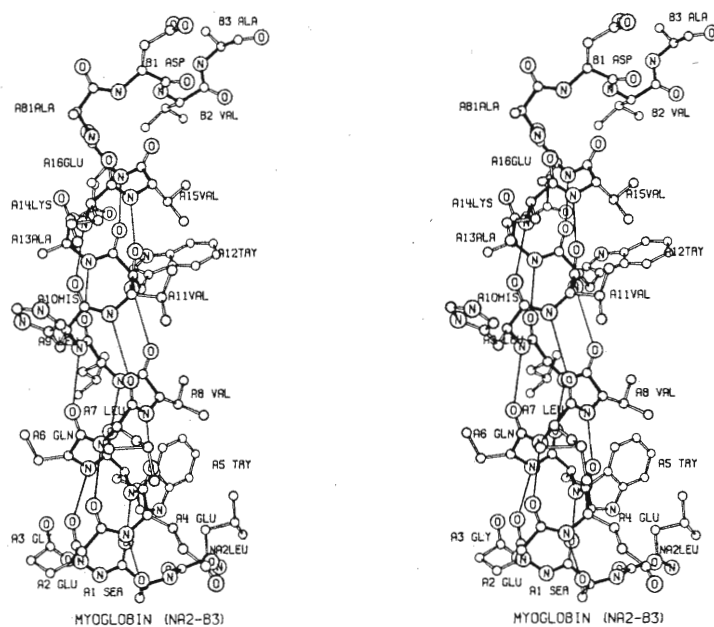


Fig. 2. The A Helix of Myoglobin. The amino end of the myoglobin chain is at the lower right corner. The first amino-acid residue, NA1 valine, is disordered and was not found in the x-ray analysis. The side chains of residues A6 and A14 are also incomplete.

In Figs. 2–14, the covalent bonds of the myoglobin backbone are shown as wide solid lines, the covalent bonds of the side chains are shown as wide unfilled lines, and the hydrogen bonds are indicated as narrow solid lines. Several possible hydrogen bonds are not shown in these drawings. Carbon-atom positions are designated by unlettered small circles; oxygen-, nitrogen-, sulfur-, and iron-atom positions are designated by larger circles with the chemical symbols inside. Hydrogen atoms are not shown. The last three letters of each identifying symbol specify the chemical nature of the amino-acid residue. The single letters A to H at the beginning of the identifying symbol denote helical segments, and the double letters refer to the regions between successive helices or to the N- and C- termini of the protein.

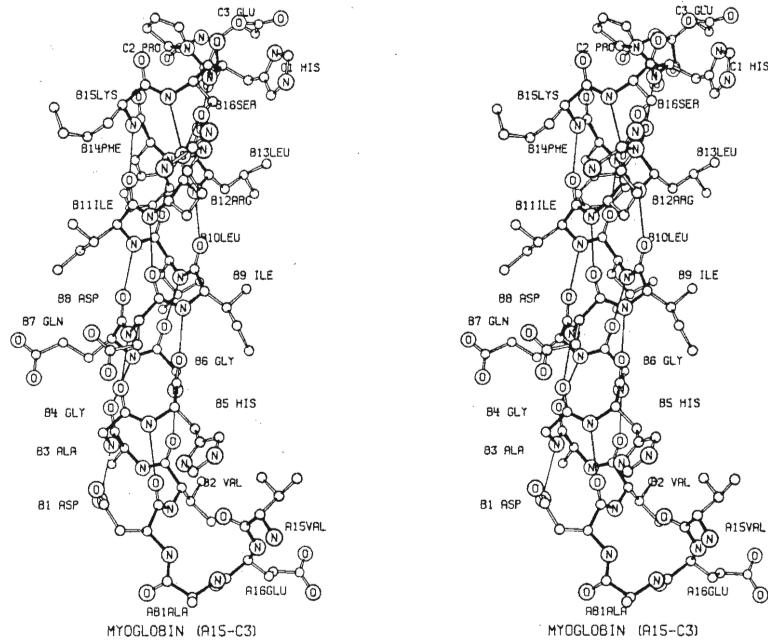
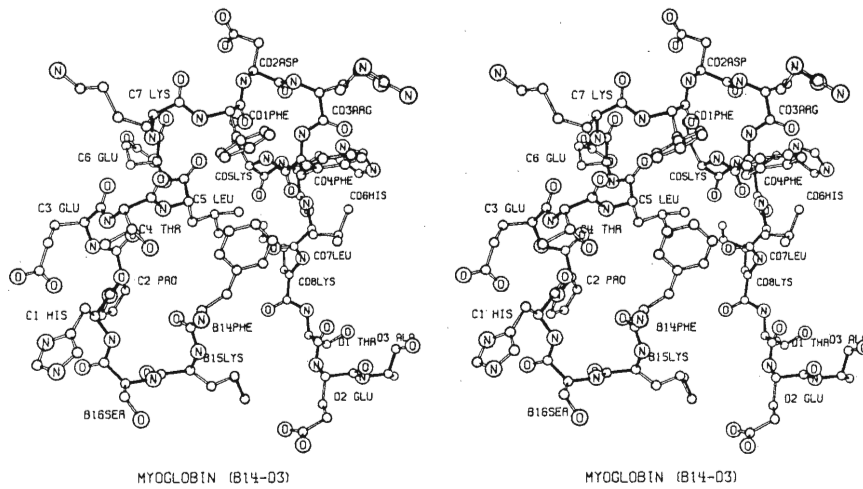


Fig. 3. The B Helix of Myoglobin. The side chain of residue B15 is incomplete.



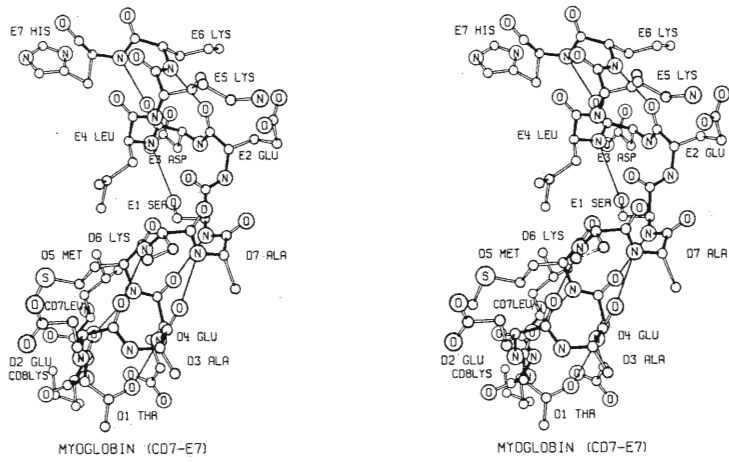


Fig. 5. The D Helix of Myoglobin. The side chains of residues CD8, D6, and E6 are incomplete.

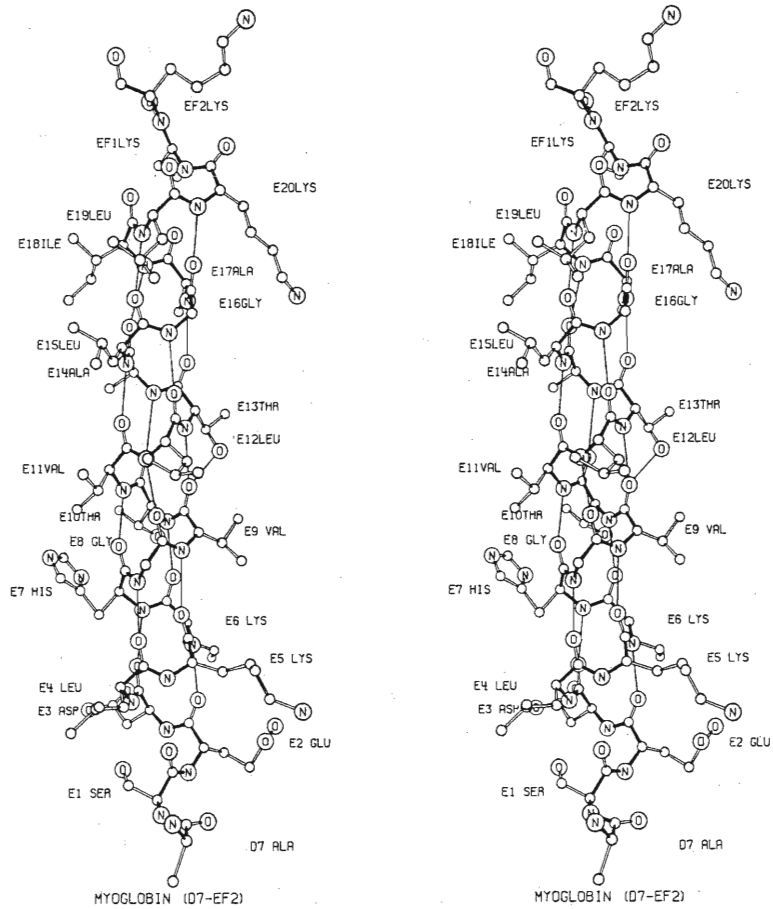


Fig. 6. The E Helix of Myoglobin. The side chains of residues E6 and EF1 are incomplete.



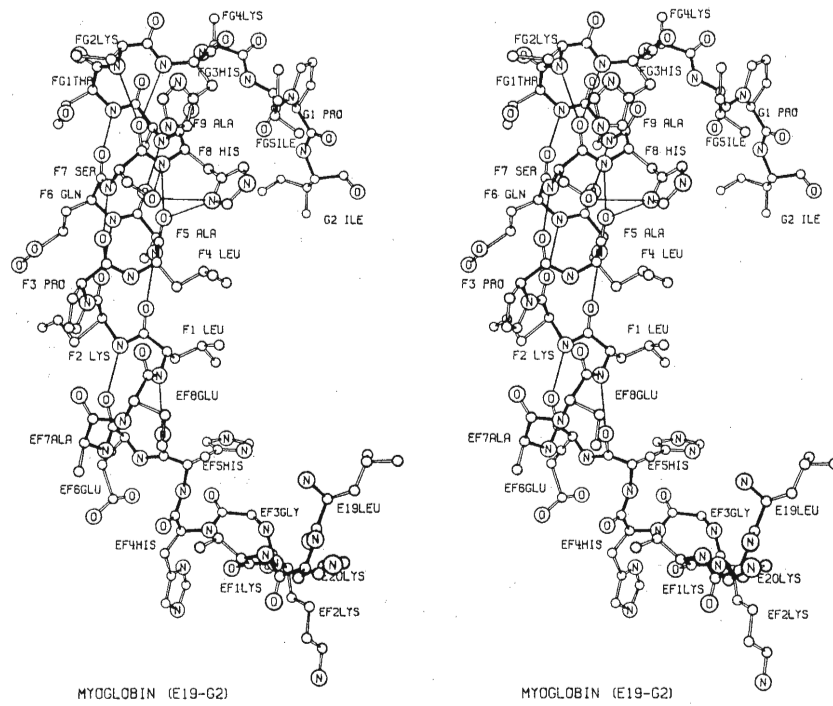


Fig. 7. The F Helix of Myoglobin. The side chains of residues EF1, EF8, F2, FG2, and FG4 are incomplete.

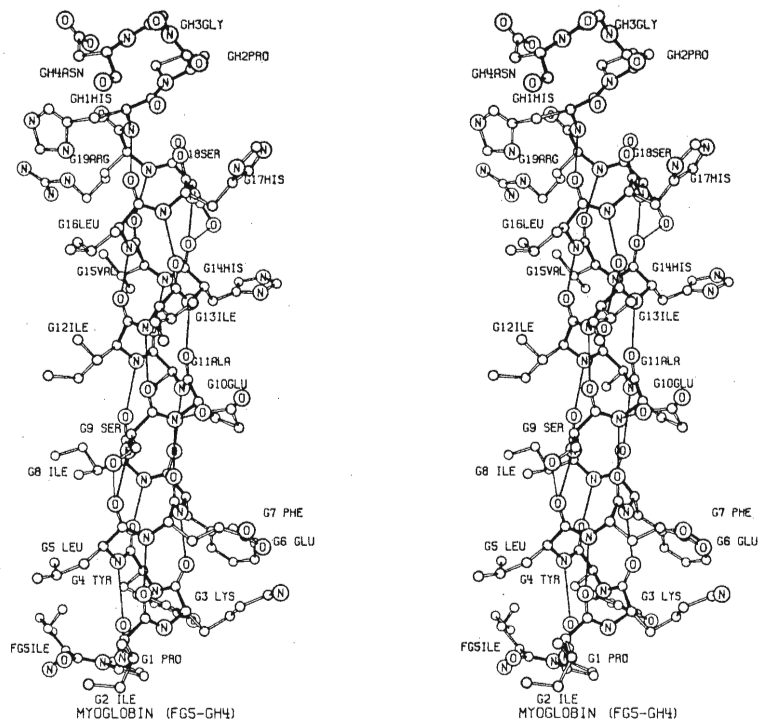


Fig. 8. The G Helix of Myoglobin.

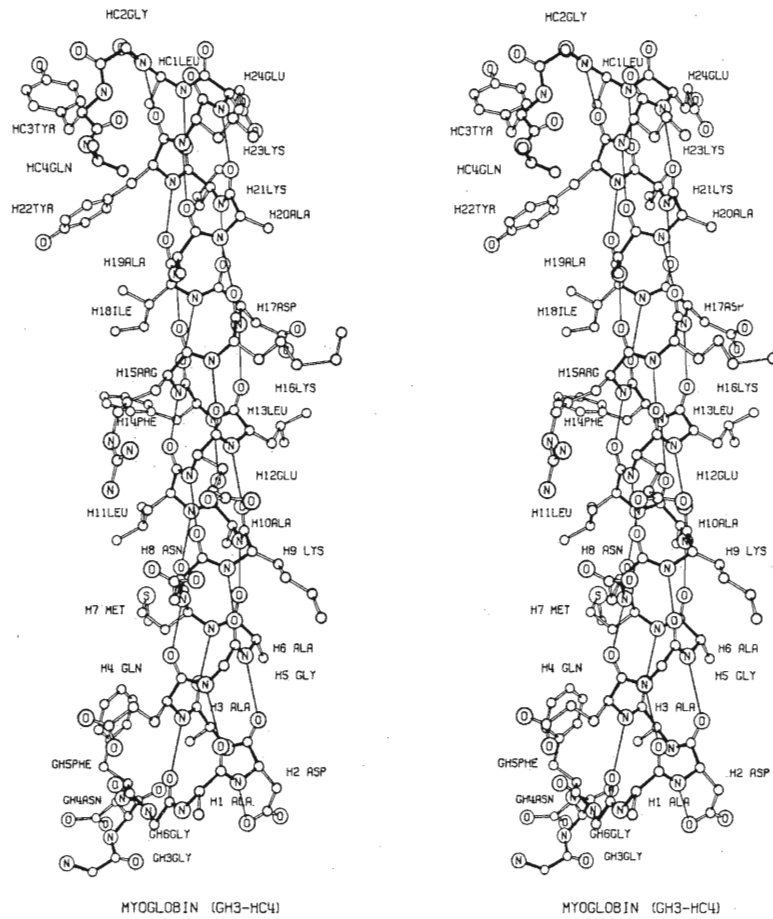


Fig. 9. The H Helix of Myoglobin. The carboxyl end of the myoglobin chain is at the upper left. The last amino-acid residue, HC5 glycine, was not located. The side chains of residues H9, H21, H23, and HC4 are incomplete. The terminal side-chain atom of residue H16 is a nitrogen atom and not a carbon atom as shown here.

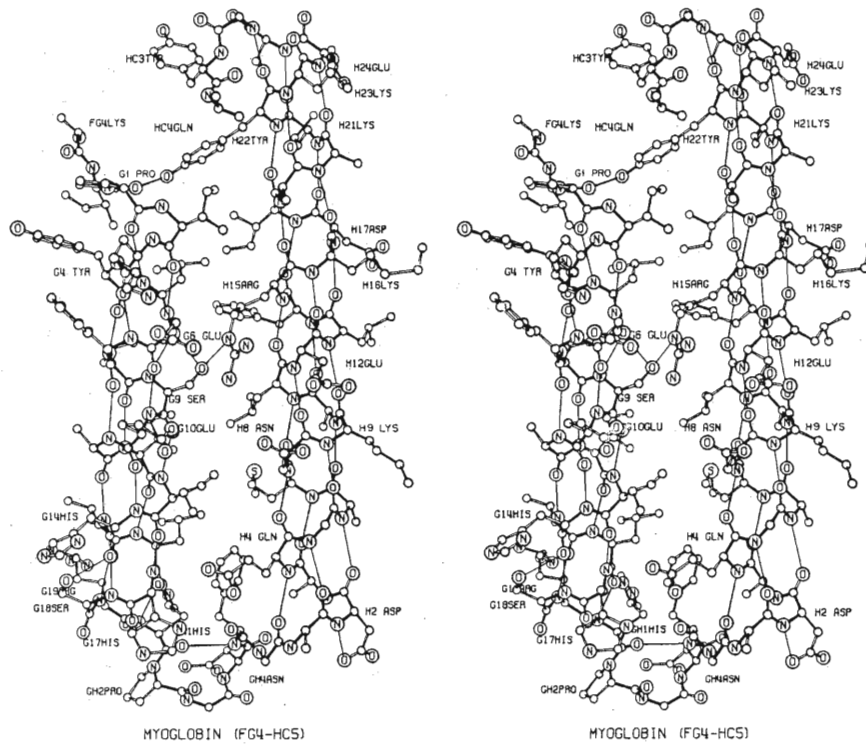


Fig. 10. The G and H Helices of Myoglobin. About one third of the myoglobin molecule is present in the figure. Identifying labels are on the polar and proline residues only. Also see caption for Fig. 9.

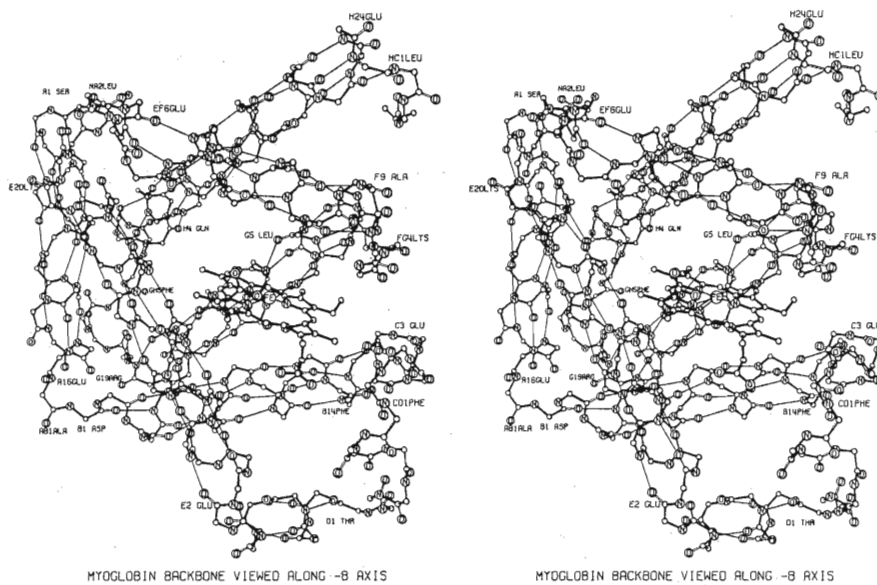


Fig. 11. The Backbone of Myoglobin. All side-chain atoms are omitted. A few residues are labeled to identify the various helical segments. The heme group is actually planar, but appears nonplanar in these figures because of an error in the positional parameters of one nitrogen atom.

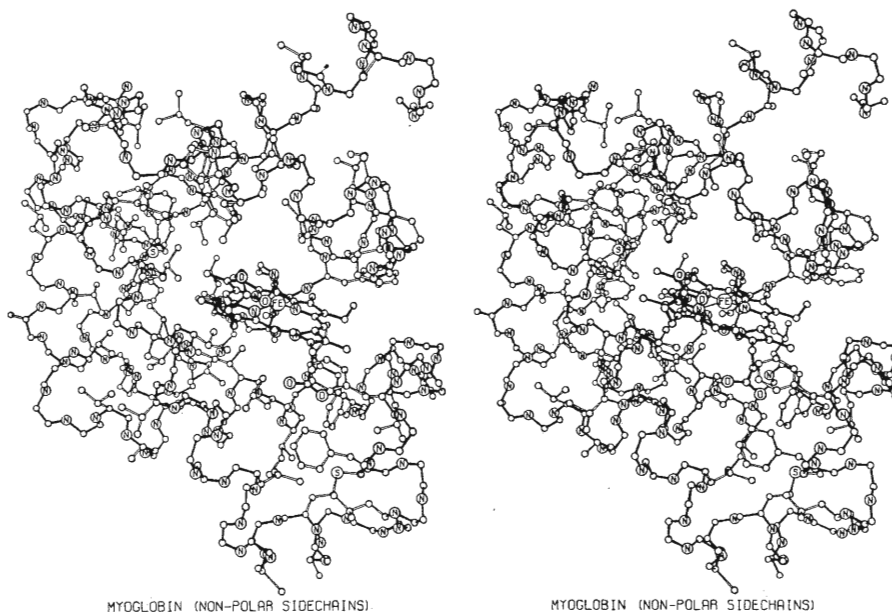


Fig. 12. The Backbone and the Nonpolar Side Chains of Myoglobin. The carbonyl oxygen atoms of the backbone and all polar side-chain atoms are omitted. Note that the nonpolar side chains are usually inside the surface of the molecule. The orientation of the molecule is the same as that in Figs. 11 and 13.

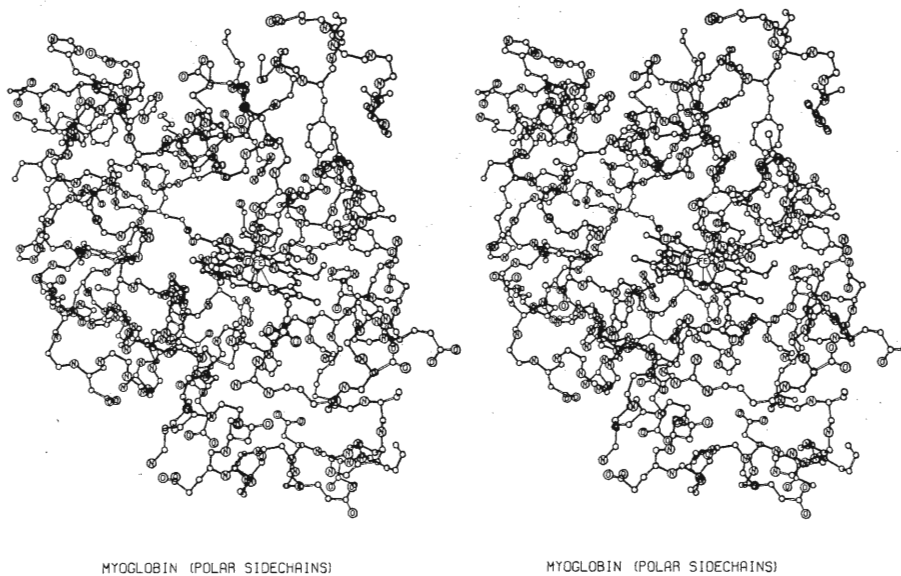


Fig. 13. The Backbone and the Polar Side Chains of Myoglobin. The carbonyl oxygen atoms of the backbone and all nonpolar side-chain atoms (except those in proline) are omitted. Note that the polar side chains are usually at the outside surface of the molecule. The orientation of the molecule is the same as that in Figs. 11 and 12.

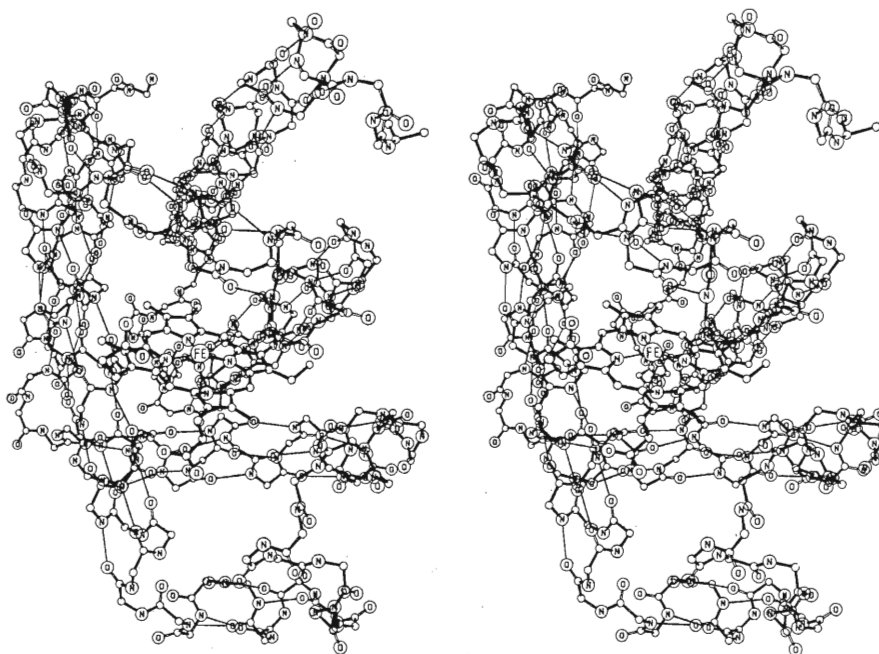


Fig. 14. The Backbone of Myoglobin. See caption of Fig. 11. The orientation of the molecule is different from that in Figs. 11, 12, and 13.

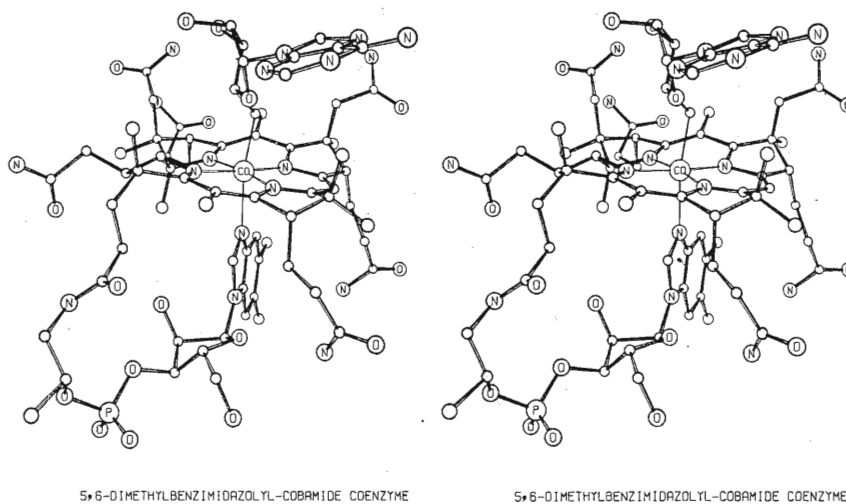


Fig. 15. Vitamin B-12 Coenzyme in the "Conventional Molecular Orientation." Carbon atoms are denoted by the smallest unmarked circles, and methyl groups are denoted by slightly larger unmarked circles. The oxygen, nitrogen, phosphorous, and cobalt atoms are so designated on the figure. Hydrogen atoms are not shown.

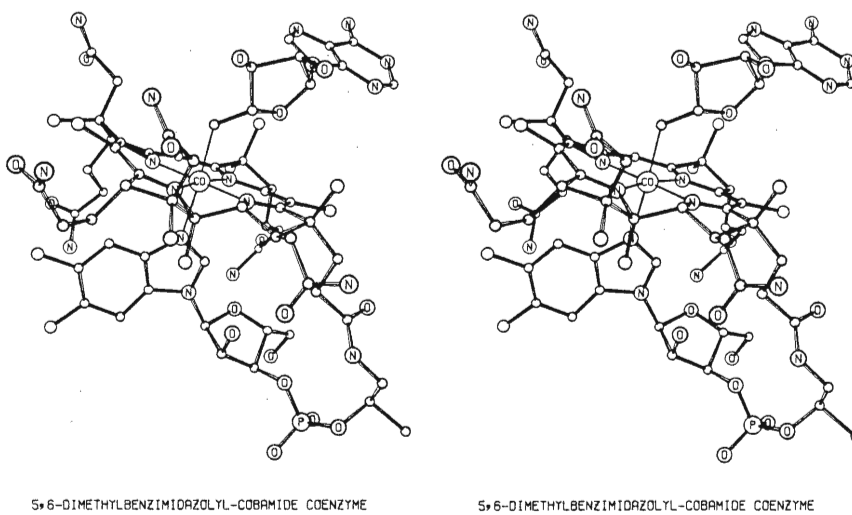


Fig. 16. Vitamin B-12 Coenzyme in an Alternate Orientation. See caption of Fig. 15.

MEDICAL RESEARCH COUNCIL

Telephone:  
Cambridge 48011



LABORATORY OF MOLECULAR BIOLOGY,  
UNIVERSITY POSTGRADUATE MEDICAL SCHOOL,  
HILLS ROAD,  
CAMBRIDGE.

29th July, 1966

Dr. Carroll K. Johnson,  
Oak Ridge National Laboratory,  
Post Office Box X,  
Oak Ridge,  
Tennessee. 37830

Dear Dr. Johnson,

I have just had a letter from Herman Watson enclosing your extremely beautiful pictures of myoglobin. I am quite delighted by them and do congratulate you on the quality of the results. I should very much like to have the opportunity of discussing all this with you, and I hear from Herman that there is some chance you may be coming to the Vienna Congress. If you do, I wonder whether we could persuade you to visit Cambridge and give us a seminar. I shall not be back in Cambridge until about the 14th of September, so I wonder whether some date within the week following that would be possible. I look forward to hearing your plans.

Yours sincerely,

*John C Kendrew*

John C. Kendrew

cc. Dr. Herman Watson

---

## What you can expect from Jana2006

**Václav Petříček and Michal Dušek**

*Institute of Physics AVCR, Cukrovarnicka 10, 162 53 Praha, Czech Republic. E-mail: [petricek@fzu.cz](mailto:petricek@fzu.cz) ;  
WWW: <http://www-xray.fzu.cz/jana/Jana2000/jana.html>*

### 1. Introduction

The program Jana is a well known system for solution and refinement of regular, modulated and composite crystals. It is distributed as freeware. Jana was originally oriented to data collected from a single crystal with a wide support for handling of twinning. In the version Jana2000 the program was generalized for structure refinement from powder data including multiphase option [1]. Finally the multiphase option has been generalized for single crystal refinement.

Many new features were gradually included into Jana2000. Thus the latest version of Jana2000 contains a lot of advanced tools such as transformation of complete structure to a lower space group, transformation to the supercell for commensurately modulated structures etc. The support for working with 5d and 6d structures has been also gradually improved. Moreover a direct connection has been established with drawing programs as well as with the SIR program for structure solution.

Jana2000 has been written in the programming language Fortran77 in order to give the LINUX users the possibility to use the free g77 compiler. Unfortunately it put severe limits to the program size. In last several years, modern Fortran compilers became more accessible and now all LINUX systems have free and relatively good g95 or gfortran compilers that can be used for compilation of Jana. This opened up new possibilities for implementation of additional options into the program. For this reason we have decided to create a new program, version Jana2006, utilizing the modern programming tools, namely the possibility to allocate and deallocate memory.

The code of Jana2000 has been completely rewritten (it took almost one year of work) and many new options have been introduced. Probably the most important change is the option for making joint refinements from different data collections. Thus data sets from powder and single crystal measured with X-rays and neutrons can be used simultaneously.

The Rietveld and profile (Le Bail) refinement were improved by implementation of the fundamental parameters approach and the anisotropic line broadening for modulated structures. Moreover a direct support for using TOF data has been introduced.

The magnetic scattering has been implemented as well. It can be used not only for structures having both (nuclear and magnetic) lattices identical but also for commensurately and incommensurately magnetic arrangements.

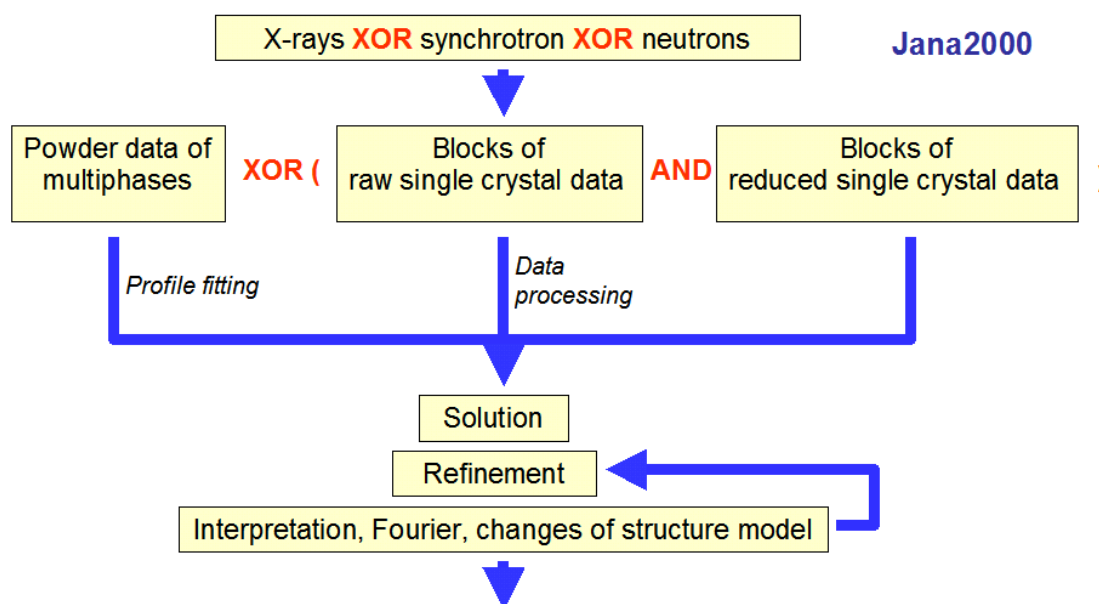
Jana2006 has a direct connection to the program Superflip [2]. This is especially important for modulated crystals which can be solved by Superflip without intermediate solution of average structure.

The graphics have been considerably improved but we are still using our own GUI as in Jana2000.



## 2. Multisource option

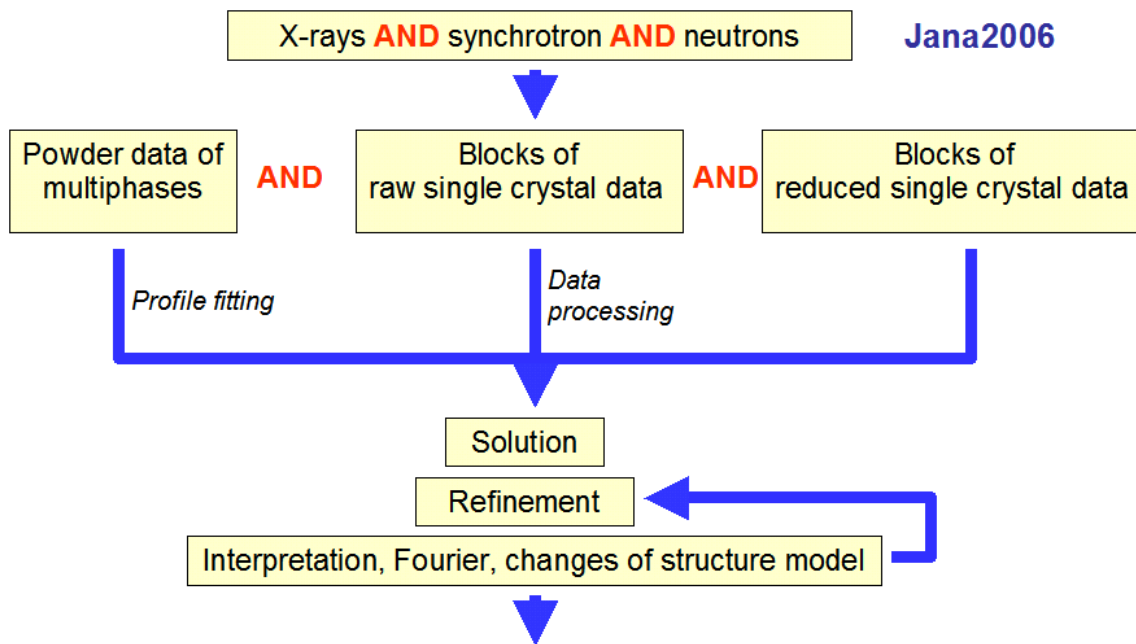
Combining data from different sources was limited in Jana2000:



In the previous version of Jana, only data collected on single crystal diffractometers using the same wavelength could be combined. Such a combination could not bring anything really new except of possibility for combination of satellites measured on synchrotron with main reflections collected with indoor diffractometers.

The new possibilities for data combination in Jana2006 can be easily understood when we take the scheme for Jana2000 and replace all “XOR” conditions with “AND”. In Jana2006 we can take benefit from combination of diffraction techniques with different sensitivity to get more precise information about the structure. This can be helpful:

- For structures containing very heavy atoms such as Pb, Bi, etc. and also some light atoms (namely hydrogen atoms). Then information from the neutron diffraction can considerably enlarge a chance to make complete analysis. The reason why we need also X-ray data is that they are usually more complete.
- For charge density studies [3] i.e. multipole refinement where from neutron data collection we can get central positions of atoms which are more realistic. On the other hand the bonding effects are apparent only from X-rays.
- For detailed analyses using X-ray data taken at different wavelengths with help of anomalous scattering effects.
- For magnetic structure analysis where we have usually only a short data record from neutron source and the combination with a full X-ray data set can considerably improve atomic positions and ADP's.



The function to be minimized is now composed from three parts:

$$\begin{aligned}
 S = & \sum_i w_{s1i} (F_{obs,1}^2 - F_{calc,1}^2)^2 + \sum_i w_{s2i} (F_{obs,1}^2 - F_{calc,1}^2)^2 + \dots \\
 & + \sum_i w_{p1i} (y_{obs,1} - y_{calc,1})^2 + \sum_i w_{p2i} (y_{obs,2} - y_{calc,2})^2 + \dots \\
 & + \sum_i w_{gi} (g_{obs,i} - g_{fix,i})^2
 \end{aligned}$$

where the first part stands for single crystal data, the second part for different powder data blocks and the third line stands for various geometrical or chemical restraints whenever necessary. The each diffraction structure factor used in the formula is calculated as follows from the used radiation and wave length. Similarly for powder data each data set can have generally different powder parameters such a background coefficients.

From this equation it is also apparent that the weighting scheme plays a crucial role in the refinement. Jana2006 does not allow any additional corrections of weights which should be based on experimental values derived from real statistics of each data block.

Another weak point of such joint refinement is that structural parameters need not be identical if the experimental conditions are not exactly same. Moreover, positions of atoms for neutron radiations are related to the positions of nuclei whereas for X-ray diffraction they are connected with the centre of a density cloud. For this reason joint refinement can be useful for a multipole analysis; on the other hand this complicates results for normal studies.

Similarly ADP parameters need not describe atom distribution as inducted by thermal motion. These parameters are strongly affected by data corrections, especially by absorption correction. Another problem is that TDS effects are different for neutrons and X-rays. As a simple correction of the mentioned differences an isotropic overall ADP has been introduced into the program.

The new option has been successfully tested but not for all cases as listed above. We are waiting for responses from users.

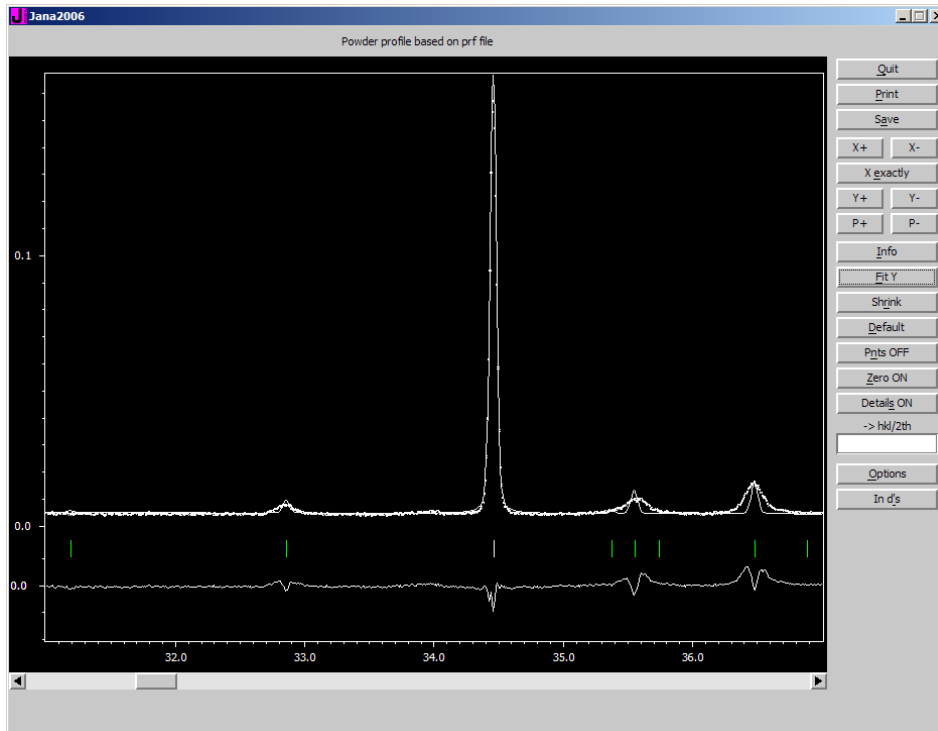
### 3. New powder diffraction options

#### 3.1. Anisotropic line broadening of modulated samples

The anisotropic line broadening  $b$  as it has been introduced by Stephens:

$$b(\langle 2\theta_{hkl} \rangle) = \tan\langle \theta_{hkl} \rangle A(hkl) \quad \text{where} \quad A(hkl) = \left[ \langle d_{hkl} \rangle^4 \sum_{H+K+L=4} G_{HKL} h^H k^K l^L \right]^{1/2} \quad (1)$$

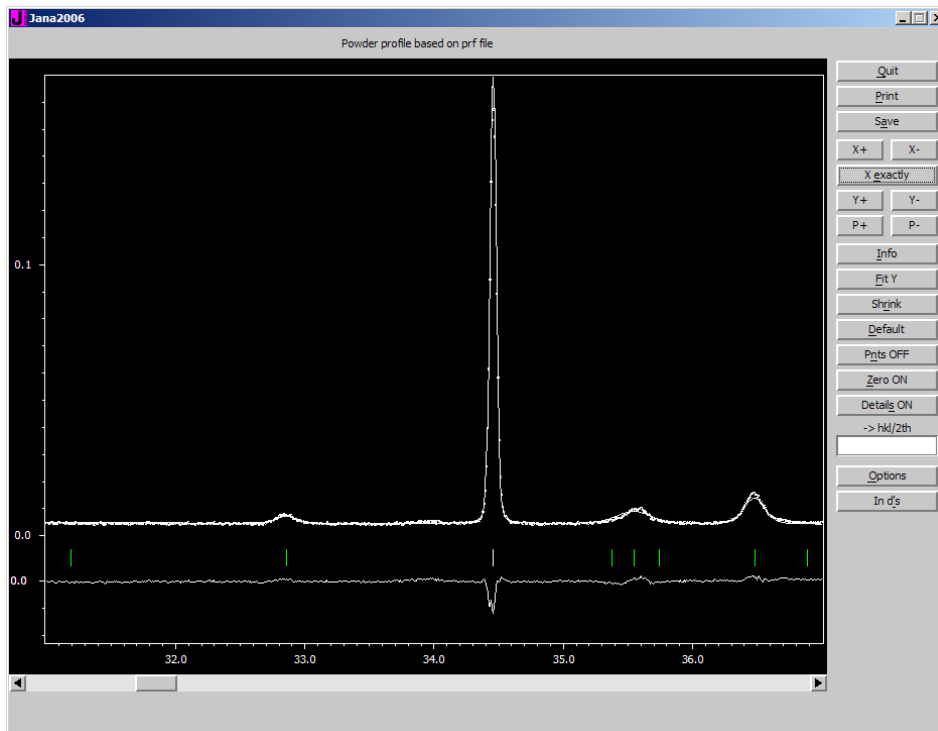
does not account for line broadening originating from strain induced by fluctuation of the modulation vector and therefore it cannot give a good profile fit as visible in the following example:



The original symmetric tensor of the 4<sup>th</sup> order connected with anisotropic broadening has generally 15 independent components. The method can be generalized for modulated structures by using similar tensor but now in 4d space. Then the number of tensor components will change to 35 and the equation for  $A(hklm)$  will take the following form:

$$A(hklm) = \left[ \langle d_{hklm} \rangle^4 \sum_{H+K+L+M=4} G_{HKL} h^H k^K l^L m^M \right]^{1/2} \quad (2)$$

A more detailed analysis made by Leineweber and Petříček [5] lead to the conclusion that all 35 components are not independent and that they can be reduced to 31. This is connected with the fact the super-space approach uses the 4d space in a specific way and only its projection to the 3d reciprocal space has real physical meaning. Application of anisotropic broadening leads to considerably better fit.

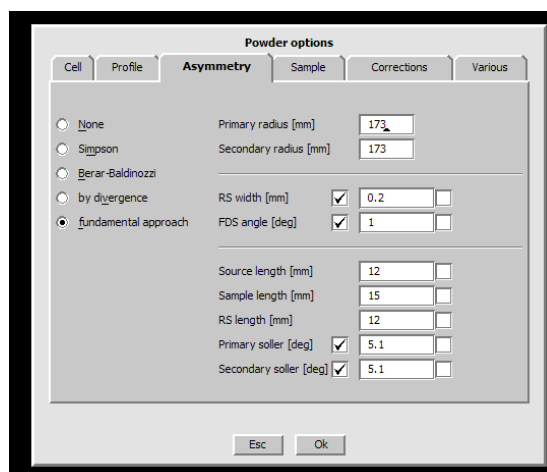


The number of coefficients for refinement is dramatically reduced by symmetry. For example for orthorhombic crystal there are just 12 independent parameters.

In cases where broadening affects satellites so strongly as in the previous figures the refinement without applying this correction can lead to systematically wrong modulation waves.

### 3.2. The fundamental approach to X-ray profiles

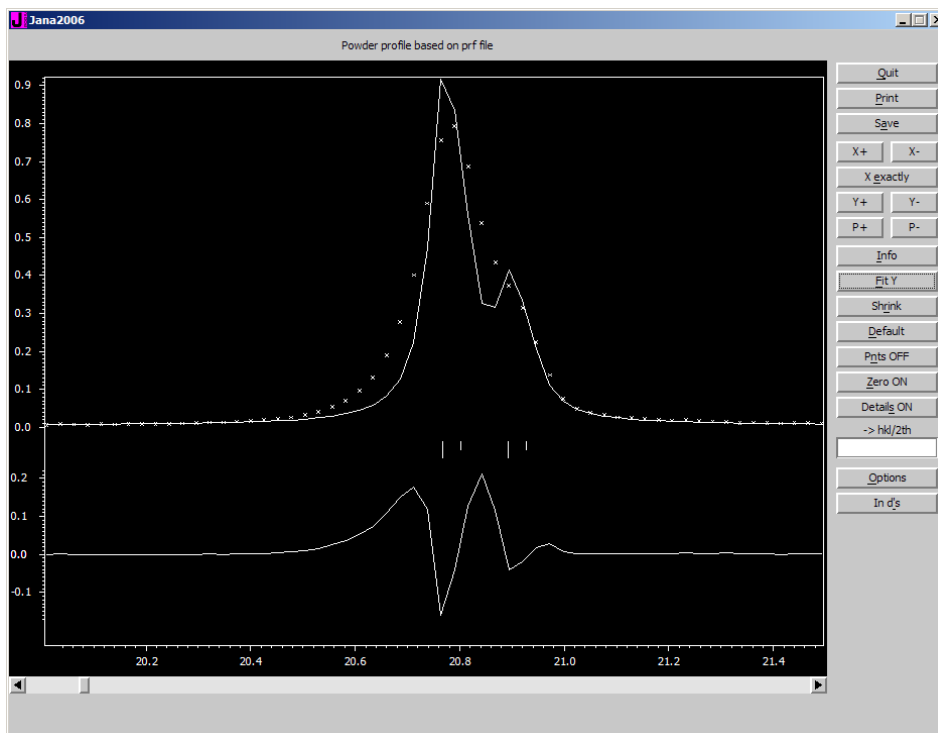
This new option in Jana2006 is fully based on the theoretical works done by R.W. Cheary and A.A. Coelho [6], [7], [8]. The main advantage of this approach for conventional X-ray powder diffractometer is that all used parameters are closely related to the experimental arrangement. A crucial function used in the general convolution procedure is the axial divergence function which is - according to the derivation made in [7] - a function of simple experimental parameter such as axial length of the X-ray source, the sample and receiving slit. In the case that Soller slits are used another modification of the basic profile have to be made. All used parameters are known from the device and they can be used as starting values. They can also be refined but a good idea is to adjust them with some standard sample. The set of parameters used in Jana2006 implementation again corresponds to what used by A.A. Coelho in the TOPAS program [9, 10]:



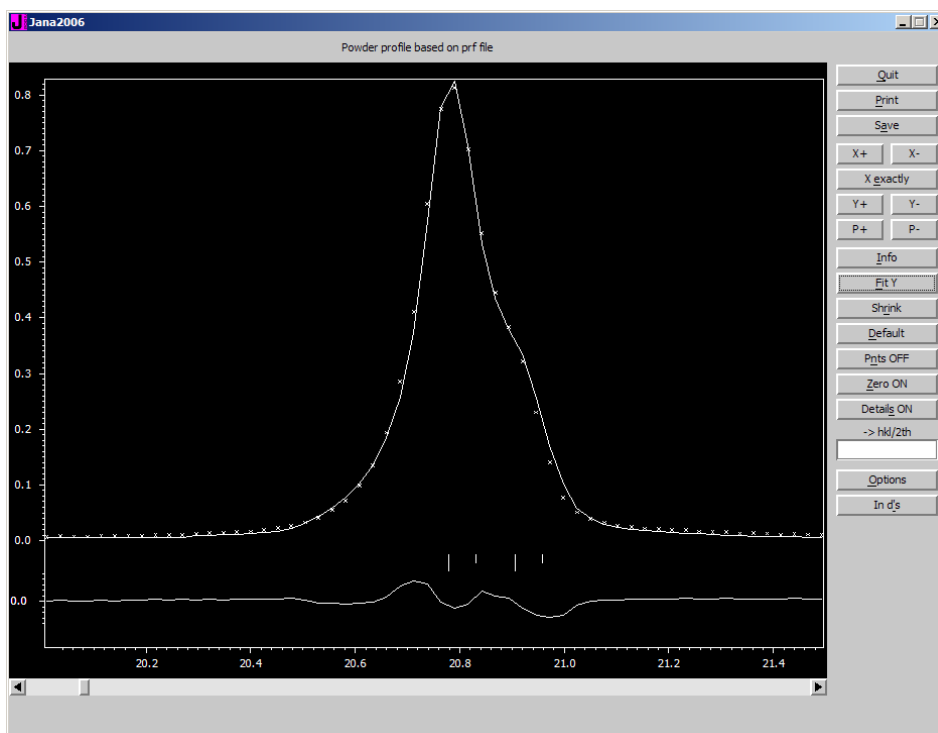
The pure axial divergence profile function is a discontinuous function and therefore its implementation into the convolution procedure is not straightforward. We have used a similar procedure as proposed in [7], [8].

The possibility to use different emission profiles has been introduced as well. The user can select from different profiles for Co, Cr, Cu, Fe, Mn and Ni tubes.

The following figure shows a peak profile for simple  $\text{PbSO}_4$  how it was refined without any correction for peak asymmetry.



Fundamental parameters as known from the experiment lead to considerable improvement:



The fundamental approach works correctly not only in the low angle region but also for high angles. With this method the zero asymmetry can be detected as predicted in the original papers at  $2\theta=120^\circ$ .

Another very positive point is that the instrumental parameters are now separated from the sample parameters and therefore we have better chance to check and control the sample quality from the Lorentzian and Gaussian parameters. The interpretation of the width parameters in terms of the crystalline size and strain is much more realistic.

### 3.3. Implementation of direct handling of TOF data

This option reflects what has been already done in the GSAS program [11]. Several data formats GSAS, ISIS and VEGA/IGOR can be used to import data and TOF parameters into the program. The profile functions were also implemented in the way described in the GSAS manual.

### 3.4. Magnetic scattering

The magnetic structure factor is a vector defined by the equation:

$$\mathbf{F}_M(\mathbf{h}) = p \sum_i f_i(h) T_i(\mathbf{h}) \mathbf{M}_i \exp(2\pi i \mathbf{h} \cdot \mathbf{r}_i) \quad (2)$$

where  $p$  is a normalization constant to transfer magnetic scattering calculated in Bohr magnetons to the scale used nuclear neutron structure factors,  $f_i(h)$  magnetic form factor,  $T_i(\mathbf{h})$  is the ADP (temperature) factor and  $\mathbf{M}$  is the magnetic moment of the  $i^{\text{th}}$  atom. The geometrical part  $\exp(2\pi i \mathbf{h} \cdot \mathbf{r}_i)$  is a function of the atom position  $\mathbf{r}_i$ . Intensity of a magnetic reflection is related to the square length of the magnetic structure factor projected into the reflection plane:

$$I_M(\mathbf{h}) = \mathbf{F}_M^2(\mathbf{h}) - [\mathbf{h}/h \cdot \mathbf{F}_M(\mathbf{h})]^2 \quad (3)$$

The intensity of the magnetic reflection is to be combined with the intensity originating from the nuclear scattering. The combination is made as from independent object (twins):

$$I(\mathbf{h}) = I_N(\mathbf{h}) + I_M(\mathbf{h}) \quad (4)$$

The magnetic moments of atoms can follow the same translation periodicity of the nuclear structure or they can have their own periodicity either commensurate or incommensurate with the nuclear lattice. Generally the magnetic moment can be written as a combination of harmonic functions:

$$\mathbf{M}_i(x_4) = \mathbf{M}_{i0} + \sum_{n=1}^N [\mathbf{M}_{ins} \sin(2\pi n x_4) + \mathbf{M}_{inc} \cos(2\pi n x_4)] \quad (5)$$

where  $\mathbf{M}_i(x_4)$  is the actual magnetic moment in the cell characterized by the translation  $\mathbf{l}$   $\mathbf{M}_i(x_4)$  and  $x_4 = \mathbf{q}(\mathbf{r}_{i0} + \mathbf{l}) + t$  is the internal coordinate. The refinable parameters are the components of vectors  $\mathbf{M}_{i0}$ ,  $\mathbf{M}_{ins}$ ,  $\mathbf{M}_{inc}$ .

For description of symmetry the concept of magnetic group has been generalized to magnetic supergroup groups in a similar way as space groups for nuclear structures were generalized to superspace groups. Such an approach has following advantages:

- Simple relationship to the Laue diffraction group allows easier symmetry recognition
- The magnetic structure can be handled even for regularly modulated and composite crystals

- The general modulation wave can account for complicated magnetic modulation – more harmonics, step like modulations, ...

But there are also some disadvantages:

- It is too complicated for simple cases i.e. double magnetic supercells
- The method to handle cases, in which the magnetic moments are arranged according to irreducible representation having dimension larger than 1, is a little bit cumbersome. We have to select a proper subgroup and make restrictions to keep coordinates of atoms and ADP as in the original space group.

A testing tool has been created to make a symmetry analysis easier. It allows selecting a proper magnetic group from the local and global magnetic moment of each atom and preliminary tests.

### 3.5. Interface to the Superflip

The solution of modulated structures depends on the size of the periodic distortions (modulations) in the crystal. For small displacements leading to weak satellites the average structure can be solved by a standard way (direct methods, heavy atom methods) from main reflections. The modulations can be found directly from subsequent refinements. As starting values for modulations we can use just small random starting values. Recommended strategy is to refine first modulations of atoms exhibiting some anomalies such as large ADP's or split positions in the average structure.

For stronger modulation special methods for solution has been developed. Usually even for such structures we can find an average structure but now with higher degree of disorder. Then we can apply direct methods [12] or the heavy atoms methods [13] and determine modulations of dominantly modulated atoms.

There are also cases where modulation is so strong that all these methods fail. However, the newly discovered method based on Charge flipping algorithm by Oszlányi and Sütö [14] and generalized by Palatinus [2] to the modulated structures works even in such cases. Jana2006 connects directly the program Superflip [15] for solution of standard and modulated structures by the charge flipping method.

## 4. Conclusions

The development of Jana2006 took a much longer time than originally predicted. Thus only now a testing version, which contains all options mentioned in this paper, is accessible through our Jana home page <http://www-xray.fzu.cz/jana/Jana2000/jana.html> and all responses from users will be welcomed.

## 5. References

- [1] Dušek, M., Petříček, V., Wunschel, M., Dinnebier, R. E., Smaalen, S. van (2001). *J. Appl. Cryst.*, **34**, 398-404.
- [2] Palatinus, L. (2004)., *Acta Cryst.*, **A60**, 604-610.
- [3] Hansen, N., Coppens, P. (1978). *Acta Cryst.*, **A34**. 909-921.
- [4] Stephens, P. W. (1999). *J. Appl. Cryst.*, **32**, 281-289.
- [5] Leineweber, A., Petříček, V. (2007). *J. Appl. Cryst.* *Accepted for publication.*
- [6] Cheary, R. W., Coelho, A. A. (1992). *J. Appl. Cryst.*, **25**, 109-121.

- [7] Cheary, R. W., Coelho, A. A. (1998). *J. Appl. Cryst.*, **31**, 851-861.
- [8] Cheary, R. W., Coelho, A. A. (1998). *J. Appl. Cryst.*, **31**, 862-868.
- [9] TOPAS, Bruker AXS Inc., Madison, Wisconsin, USA.
- [10] Coelho, A. A. (2007a). *TOPAS-Academic V4.1-beta*. <http://members.optusnet.com.au/alancoelho/>.
- [11] Larson, A. C. and R. B. Von Dreele. (2004). General Structure Analysis System (GSAS). Los Alamos National Laboratory Report LAUR 86-748.
- [12] Fan, H-F., van Smaalen S., Lam E. J. W., Buerskens P. T., (1993). *Acta Cryst*, **A49**, 704-708.
- [13] Peterková, J., Dušek, M., Petříček V., Loub, J. (1998). *Acta Cryst*. **B54**, 809-818.
- [14] Oszlányi G., Süto A., (2004). *Acta Cryst*. **A60**, 134-141.
- [15] Palatinus L., Chapuis G., (2007). *J. Appl. Cryst.* **40**, 786-790.



---

## Report from the GSAS-II Workshop: May 10-11, 2007

**Brian H. Toby and Robert B. Von Dreele**

*Advanced Photon Source, Argonne National Laboratory, Building 401, 9700 S. Cass Avenue, Argonne, Illinois, 60439, USA. E-mail: [brian.toby@anl.gov](mailto:brian.toby@anl.gov) and [vondreele@anl.gov](mailto:vondreele@anl.gov) ; WWW: <http://aps.anl.gov/>*

Place holder page. Report-proper starts on following page.

# Report from the GSAS-II Workshop

May 10-11, 2007

*Brian H. Toby and Robert B. Von Dreele*

*Advanced Photon Source and  
Intense Pulsed Neutron Source  
Argonne National Laboratory  
Argonne, IL 60439 (USA)*

## Executive Summary

The GSAS crystallographic package is the only tool designed to be used for all types of problems and use all types of diffraction data. The package is important for a wide range of fields: geosciences, solid-state and inorganic chemistry, condensed-matter physics, materials engineering, pharmaceuticals and even extraterrestrial studies. In nearly two decades of use, it has been cited well over 4,000 times and continues to be cited more than once per day. Nonetheless, many aspects of the package are showing their age, so a workshop was convened to discuss the needs and directions for crystallography.

Conclusions were that structural analysis software is a significant limitation to scientific productivity. Software needs to be more flexible in the hands of experts and be better suited to handle large amounts of data but more forgiving and instructional in the hands of novices, who are less likely than past users to have a strong education in crystallography. Starting a new software will enable new science by allowing better use of nondiffraction data and pair distribution functions. This is needed for structural characterization of complex materials, such as nanostructured composites, catalysts and partially ordered electronic materials. Such a project will bring new staff and keep these tools from dying when their maintainers retire.

The workshop participants strongly supported a new package, GSAS-II, building on the pioneering approach of GSAS. The new code should be more modular, able to be customized in the hands of experts and should also be designed for use by non-crystallographers, with significant consistency checking, documentation, and tutorial material.

<p>This report has been created by UChicago Argonne, LLC, Operator of Argonne National Laboratory ("Argonne"). Argonne, a U.S. Department of Energy Office of Science laboratory, is operated under Contract No. DE-AC02-06CH11357.</p>
---

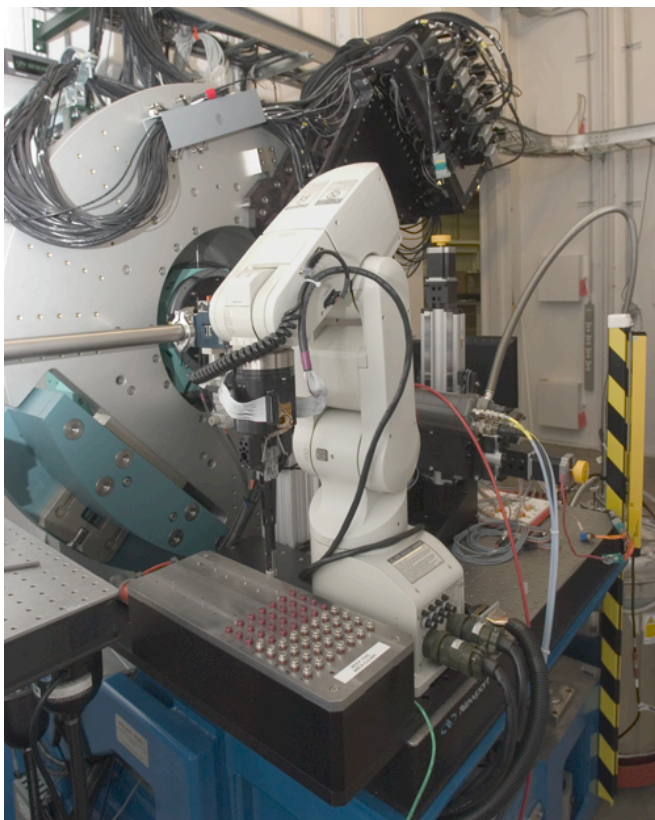
## Motivation

More than two decades have passed since the GSAS package was initiated. During these years, GSAS has been extremely valuable for crystallographic computing and continues to expand in capabilities. When first released, a relatively small community utilized it, primarily scientists using time-of-flight neutron scattering. It is now widely used in virtually every area of the physical and biological sciences where solid-state materials are studied. One measure of success is citations: Since its introduction, GSAS has been cited over 4400 times. Its use continues to grow: At present it is cited on average 10 times per week.

Reasons for the success of this endeavor are multifold:

- It was the first software package designed to be comprehensive: to address all types of crystallographic problems, utilizing any type of x-ray or neutron diffraction data in any combination including single-crystal and powder experiments.
- The software was written and updated by scientist(s) who were involved at the forefront of the field, who added support for new types of measurements and models, as they became available.
- While GSAS was created to run on VAX/VMS computers, it was adapted to run on all commonly used computing platforms, as those systems developed.
- An allied project released a graphical user interface (EXPGUI) that eased the learning experience for novices; it also supplied simple-to-use self-installing packages for GSAS & EXPGUI that made the software more accessible. EXPGUI has been cited over 400 times since 2001 and is currently cited 2-3 times per week.

However, while the applications for GSAS have grown dramatically, maintenance of the GSAS and EXPGUI packages remains largely a hobby of the authors. One of the two GSAS originators (Allen Larson) has been retired from the project for more than a decade, and there is no succession plan should the other developer (Robert Von Dreele) also retire. While GSAS can continue to be augmented and adapted to suit nearly all contemporary uses, the structure of underlying code does limit future growth and expansion. New instruments, such as the APS 11-BM high-resolution and high-throughput x-ray powder diffractometer and the SNS POWGEN-III will generate huge amounts of diffraction data that will challenge our ability to perform analysis. To consider the current and future applications for crystallographic structural analysis and needs for software, particularly for the work of US scientists, a workshop was convened May 10 & 11, 2007. This report documents the discussions and general conclusions of this workshop.



**The 11-BM powder diffractometer at the APS. This instrument is equipped with twelve analyzers and a robotic sample changer to collect high-resolution diffraction data with high throughput.**

## Background

Crystallography has a unique place in the history of science because it was the first physical technique that provided measurements that could be directly correlated to atomic structure. Starting a century ago, it became an extremely powerful tool for understanding the physical, chemical or biological function of a material. While other tools now allow scientists to “see” atoms, crystallography remains unique for characterization of bulk atomic structure; a measure of its importance can be appreciated by the fact that more than 20 Nobel Prizes have been awarded for crystallographic work.

Improvements in diffraction theory later allowed for *quantitative* simulation of diffraction observations from an atomistic model. Advancements first in manual methods and later in automated computation made it possible to optimize these models (*crystal structures*) to best fit diffraction data sets. The excellent agreement between experiment and scattering theory means that very low levels of systematic error are present in fitting, which allows highly accurate models to be developed. A number of other physical measurements can now be simulated from atomistic models, though few offer the excellent agreement currently possible with x-ray and neutron diffraction. However, as

theory and computation improve, quantitative simulation capabilities should be increasingly common for other physical measurements.

Crystallography offers one additional unique capability: a data set can contain a huge number of independent observations that provide structural information. For single crystals, this typically allows the fitted parameters that describe the molecular structure to be significantly over-determined, which in turn improves the precision of the result. Having a significantly over-determined result yields greater confidence: When a crystallographic model is developed, which is chemically reasonable and provides a very good fit to the observations, we can have reasonable faith that the model is very likely accurate. This is not always true for powder diffraction, particularly for materials where significant levels of disorder are present, since fewer observations are available.

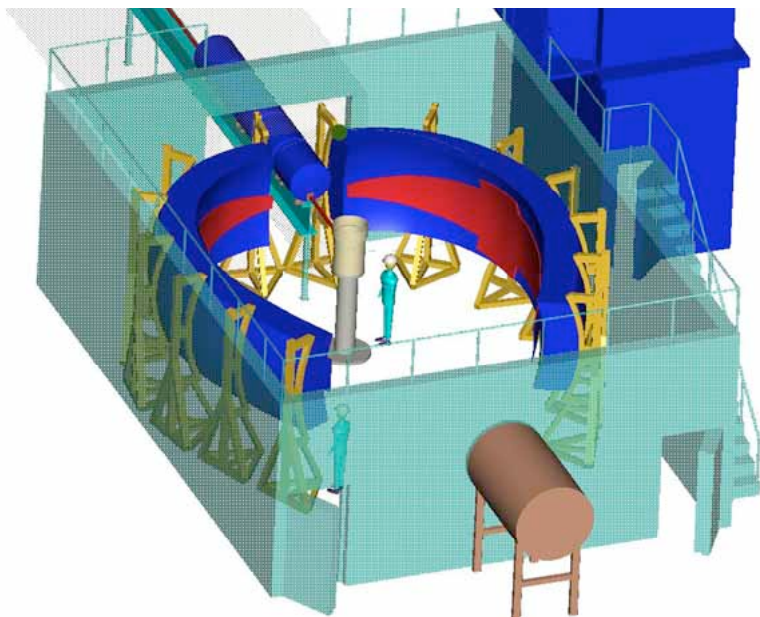
## Applications of Structural Characterization

Structural characterization traditionally has been a key technique in solid-state, inorganic and organic chemistry, to demonstrate that the desired species is indeed what has been synthesized. It has also been a key technique in mineralogy, for phase identification. In more recent years, however, structural characterization, particularly from powder diffraction, has seen very widespread application. Structural characterization is widely used in condensed matter physics for understanding the structure-property relationships in superconductors, magnetoresistors and other oxides and alloys with key magnetic or electronic properties. For materials engineering and science, determination of phase and microstructure composition, as well as crystallographic texture, provides a physical basis for understanding the strength of materials. Residual stress characterization from diffraction provides the basis for understanding failure processes, such as cracking in building materials, as well as high-tech components of airplanes, etc. Increasingly, the same diffraction techniques are now being applied to biomechanics studies of bones, teeth and other biological materials. In the areas of catalysis and separations, crystallography continues to be a very important resource for the characterization of new functional materials, such as zeolites. Pharmaceutical science is increasingly depending on structure elucidation from powder diffraction. Because polymorphs may have different bioavailability, the FDA requires characterization of the crystalline phase used in medical formulations. Utilization of powder diffraction even extends to space. GSAS is currently in use for the evaluation of data from a prototype diffractometer that will fly on the 2009 Mars Rover mission and will likely be used to analyze rocks on that planet (see photo).



**Professor David Bish using GSAS (& EXPGUI) north of the Arctic Circle. Adjacent to his left shoulder is a prototype of an x-ray diffractometer (CheMin IV) that will fly on the 2009 Mars Rover; above his right shoulder is a rifle for protection from polar bears. [David Bish, University of Indiana]**

The wide demand for powder-diffraction crystallography has led to the development of a number of advanced instruments. At the APS, two high-throughput instruments have been constructed. The 11-ID-B powder diffractometer is dedicated to pair distribution function analysis and can collect a complete data set in a fraction of a second. The 11-BM instrument can collect a high-resolution data set in under an hour or a lower resolution data set in minutes. An even more advanced instrument is planned for the NSLS-II. At the SNS, the POWGEN-III instrument advances neutron powder diffraction to a new generation, with a continuous array of detectors that allows instrumental resolution to be traded off against throughput in data reduction. This will offer unique capabilities for the first time in the US.



**The POWGEN-III diffractometer at the SNS. This instrument is expected to collect as quickly as ~20 minutes/data set. [J. Hodges, SNS]**

## Outlook for Crystallographic Computing

Up to the middle 1980s, when GSAS was first developed, a typical computer might cost as much as the annual salary of all its users combined. Codes needed to be highly efficient, since access was limited and charges for computer usage could eat up a large fraction of a research budget. Days were spent to improve computation times by a few percent or trim the memory demands by kilobytes. In that period, crystallographic computer programs were written and used by specialists. The users had substantial training in crystallography and expected to invest time learning software, which would be amortized against a career in the field.

That has changed completely. Computers are inexpensive and ubiquitous; a \$500 computer available in a department store is probably 5000 times faster than the departmental computer of the 1980s. If consuming an extra day of computer time or a gigabyte of memory would help improve scientific productivity, no one would think twice. The user base has changed. Structural characterization tools are now widely used, frequently by scientists with minimal crystallographic training. Today's scientists will use thousands of programs across their careers. They cannot invest significant time in learning the idiosyncrasies of very many tools. The data-analysis paradigm must be rethought from the perspective of how to improve efficiency of scientists and reliability of results through maximal deployment of computer hardware.

As science advances to more demanding problems, diffraction data alone are not sufficient for unique determination of structural parameters – at least not at the level needed in the research. In many modern engineered materials, for example in nanoparticles, shape-memory alloys, catalysts, and thermoelectric materials, the defects,

i.e., local deviations from long-range order, are as important for understanding materials properties as the average crystal structure. Such materials typically do not diffract well, and only a paucity of crystallographic observations is obtained. The pair distribution function approach to powder-diffraction data analysis offers an alternate tool for probing local structure. However, in many cases this technique is best used in conjunction with crystallographic techniques, since the local structure must average over long range to agree with the crystallographic result. Many other spectroscopic and microscopic techniques are used to probe structure. As the state of the art in these techniques improves, an increasing number may be quantitatively simulated from atomistic models. In practice, however, seldom are complex atomistic models fit directly to spectroscopic and microscopic data. This is in part due to the fact that these techniques, while offering valuable observations related to structural parameters and materials dynamics, alone do not offer enough independent observations for unconstrained fitting.

## Review of Comprehensive Crystallographic Software

There are now three comprehensive crystallographic software packages (powder/single crystal, x-ray/neutron): GSAS, FullProf and Topas, all of which can analyze diffraction data obtained at any national facility or home laboratory. Also related is the DANSE project, an NSF-funded effort for software related to analysis of all types of neutron scattering data. A 2005 DANSE survey in the powder-diffraction community found that of 140 participants, 75% use GSAS and 40% use FullProf. Only 15% reported using Topas, but that has very likely expanded considerably.

GSAS offers the widest range of constraints, restraints and correction models of these packages. It is the only software package capable of macromolecular fitting to single-crystal and powder data, and GSAS is the only program explicitly designed to process multiple combinations of diffraction data. GSAS-II workshop participants commented on the ease of use of the graphical user interface; GSAS was their preferred choice for instructional purposes. Some of the code that implements symmetry in GSAS was originally written by Allen Larson for the NRCVAX package, but all code in GSAS was written by the program authors or was contributed by others specifically for the project. GSAS is distributed for all common computer platforms (Windows, Mac & Linux). Source code is distributed only to individual scientists who request it and agree not redistribute it.

FullProf has unique features for fitting magnetic scattering using irreducible representations. This approach is being extended to a generalized treatment of incommensurate structures. FullProf was originally based on code dating back to the original Rietveld program but is being rebuilt in stages internally to use modern object-oriented Fortran code contained in an open-source crystallographic computation library, CrysFML, provided by the same developers. Most of the commonly used capabilities in GSAS are now present in FullProf. FullProf likely sees greater usage in the neutron diffraction community than GSAS, though many scientists use both codes depending on the needs of the project. FullProf runs a variety of platforms. It is not presently open source.



Topas is a completely modern code with roots in the fundamental parameters approach to powder peak-shape description and is the first comprehensive commercial crystallographic software package. It is sold through Bruker AXS, Inc., as part of their diffractometer analysis suite and is also sold directly, with a very substantial discount, to academic users. It is less comprehensive than GSAS or FullProf (for example, magnetic scattering is not available) but offers more modern fitting algorithms. It implements a symbolic algebra processor (called computer algebra by the developer) that allows users to reconfigure internal computations. Several workshop participants presented examples where this capability allowed models to be developed to treat diffraction phenomena that could not be fit in other packages. Topas also offers several exciting new approaches to commercially important problems, such as indexing and structure solution from powder diffraction. The developer of the software, Alan Coelho, plans to continue development of the code but primarily in areas where there is demand from customers. He noted at the workshop that he uses GSAS to validate his computations. Topas runs only under Windows.

## Scientific Limitations of Current Software

A central focus of the workshop was how crystallographic software limits science. A point was made that many users are happy with what they have, but science advances in the hands of practitioners who push the frontiers back, in measurement techniques, theory and in data analysis. However, it was also often expressed that effort needed to learn the software and the time required to utilize it already serve as a bottleneck limiting scientific output. This will become more acute as data can be measured with higher throughput, as well as in the hands of future less-experienced users, who will have less time available to invest in learning software.

The topics discussed at the workshop are summarized here:

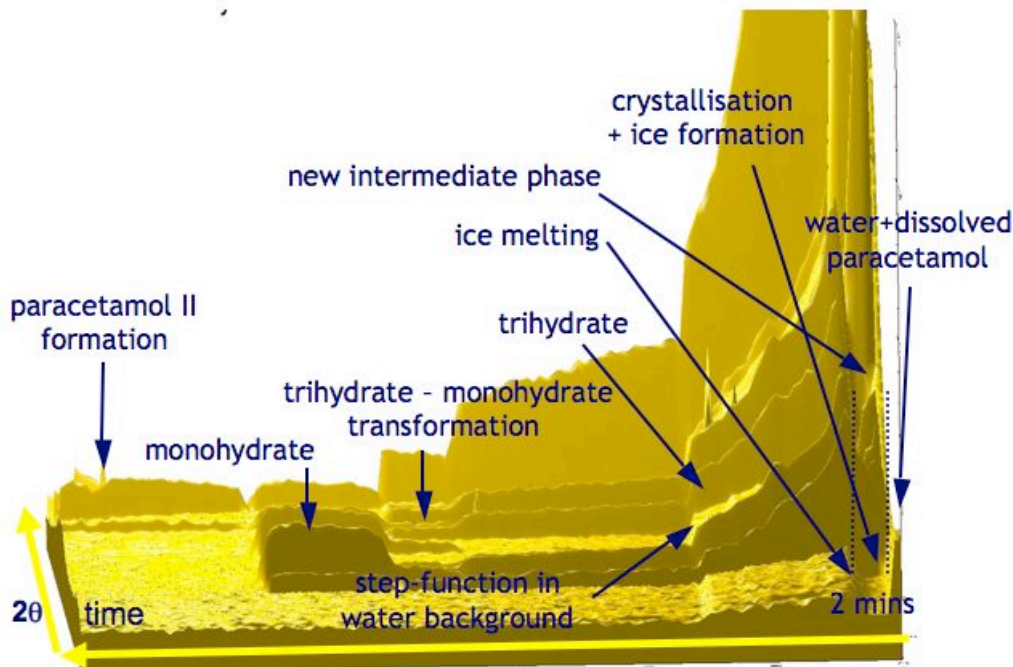
**Crystallography needs to be extended to the nanoscale.** This seemingly simple statement captures quite a range of materials-characterization research. While diffraction is sensitive to ordering on all distance scales, conventional crystallographic analysis ignores distortions in the shapes of diffraction peaks, which can provide detail about crystal defects. It does not model diffuse scattering, which provides information about local ordering. The total scattering method, where models are fit to a pair distribution function (PDF), provides sensitivity to ordering on a distance scale ranging from interatomic through the local nanoscale level. Just as Rietveld tosses away the non-Bragg scattering as background, total scattering discards periodicity. The ideal is a marriage that uses model descriptions reflecting both long- and short-range order that is fit simultaneously to both the diffraction data and the PDF.

Further, the treatment of crystallite-broadening contributions to the diffraction peak-shape use for data fitting have not developed significantly from the pioneering work of Scherrer in 1918. This is an area of active research interest. Characterization of domain sizes and shapes is of considerable importance for study of nanomaterials, including catalysts and nanocomposites.

For **mechanical characterization** by diffraction, a number of approaches for treatment of lattice strain anisotropy, including load-sharing models in the elastic regime, were identified as immediate needs in the field. In the longer term, treatment of lattice strain anisotropy due to inelastic deformation will afford the direct modeling of systems under deformation – allowing a major step forward. The adoption of a modular design in fitting software would allow code development to be decentralized; this would help in developing additional tools for these types of data analysis, including sophisticated and realistic macrostrain averaging models.

**Collaboration tools** are needed to foster long-distance collaborations. At present, it is quite difficult to pass a fitting project back and forth between collaborators and understand what has been tried – what improved the model and, more significantly, what failed and was abandoned. To help train students, the analogy was made to an airplane “black box,” which records everything the pilots do and is indispensable for error recovery. When presented with a refinement, one would like to replay the steps followed to see where problems occurred.

**Parametric fitting of multiple data sets** is needed to treat the large numbers of diffraction data sets produced by modern high-throughput instruments as a function of variables such as time, pressure or temperature. Note how clear it the evolution of phases becomes with the wealth of data collected upon heating acetaminophen in the figure below.



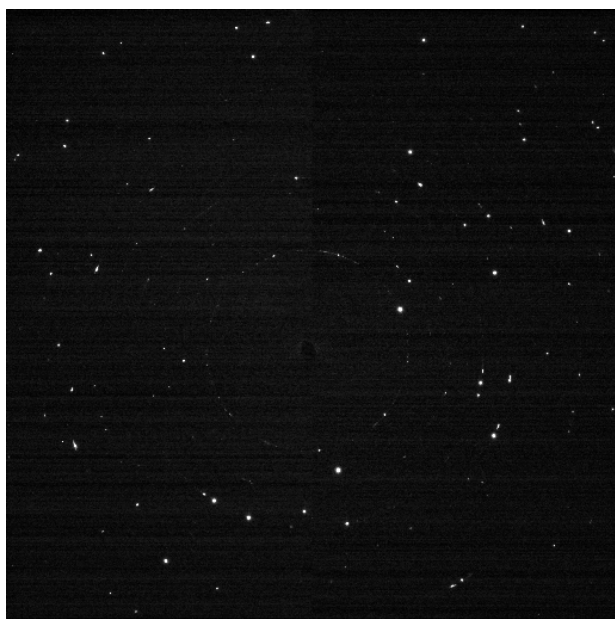
**Evolution of paracetamol (acetaminophen) phases upon heating. [W.I.F. David, Rutherford-Appleton]**

The APS is already able to measure diffraction data suitable for crystallographic analysis as rapidly as 10 data sets per second. When the SNS begins full operation, it will likewise advance neutron data collection times from hours to minutes. At present, it is quite

difficult to fit equations of state to the sets of derived structural parameters, which requires using the covariance results as a weight matrix. In rare cases, there may be advantages to building a structural model that directly incorporates an equation of state.

**Area detector data** utilization has revolutionized both single-crystal and powder diffraction. In the case of powder diffraction, sensitivity is dramatically improved, while susceptibility to preferred orientation and graininess (poor crystallite counting statistics) are largely removed. At present, in a painful manual process, these data are reduced by radial averaging prior to use in a conventional Rietveld program. However, if fitting is performed directly to the raw data, geometric corrections can be made part of the fitting procedure. Texture information can also be directly extracted. Application of external stress to a sample distorts the Bragg rings into ellipses. Data reduction for area-detector data is currently time consuming, and contemporary software has not been designed to take the best advantage of the information content in the images. This is particularly true in the area of mechanical characterization of materials by diffraction.

Area detectors, combined with microfocus x-ray optics, have made possible a new class of measurements, where diffraction spots from the individual crystallites comprising a small volume in a polycrystalline material are individually indexed and integrated. Samples with tens to perhaps hundreds of crystallites can be handled at present. However, this new approach to data collection suggests new approaches to software, which would couple the process of image analysis with data fitting.



**A diffraction image of a novel perovskite, with reflections present from ~15 crystals. Combined with images at many sample settings, it is possible to determine orientation matrices for each crystal. [J. Wright, *et al.*, ESRF]**

**Universal input file** handling is frequently sought by scientists. For a number of reasons, diffraction data are recorded in a variety of different file formats. One of the most

commonly posted questions on the Rietveld mailing list is “how do I get data from instrument  $X$  into computer program  $Y$ . Top scientists, who frequently design experiments that can only be performed on specifically optimized instruments at facilities around the world frequently complain about the time spent figuring out how to get information into the software tool of choice. Effort put into easing the handling of data will be repaid in greater productivity.

**Symbolic processing** or “computer algebra,” as implemented in Topas, allows abstraction of the computational structure of the software to be written in a high-level algebra-like manner. These equations can then be *modified by users* to perform computations that were never anticipated by the software developers. As an example, Peter Stephens showed how he modified the peak-shape equation in Topas to account for sample effects in a way that had never been planned by the software designer. While most users will not need the ability to customize computations, this ability is what allows cutting-edge science to be done. In the past, this capability was only available to people with the skills to do sophisticated programming, but, with much greater computing power, customization can be done either by parsing of equations written in symbolic form or by writing the upper level code in a scripting language.

**Combined fitting to nondiffraction measurements** would allow other physical information to be used for problems where crystallographic information is on its own inadequate. For many complex materials, where ordering is not long range, for example catalysts and nanostructured materials, the number of diffraction observations is not adequate to develop unique structural models or models with sufficient precision to differentiate research questions. Other measurements, such as XAFS, NMR, Raman, etc., probe structure. A plausible structural model should be consistent with all available data, but our ability to actually fit a model to multiple types of data is limited by availability of software.

## Why a Fresh Start?

The GSAS software was written with the most modern tools and the most modern programming concepts that were available when the project was first started, but this code is now very dated. The extensive use of named Fortran COMMON blocks within “include files” then facilitated efficient implementation of data structures within the programs, but also nearly prohibits the reuse of code. In fact, some algorithms are implemented more than once in GSAS, to be used with differing sets of COMMON block structures.

The original user interface in GSAS (EXPEDT) was designed for slow terminals with limited display capabilities. The philosophy employed in its design was to “ask a question only once and only ask questions the user can answer.” The resulting menu/tree structure with one letter commands and on-demand help listings, lead the state of the art when new but now is now clearly dated. However, it does contain the elements of structural design for a modern graphical user interface.

The heart of GSAS, the “Experiment File” where the project and all experimental and fitted parameters are stored is still an important key concept that is still not fully appreciated. However, the internal structure used in the GSAS experiment file is not as expandable and adaptable as would be desired for a package that will extend structure modeling to new length scales and utilize other types of data.

The coding of GSAS employed a rudimentary version of the now widely used principles of object oriented programming, where each parameter has its own suite of input-output and data-processing routines. However, the monolithic structure of GSAS, where one large program simulates all types of data, computes restraints and constraints, does fitting, etc., limits extension of the code. To develop new functionality, a scientist programmer must understand how much of the code operates. This will certainly inhibit development of simulation codes for other techniques. How many NMR or XAFS experts know enough diffraction and crystallography to wade through a complex program such as GSAS?

While one might think that most coding effort goes into the algorithms that implement the models and their fitting, in fact nearly half of the GSAS code (~200,000 lines) provides users with the ability to enter information into the experiment file (program EXPEDT). The EXPGUI program replaces a subset of the functionality of EXPEDT with a graphical user interface, but neither approach provides the data validation tools and user friendliness that modern computer users have grown to expect from software. The process of how users will interact with these programs should be thought through from the simultaneous paradigms of novice-friendly and expert-efficient.

## Goals for a New Software Package

The goal for a new generation of crystallographic software should be nothing short of the grand challenge to fit any type of model to all the relevant data and theory. The framework should be extensible, so that new concepts in simulation and new types of experiments can be incorporated. There is no reason to differentiate tools for fitting macromolecular structures from those for small-molecule or extended frameworks, nor is spectroscopic investigation of structure fundamentally different from that using diffraction. This is science at the highest level: the quantitative simulation of scientific observations based on physical models. It is vital for reaping the full benefits of our scientific user facilities.

Work in this software should begin with creation of a data structure that will eventually allow development of flexible descriptions of structural models on several length scales, so that eventually the software can be deployed for crystallographic, PDF, and small-angle scattering fitting as well as theory. The parameter descriptions should be appropriate for all types of crystallographic computations, from simple lattice compounds, through small-molecule structures up to the most complex macromolecular structures, so that all types of projects can be tackled with all types of data.

Parameters should include defect descriptions, so that Hendrick-Teller computations can be used for “stacking fault” modeling. The models should also anticipate the needs to

model NMR, XAFS, inelastic scattering and other spectroscopic simulations, so that this type of fitting can be done. Likewise, descriptions are needed for empirical parameters that are used for data fitting, as well as experimental conditions. Where possible, these descriptions should follow the nomenclature developed in the IUCr's CIF dictionaries so that results are directly and electronically communicable to the crystallographic community. Where these descriptions cannot follow CIF, this likely indicates inadequacies of CIF. This should be addressed with the CIF maintainers.

Just as GSAS has always allowed users to input the commonly used space group's Hermann-Mauguin symbols rather than having to look up and type in the symmetry operations generated by these space groups, as is required even to this day in many contemporary programs, GSAS-II should implement many other types of derivable relationships, such as subgroup-supergroups. Every user supplied input should be considered for potential validation and should be documented such as may be needed for comprehension by someone with fairly minimal crystallographic training. These concepts should be implemented in a novice-friendly manner that still allows expert users to navigate quickly and easily.

Different minimization implementations should be available:

- Traditional least-squares provides uncertainty analysis and provides the minimum uncertainties where the data are free from systematic error
- Robust and resistant minimization limits the leverage of systematic errors that affect only a small number of observations
- Modern minimization algorithms such as BFGS provide more rapid and stable convergence than least-squares
- Monte-Carlo approaches are useful for identification of likely models (structure solution). When implemented with a full Markov chain, this provides good evidence that the identified model(s) are the unique solutions, at least within the parameterization utilized.

Fitting routines should optimize against powder-diffraction data sets, reflection lists (as obtained in single-crystal measurements), or "peak" lists, where observations are integrated intensities that may include multiple overlapped reflections, as obtained from either CW-Laue diffraction or Pawley- or LeBail-extracted powder data. Other data types should be considered, for example to model texture or externally applied strain from area detector data. For structure solution from powder diffraction, it may fit against peak lists for speed when testing and optimizing large numbers of models, but, after a model is identified for serious consideration, the fit is made against the powder diffractogram.

Data-simulation modules should be written as independent programs that compute expected values for physical measurements and, where convenient, their derivatives with respect to the model parameters. Numerical derivatives should also be implemented for algorithms that do not lend themselves to analytic derivative computation. These modules should be provided as independent programs that read the experimental and model description information and then provide results that can be included in the design matrix and least-squares vector. This allows inclusion of new approaches to modeling and utilization of new types of experimental data without having to modify existing

programs. Diffraction simulation modules should feed information to convolution modules that convert structure factor values into powder-diffraction traces.

Likewise restraints are written in the same fashion. These compute internal agreements of the model to user-supplied information and perhaps directly to likelihood estimates made from crystallographic database or theory computations.

The data simulation and minimization routines should be linked together with a scripting language, so that customization does not require source-code changes to either the simulation or minimization routines, further allowing experts to introduce new concepts to their analysis.

Constraint modules should be written to implement crystallographic and non-crystallographic symmetry through matrix reduction. Alternate constrain formulations should implement user-supplied equations as implemented by Finger and Prince.

## Interaction with the DANSE Project

The DANSE project (<http://wiki.cacr.caltech.edu/danse/>) has been funded by the NSF to package, improve and develop software for neutron scattering, as well as to develop infrastructure. The project had an initial scope to cover several of the goals listed here, at least with respect to neutron powder diffraction, however the project was not fully funded and the scope was reduced. Two of the five DANSE science subproject leaders (Simon Billinge and Ersan Üstündag, for structural diffraction and engineering diffraction, respectively) attended the GSAS-II workshop and expressed strong support for a GSAS-II package. It would fit in well with the goals of each subproject and would strengthen the project outcome. There are considerable areas for collaborative development, which would need further discussion.

## Recommendations

Software development is a long-range project. Developing a software project to the point where it can be used for analysis on real projects takes years. Once it is deployed, it must be supported: bugs need to be addressed promptly; users need to be taught how to use the software; new features need to be added; documentation must be revised; changes in computing platforms must be accommodated. Once maintenance and upgrades end, the software will soon be obsolete. The extensive expectations for modern software require a team approach, where scientists, numerical analysts and programmers work together. The commercial developers of software will follow the needs for scientific analysis using techniques that have been demonstrated to have value but will not explore the uncharted territories of cutting-edge research since the market place has not yet been established.

Since the development of cutting-edge software for research purposes will require groups of diverse specialists to work for several times longer than the duration of the average grant, the only place where this type of development can be performed is in a national laboratory. This type of scientific development is not nurtured in academia. Further, since the motivation for much of the development arises from interaction with state-of-the-art

theoretical and experimental projects, the scientists leading this work must be directly involved with the research projects that require the new analyses, so these individuals should also be involved in experimental projects, preferably in a scientific user facility. It is difficult to recruit successful scientists to work full time on software projects; those scientists who work only in software, soon lose contact with the latest experimental techniques. The GSAS-II project should be considered as a long-range effort, with an integrated goal of bringing new generations of crystallographer/software-development leaders into the field.

If the GSAS-II project is not begun, then future software development efforts in this area will be led exclusively by researchers overseas, since no other domestic groups educated and experienced with broad-scale crystallographic computation are active. Abdication of this effort to the international community will put American scientists at a disadvantage, since their access to education from the developers and their ability to influence development directions will be compromised.



### **GSAS-II Workshop organizers**

Simon Billinge, Michigan State University  
 Juan Rodriguez-Carvajal, Institute Laue-Langevin (unable to attend workshop due to a scheduling conflict)  
 James Richardson, Intense Pulsed Neutron Source, Argonne  
 Brian Toby, Advanced Photon Source, Argonne  
 Robert Von Dreele, Intense Pulsed Neutron Source and Advanced Photon Source, Argonne

### **Other Participants**

Alan Coelho\*, Coelho Software, Australia  
 Jon Wright\*, ESRF, France  
 Ralf Grosse-Kunstleve\*, Lawrence Berkeley National Laboratory  
 Vincent Favre-Nicolin\*, Université Joseph Fourier & CEA, France  
 William I. F. David\*, Rutherford-Appleton, United Kingdom  
 Ray Teller, IPNS  
 Angus Wilkinson, Georgia Tech  
 Jason Hodges, SNS  
 Ashfia Huq, SNS  
 James Kaduk, INEOS  
 Ken Evans\*, APS  
 Pete Jemian, APS  
 Peter Stephens, Stony Brook University  
 Ersan Üstündag, Iowa State University and Ames National Laboratory  
 Thomas Proffen, Los Alamos National Laboratory  
 Wenduo Zhou, Michigan State University  
 Thomas Worlton, IPNS  
 Emil Bozin, Michigan State University  
 Pavol Juhas, Michigan State University  
 Thomas Degen, PANalytical, Netherlands  
 Cevdet Noyan, Columbia University  
 William Bisson, Collaborative Computational Project No. 14 in Powder and Small Molecule Single Crystal Diffraction (CCP14), United Kingdom  
 Jeremy Cockcroft, CCP14 and University College, United Kingdom  
 Sytle Antao, APS  
 Ryoji Kiyonagi, IPNS  
 Jennifer Doebbler, APS  
 John Mitchell, Materials Science Division, Argonne

\* invited speakers

**Luc J. Bourhis<sup>a</sup>, Ralf W. Grosse-Kunstleve<sup>b</sup>, Paul D. Adams<sup>b</sup>**

*a) University of Durham, Durham, DH1 3HP, UK and b) Lawrence Berkeley National Laboratory, Berkeley, CA 94720, USA. E-mail: [rwgk@cci.lbl.gov](mailto:rwgk@cci.lbl.gov) and [luc\\_j\\_bourhis@mac.com](mailto:luc_j_bourhis@mac.com) ; WWW: <http://cctbx.sourceforge.net/>, <http://www.phenix-online.org/>, <http://cci.lbl.gov/>*

### Abstract

We describe recent developments of the Computational Crystallography Toolbox.

### Preamble

In order to interactively run the examples scripts shown below, the reader is highly encouraged to visit [http://cci.lbl.gov/cctbx\\_build/](http://cci.lbl.gov/cctbx_build/) and to download one of the completely self-contained, self-extracting binary cctbx distributions (supported platforms include Linux, Mac OS X, Windows, IRIX, and Tru64 Unix). All example scripts shown below were tested with cctbx build 2007\_10\_29\_2045.

In the following we refer to our articles in the previous editions of this newsletter as "Newsletter No. 1", "Newsletter No. 2", etc. to improve readability. The full citations are included in the reference section.

### Introduction

The *Computational Crystallography Toolbox* (cctbx, <http://cctbx.sourceforge.net/>) is the open-source component of a structure determination suite for macro-molecular crystallography (Phenix, <http://www.phenix-online.org/>). However, the cctbx was started with a code base developed in the context of small-molecule crystallography, most notably SgInfo (<http://cci.lbl.gov/sginfo/>). Although in recent years most new developments were targeted towards macro-molecular work, the small-molecule heritage has been carefully maintained in the core modules of the cctbx project. For example, all algorithms in the `cctbx` module (for the distinction between the *cctbx module* and the *cctbx project* see Newsletter No. 1) work for all 230 crystallographic space groups and are routinely tested with symmetries not found in macro-molecular crystals.

Recently, we have started a new `smtbx` module with algorithms specifically for small-molecule work. This is very much work in progress, but below we present some related developments. We give an example of least-squares minimization with a target function and a weighting scheme commonly used in the refinement of small molecules. Another development that grew out of small-molecule context is the handling of special position constraints. We also highlight important new developments of the *Phil* system introduced in Newsletters No. 5 and No. 7. Finally, we give a brief summary of the transition of the cctbx source code repository from CVS to Subversion (SVN).

# Refinement tools for small-molecule crystallographers

## Refinement against $F^2$

Small-molecule crystallographers almost exclusively rely on the minimization of a least-square target to refine a structure. The cctbx has provided one for a long time but only for  $F$ . Since  $F^2$  refinement is very popular among small-molecule crystallographers, a new target has recently been added to the cctbx. The class `cctbx.xray.unified_least_squares_residual` provides a single entry point to both  $F$  and  $F^2$  refinement.

To keep the example self-contained, and also to demonstrate some tools useful to develop and debug crystallographic algorithms, instead of starting from real data, we will use randomly generated crystal structures. Atoms are randomly spread in the unit cell and the structure factors are then computed:

```
from cctbx.array_family import flex
from cctbx import xray
from cctbx import crystal
from cctbx import miller
from cctbx.development import random_structure
import random

indices = miller.build_set(
    crystal_symmetry=crystal.symmetry(unit_cell=(10,11,12, 90,105,90),
                                         space_group_symbol="P21/c"),
    anomalous_flag=False,
    d_min=0.8)
structure = random_structure.xray_structure(
    indices.space_group_info(),
    elements=['C']*6 + ['O']*2 + ['N'],
    volume_per_atom=18.6,
    random_u_iso=True)
f_ideal = structure.structure_factors(d_min=indices.d_min()).f_calc()
```

Then we extract the amplitudes or intensities and we put them on a different scale to make the example a bit more realistic:

```
f_obs = f_ideal.amplitudes()
f_obs.set_observation_type_xray_amplitude()
f_obs *= 2
f_obs_square = f_ideal.norm()
f_obs_square.set_observation_type_xray_intensity()
f_obs_square *= 3
```

In practice we would get `f_obs` or `f_obs_square` from a data file using the `iotbx` and the observation type would have been automatically set up for us.

Then we can construct the least-square targets and examine them:

```
ls_against_f = xray.unified_least_squares_residual(f_obs)
ls_against_f_square = xray.unified_least_squares_residual(f_obs_square)

residuals = ls_against_f(f_ideal, compute_derivatives=True)
print "against F: value=%.3f, scale=%.3f" % (residuals.target(),
                                             residuals.scale_factor())
residuals = ls_against_f_square(f_ideal, compute_derivatives=True)
print "against F^2: value=%.3f, scale=%.3f" % (residuals.target(),
                                              residuals.scale_factor())
```

The constructor of the class automatically recognizes whether the data passed to it are amplitudes or intensities and it adapts the computations accordingly, correctly getting a target value of 0 and a scale factor of 2 and 3, respectively, as expected in this trivial example.

By passing `compute_derivatives=True`, we require the computation of the derivatives of the L.S. target function with respect to  $F_{\text{calc}}(h)$  for each Miller index  $h$ . They are available as `residuals.derivatives()`. Derivatives now brings us to discuss refinement.

To demonstrate refinement, we will first add a perturbation to the crystal structure as well as allowing the refinement of atom sites:

```
perturbed_structure = structure.random_shift_sites(max_shift_cart=0.2)
for s in perturbed_structure.scatterers():
    s.flags.set_grad_site(True)
```

The simplest refinement engine in the cctbx is `cctbx.xray.minimization.lbfgs`. For a refinement against  $F^2$ :

```
refining_structure = perturbed_structure.deep_copy_scatterers()
optimiser = xray.lbfgs(
    target_functor=ls_against_f_square,
    xray_structure=refining_structure,
    structure_factor_algorithm="direct")
print "Initial L.S. residual:%.3f" % optimiser.first_target_value
structure.show_scatterers()
print "Final L.S. residual:%.3f" % optimiser.final_target_value
refining_structure.show_scatterers()
```

The LBFGS algorithm (Liu & Nocedal, 1989) used to minimize the target function needs to compute its partial derivatives with respects to the refined parameters (atomic position here). This is where the derivatives which we showed to be obtainable by `residuals.derivatives()` above come into play: they are combined, by using the chain rule, with the derivatives of  $F_{\text{calc}}(h)$  with respect to the refined parameters.

## Least-squares weights

By default, `xray.unified_least_squares_residual` tries to make sensible choices for the least-squares weights, i.e. unit weights for refinement against  $F$  and the so-called quasi-unit weights for refinement against  $F^2$ , which are  $1/(4 F_{\text{obs}}^2)$ . The latter choice is known to result in a more stable refinement. However, almost universally, experimental error estimates are available, as `f_obs_square.sigmas()`, and the least-square weights should take advantage of them. The pure statistical weights  $1/\sigma^2$  are rarely used in small molecule crystallography. The most popular choice is that of the ShelXL program (<http://shelx.uni-ac.gwdg.de/>),  $1/(\sigma(F_{\text{obs}}^2)^2 + (a P)^2 + b P)$  where  $P = 1/3 \max(0, F_{\text{obs}}^2) + 2/3 F_{\text{calc}}^2$ , which down-weights the stronger reflection while reducing statistical bias by the use of  $P$  (Wilson 1976).

This weighting scheme is available in the module `cctbx.xray.weighting_schemes`:

```
weighting = xray.weighting_schemes.shelx_weighting()
shelx_weighted_ls_against_f_square = xray.unified_least_squares_residual(
    f_obs_square, weighting=weighting)
```

This least-square target can then be used with the `lbfgs` minimizer. The default is that of ShelXL, i.e.  $a=0.1$  and  $b=0$ , which is best suited for early refinements when the structure is still incomplete. All the other weighting schemes we mentioned are also provided by that module (the reader is invited to read the comments for each Python class).

## Special position constraints

The traditional way to deal with the refinement of crystal structures with atoms on special position is to constrain the latter never to move away from the special position, in effect minimizing the target function under a set of constraints. However, the minimizer introduced above does not work in such a manner and neither does the more sophisticated `mmtbx.refinement.minimization.lbfgs`, mainly because this is less important for macro-molecular models, which usually have very few atoms on special positions. One can safely, at each refinement cycle, let those atoms move away from the special positions and move them back before the next cycle. In contrast, in the small molecule world it is not uncommon that all atoms are on special positions and the ad-hoc treatment is more problematic.

The `cctbx` does actually provide all the tools to find, store and apply special position constraints. We will therefore start by introducing those fundamental tools:

```
crystal_symmetry = crystal.symmetry(
    unit_cell=(10,10,10,90,90,90),
    space_group_symbol="Pm3m")
crystal_symmetry.show_summary()

special_position_settings = crystal_symmetry.special_position_settings(
    min_distance_sym_equiv=0.5)
```

The site symmetry of a position given in fractional coordinates is then obtained by:

```
site_symmetry = special_position_settings.site_symmetry(
    site=(0.3, 0.31, 0.111))
```

The given position is at a Cartesian distance smaller than 0.5 Å from a special position with  $x=y$ . The `site_symmetry` algorithm computes the exact location of the nearest special position (Grosse-Kunstleve and Adams, 2002). The resulting `site_symmetry.exact_site()` is (0.305, 0.305, 0.111).

Then:

```
site_constraints = site_symmetry.site_constraints()
```

gives access to the constraints on the exact site:

```
>>> site_constraints.n_independent_params()
2
>>>
site_constraints.independent_params(all_params=site_symmetry.exact_site())
(0.305, 0.111)
```

The other way around, one can determine all the site coordinates from the independent ones:

```
>>> site_constraints.all_params(independent_params=(0.2, 0.1))
(0.2, 0.2, 0.1)
```

The most interesting facility for refinement is the handling of gradients. To illustrate it, let us introduce a simple function  $f$  of the site coordinates  $x,y,z$  (during a refinement,  $f$  would instead be the L.S. target for example, considering its dependence on the coordinates of one atom only):

```
def f(x,y,z): return -x + 2*y + 3*z
```

which we then restrict onto the special position locus:

```
def g(u,v):
    x, y, z = site_constraints.all_params((u,v))
    return f(x,y,z)
```

We wish to compute the derivatives of  $g$  with respect to  $u$  and  $v$  knowing the derivatives of  $f$  with respect to  $x,y,z$  which are easily read directly from its definition:  $(df/dx, df/dy, df/dz) = (-1,2,3)$ . Those derivatives of  $g$  are then easily obtained with:

```
>>> independent_gradients = site_constraints.independent_gradients(
    all_gradients=flex.double((-1,2,3)))
(1.0, 3.0)
```

We have so far demonstrated only site constraints and only in fractional coordinates, but the `cctbx` provides more facilities:

```
frac_adp_constraints = site_symmetry.adp_constraints()
```

gives access to the constraints on ADPs in fractional coordinates whereas:

```
cart_adp_constraints = site_symmetry.cartesian_adp_constraints(  
    crystal_symmetry.unit_cell())
```

deals with the same constraints on ADPs in Cartesian coordinates.

It should be noted that the `site_symmetry` object caches all the constraints it gives access to: the necessary symmetry computations are performed only once when `site_constraints`, `adp_constraints` or `cartesian_adp_constraints` are called for the first time and the results are reused later on.

The `cctbx` special position constraints we have just expounded are the basis of the refinement engine `lbfgs` in the module `smtbx.refinement.minimization`. It is to be used exactly as `cctbx.xray.minimization.lbfgs`, the only difference being that atoms on special positions have their site coordinates and ADPs constrained properly. Our plan is to develop `smtbx.refinement.minimization.lbfgs` over time into the equivalent of the more sophisticated and versatile `mmtbx.refinement.minimization.lbfgs`.

## Phil developments

Phil (Python-based hierarchical interchange language) is a module for the management of application parameters and, to some degree, inputs. Phil was first introduced in Newsletter No. 5. In Newsletter No. 7 we presented a complete example application which uses Phil for the handling of program parameters.

Overall, Phil has been very stable after an intense development push almost three years ago. Some features were added in response to needs that arose as part of the development of other applications, and a few bugs were fixed. These changes are very conservative. However, recently there has also been an important semantic change affecting "multiple definitions" and "multiple scopes". The new features and changes are reflected in the updated documentation (URL at end of this section) which is based on parts of our original article in Newsletter No. 5. Important new features and changes include:

- The handling of multiple scopes went through a few iterations eliminating bugs, inconsistencies and inefficiencies. The latest implementation (as of October 2007) is considered mature, stable and intuitive.
- The new `.fetch_diff()` method returns only objects with non-default values. This is most useful for applications with a large number of parameters. Usually most parameters are not changed by the user. `.fetch_diff()` pin-points the (few) changes.
- The previous plain `include` syntax was changed to `include file`; the new `include scope` syntax was added. The `include scope` feature builds on Python's standard import mechanism. In practice it is found to be much more useful than the `include file` feature.
- The syntax-aware comment feature now uses `!` as the comment character. For example:

```
!crystal_symmetry {  
    unit_cell = None  
    space_group = None  
}
```

The exclamation mark comments out the entire `crystal_symmetry` scope including all embedded definitions. `#crystal_symmetry` is now a normal one-line comment as expected by most users. Based on feedback, the distinction between

`#crystal_symmetry` (syntax-aware comment) and `# crystal_symmetry` (one-line comment) was found to be too subtle.

- Again based on feedback, the `{` and `}` scope-delineation characters (compare with the `crystal_symmetry` example above) are now interpreted as one-character keywords. In contrast to the initial implementation, any `{` and `}` in strings have to be quoted. This leads to a more obvious syntax. It also enables a scope name and embedded definitions to appear on the same line. This can be convenient in certain situations, in particular for definitions specified on the command-line.
- Similarly, `;` characters are now interpreted as one-character keywords (they had no syntactical meaning in the original implementation). This enables `scope { a=1; b=2 }` all on one line.
- Related to the `{, }` scope-delineation change, the `${varname}` variable substitution syntax was changed to `$(varname)`.

For more details see the updated documentation: [http://cctbx.sourceforge.net/libtbx\\_phil.html](http://cctbx.sourceforge.net/libtbx_phil.html)

## Subversion

For six years, from April 2001, when the SourceForge cctbx project was started, to March 2007, cctbx development was based on the Concurrent Versions System (CVS, <http://www.cvshome.org/>). This era came to an end with the transition to the more modern Subversion system (SVN, <http://subversion.tigris.org/>). In the last two years, the vast majority of the open source community has gone through this transition. SVN introduces many new features, most importantly "atomic commits" which handle a set of changes as one entity, no matter how many files and directories are involved. This makes it much easier to keep track of large-scale changes, and to backtrack if necessary. Almost as important is the option to rename files and directories without introducing breaks in the development history. The need to reorganize arises frequently in the early stages of a (sub-)project. Often it is initially not very clear how all the pieces fit together. The best ideas for organizing the whole tend to crystallize only after a critical subset of the project is already implemented. SVN provides a clear path for reorganizing the sources.

The cctbx sources were converted using the `cvs2svn` script (<http://cvs2svn.tigris.org/>, it is a Python script!) which preserves the complete CVS development history, including all original time stamps, user names, and log messages. The last state of the cctbx CVS repository before the conversion is still available for viewing at SourceForge, but for all practical purposes it is completely obsolete.

The main cctbx page at Sourceforge (<http://cctbx.sourceforge.net/>) includes a link to the web view of the cctbx SVN repository. Instructions for checking out the sources using the `svn` command are posted under the cctbx installation instructions (<http://cctbx.sourceforge.net/current/installation.html>). These instructions show how to get a selection of individual cctbx modules. Note that it is also possible to get the entire cctbx project with a single command (this wasn't possible with CVS), for example:

```
svn co https://cctbx.svn.sourceforge.net/svnroot/cctbx/trunk svnroot_cctbx
```

The name of the target directory (`svnroot_cctbx`) is arbitrary. The advantage of checking out everything under one tree is that a single `svn update` or `svn commit` command works on the entire repository. The disadvantage compared to the more granular approach is that the working copy includes modules that may not be needed and therefore consumes more disk space (currently about 62 MB).

With the move to SVN, the old distinction between *anonymous* and *developer* checkouts disappeared. This is a great advantage. Everybody can checkout working copies using the exact same commands. Credentials, i.e. a user name and password, are required only for write access (e.g. svn commit). It is possible to checkout a working copy before having a SourceForge user name, make local modifications, get a user name and request cctbx svn write access, and then to commit the changes from the initial working copy.

## Acknowledgments

L.J. Bourhis gratefully acknowledge the financial support of EPSRC under grant number EP/C536274/1. R.W. Grosse-Kunstleve and P.D. Adams gratefully acknowledge the financial support of NIH/NIGMS under grant number P01GM063210. Their work was supported in part by the US Department of Energy under Contract No. DE-AC02-05CH11231.

## References

Grosse-Kunstleve, R.W., Adams, P.D. (2002). Acta Cryst. A58, 60-65.

Grosse-Kunstleve, R.W., Adams, P.D. (2003). Newsletter of the IUCr Commission on Crystallographic Computing, 1, 28-38.

Grosse-Kunstleve, R.W., Afonine, P.V., Sauter, N.K., Adams, P.D. (2005). Newsletter of the IUCr Commission on Crystallographic Computing, 5, 69-91.

Grosse-Kunstleve, R.W., Zwart P.H., Afonine, P.V., Ioerger, T.R., Adams, P.D. (2006). Newsletter of the IUCr Commission on Crystallographic Computing, 7, 92-105.

Liu C., Nocedal J. (1989). Mathematical Programming 45, 503-528.

Wilson, A.J.C. (1976). Acta Cryst. A32, 994-996.



---

# Rietveld refinement of structural distortion-mode amplitudes

Branton J. Campbell<sup>a</sup>, John S. O. Evans<sup>b</sup>, Francesca Perselli<sup>b</sup> and Harold T. Stokes<sup>a</sup>

<sup>a</sup>Brigham Young University, Department of Physics & Astronomy, Provo, Utah 84602, USA. <sup>b</sup>The University of Durham, Department of Chemistry, South Road, Durham, DH1 3LE, UK. Email:

[branton\\_campbell@byu.edu](mailto:branton_campbell@byu.edu), [john.evans@durham.ac.uk](mailto:john.evans@durham.ac.uk), [stokesh@byu.edu](mailto:stokesh@byu.edu) ;

WWW ISODISPLACE: <http://stokes.byu.edu/isodisplace.html> ;

WWW TOPAS: [http://www.dur.ac.uk/john.evans/topas\\_academic/topas\\_main.htm](http://www.dur.ac.uk/john.evans/topas_academic/topas_main.htm)

## Abstract

For any crystal structure that can be viewed as a low-symmetry distortion of some higher-symmetry parent structure, one can represent the details of the distorted structure with a list of distortion-mode amplitudes rather than the traditional list of *xyz* atomic coordinates. After importing mode definitions from the ISODISPLACE software, TOPAS Academic can now directly refine structural distortion-mode amplitudes. In this article, we demonstrate that the distortion-mode basis is well-suited to a Rietveld refinement of the room-temperature structure of WO<sub>3</sub>, which has 24 displacive atomic-coordinate degrees of freedom. Only five distortion-mode amplitudes are needed to capture the essential features of this structure.

## 1.0 Introduction

The details of a subtle superstructural distortion are often very difficult to extract from powder-diffraction data. The added structural complexity of the distorted structure is rarely compensated by the extra information in the low-symmetry powder pattern, which may include only limited peak broadening or splitting and a handful of weak superlattice reflections. This is especially true with data from lab instruments. A typical approach to this type of problem involves iterations over four basic steps: (1) use intuition and experience to select a promising distortion model, (2) transform the parent structural description into the new setting, (3) establish a complicated matrix of bond and/or angle constraints that reduce complexity by allowing only specific geometric distortion patterns, and (4) refine the model against the experimental pattern. With a little luck, a reasonable number of iterations will yield one model that is clearly better than the others. This process is almost always very time consuming, though the pain or pleasure derived largely depends on your interests and objectives!

In this article, we demonstrate that identifying and refining a superstructural distortion can be dramatically simplified by new Rietveld-refinement capabilities that take full advantage of group-theoretical distortion-mode analysis. The combined use of ISODISPLACE and TOPAS Academic eliminates the need for manual structure transformations and many structural constraints, while also streamlining the process of exploring and testing candidate models.

## 2.0 The distortion-mode basis

The free energy of any crystalline material can be expanded in terms of the order parameters of the irreducible representations of the parent space-group symmetry.<sup>1</sup> Most real phase transitions that produce distortions are energetically driven by a relatively small number of these order parameters (often just one). This symmetry-motivated basis of order parameters, which we refer to as the *distortion-mode basis*, is the most natural basis for studying structural distortions because it allows the essence of most distortions to be captured by the smallest possible number of refinable parameters. As used here, the term "distortion" could refer to any type of physical order parameter, not just an atomic displacement. In the current context, however, we will primarily be discussing atomic displacements, strains, and site occupancies.

A superstructural distortion breaks some of the symmetries of the parent crystal structure. Those parent symmetries that remain in the distorted structure comprise its *distortion symmetry*<sup>2</sup> or *isotropy subgroup*<sup>3</sup> (we use these two terms interchangeably). Thus, the distortion symmetry of a distorted structure is precisely its space-group symmetry, which can be identified by its combination of space-group type, supercell basis and supercell origin. Because the space-group symmetry of a specific structure includes both the symmetry elements of the space-group type *and* their actual locations within that structure, both the basis and the origin of the supercell are essential information.

Every superstructural distortion is associated with a *k*-point (or set of *k*-points) in the Brillouin zone, which is also the location where superlattice reflections will appear in the corresponding diffraction pattern. For a given *k*-point, the parent space group has a finite number of *irreducible representations* (irreps), each of which maps its symmetry elements onto an irreducible group of matrices. The dimension of an irrep refers to the dimension of its matrices. The group theory of irreps and irrep matrices is addressed in detail by Bradley and Cracknell,<sup>4</sup> though one does not need to be acquainted with irrep theory to follow the concepts presented here. Loosely speaking, each irrep corresponds to a specific set of parent symmetries that can be broken, which in turn determines which subgroups of parent symmetries might be preserved. A physical distortion that breaks only the symmetries associated with a specific irrep is said to be an *order parameter* of that irrep.

An order parameter of a multidimensional irrep can belong to any one of several different *order parameter directions* (OPDs) in representation space, each of which breaks only a special subset of the symmetries that the irrep is able to break. The general OPD of an irrep (also called the *kernel*) breaks as much symmetry as possible. The special OPDs, on the other hand, break less symmetry than the kernel, and result in distortion symmetries that are both subgroups of the parent symmetry and supergroups of the kernel symmetry. For a given *k*-point and irrep, each available OPD leads to a different distortion symmetry. If (a,b,c,d) is the *general* OPD of some four-dimensional irrep, then (a,-a,b,b) would be called a *special* OPD of that irrep. The OPDs of an irrep are somewhat analogous to the Wyckoff sites of a space group – just as an atom at the special (x,0,½) Wyckoff position has fewer degrees of freedom than an atom at the general (x,y,z) position, a physical order parameter that lies along the special (a,-a,b,b) OPD will have fewer structural degrees of freedom than an order parameter that lies along the general (a,b,c,d) OPD. We refer to an OPD's variable parameters as *branches*, and refer to an order parameter's structural degrees of freedom as *distortion modes*. Thus, any order parameter with direction (a,-a,b,b) will have two distortion modes: an "a" branch mode and a "b" branch mode.

While irreps and OPDs are purely mathematical abstractions, their order parameters have real physical meaning. A specific distortion symmetry may accommodate many different types of physical order parameters (e.g. strains, displacements, occupancies, etc.), and many distinct order parameters of the same type. Each order parameter will have as many modes as there are branches of the OPD. Each mode is associated with one degree of freedom that has zero *amplitude* in the undistorted parent structure. Though crystal strain modes (i.e. unit cell parameter changes) are macroscopic, an occupancy mode or a displacive mode is microscopic in nature, and must be associated with a unique atom of the parent structure. Thus, a single microscopic mode may affect many supercell atoms, but only one unique parent atom. For a displacive distortion, there will be as many displacive modes as there are variable atomic-coordinate parameters, all of which will be linearly independent, so that any superstructure that can be described with atomic coordinates can be equally-well described with distortion-mode amplitudes. Atomic coordinates and displacive distortion-modes comprise two equivalent bases of the vector space of all displacive distortions, and are related by a linear transformation.<sup>5</sup>

The traditional atomic-coordinate description of a given superstructure is entirely independent of any other structure that it may be related to. The distortion-mode description, on the other hand, is a decomposition of the superstructure into the distortion modes of a higher-symmetry parent structure. In this sense, the two bases are quite different, and provide complimentary views of a structure. The distortion-mode basis is considerably more convenient for some applications. In the examples that follow, we will demonstrate that the distortion-mode basis is the most natural basis for exploring phase transitions and refining structural distortions.

### 3.0 The WO<sub>3</sub> phase diagram

The structure of WO<sub>3</sub>, at first glance, is remarkably simple, consisting of a three-dimensional network of corner-sharing WO<sub>6/2</sub> octahedra with a ReO<sub>3</sub>-like connectivity. In reality, WO<sub>3</sub> has a very complicated structural phase diagram<sup>6-10</sup> and undergoes at least 6 transitions upon cooling from 1000°C. These transitions involve off-centre distortions of W within the WO<sub>6/2</sub> octahedra, as commonly observed for d<sup>0</sup> transition metal ions, and coupled tilting of the WO<sub>6/2</sub> octahedra, as commonly observed in perovskite-related structures. Howard *et al.*<sup>6</sup> provide a good review the seven known polymorphs of WO<sub>3</sub> (see Table 1). These structures can each be described as distortions of a hypothetical cubic ( $Pm\bar{3}m$ ) parent phase that places W at a(0,0,0) and O at d(½,0,0). The irreps of  $Pm\bar{3}m$  that are relevant to the WO<sub>3</sub> phase diagram are located at the  $\Gamma$ [0,0,0], X[½,0,0], M[½,½,0] and R[½,½,½] points. In describing the order parameters of these irreps, we will refer to the *a*, *b* and *c* axes of the cubic parent structure as **d**<sub>1</sub>, **d**<sub>2</sub> and **d**<sub>3</sub>, respectively.

**Table 1:** Summary of the ambient pressure WO<sub>3</sub> phase diagram. For each phase, we include the temperature range, space-group, supercell shape relative to cubic parent, literature references, Glazer tilt-pattern symbol,<sup>11,12</sup> number *p* of refinable atomic-coordinate parameters, number *n* of distortion-modes with relatively-large amplitudes, and selected irreps/OPDs of the cubic parent symmetry that are relevant to the distortion. Because the  $M_3^-$ ,  $R_4^+$ ,  $X_5^-$  and  $M_3^+$  irreps are consistently important across the phase diagram, they are listed wherever they are capable of coupling to a distortion, even when they have no clearly-active (i.e. large-amplitude) modes. Irreps that are not essential to the distortion symmetry are separated from the others by a semicolon, and order-parameter branches giving rise to clearly-active modes are indicated with a bold-face font.

Temp. (°C)	S.G.	Supercell	Refs.	Tilts	<i>p</i> ( <i>n</i> )	Important irreps and order parameter directions
above 900	$P4/nmm$	$\sqrt{2} \times \sqrt{2} \times 1$	<sup>6</sup>	$a^0 a^0 c^0$	2(1)	$M_3^-(\mathbf{a},0,0)$
790 to 900	$P4/nnc$	$\sqrt{2} \times \sqrt{2} \times 2$	<sup>6,7</sup>	$a^0 a^0 c^-$	3(2)	$M_3^-(\mathbf{a},0,0) \oplus R_4^+(\mathbf{a},0,0)$
760 to 790	$P2_1/c$	$\sqrt{2} \times \sqrt{2} \times 2$	<sup>6</sup>	$\bar{a}^- \bar{a}^- c^-$	12(3)	$M_3^-(\mathbf{a},0,0) \oplus R_4^+(\mathbf{a},\mathbf{b},\mathbf{b}); X_5^-(0,0,\mathbf{a},0,0,0)$
400 to 760	$Pbcn$	$2 \times 2 \times 2$	<sup>6,7</sup>	$a^0 b^+ c^-$	12(4)	$M_3^-(\mathbf{a},\mathbf{b},0) \oplus R_4^+(\mathbf{a},0,0) \oplus X_5^-(0,0,0,0,\mathbf{a},-\mathbf{a}); M_3^+(0,0,\mathbf{a})$
17 to 400	$P2_1/n$	$2 \times 2 \times 2$	<sup>6,7</sup>	$\bar{a}^- b^+ c^-$	24(5)	$M_3^-(\mathbf{a},\mathbf{b},0) \oplus R_4^+(\mathbf{a},\mathbf{b},0) \oplus X_5^-(0,0,\mathbf{a},\mathbf{a},\mathbf{b},-\mathbf{b}); M_3^+(0,0,\mathbf{a})$
-40 to 17	$P\bar{1}$	$2 \times 2 \times 2$	<sup>8,9</sup>	$\bar{a}^- \bar{b}^- c^-$	48(6)	$M_3^-(\mathbf{a},\mathbf{b},0) \oplus R_4^+(\mathbf{a},\mathbf{b},\mathbf{c}) \oplus X_5^-(0,0,\mathbf{a},\mathbf{b},\mathbf{c},-\mathbf{d}); M_3^+(0,0,\mathbf{a})$
below -40	$Pc$	$\sqrt{2} \times \sqrt{2} \times 2$	<sup>8,10</sup>	$\bar{a}^- \bar{b}^- c^-$	24(6)	$M_3^-(\mathbf{a},0,0) \oplus R_4^+(\mathbf{a},\mathbf{b},\mathbf{b}) \oplus \Gamma_4^-(\mathbf{a},\mathbf{a},\mathbf{b}); X_5^-(0,0,\mathbf{a},0,0,0)$

The most important distortion modes induced by  $R_4^+$ ,  $M_3^+$  or  $\Gamma_4^-$  all involve oxygen displacements, whereas those induced by  $M_3^-$  or  $X_5^-$  involve tungsten displacements. These irreps also induce other less important (i.e. small-amplitude) modes that are not discussed in detail. Note that the  $R_4^+$  octahedral-tilt modes produce anti-phase tilt arrangements, meaning that adjacent octahedra along the tilt axis rotate out of phase, whereas the  $M_3^+$  octahedral-tilt modes produce in-phase tilt arrangements.

An  $M_3^-$  pattern of tungsten displacements directed parallel to the tetragonal axis (**d**<sub>3</sub>) is initially present at high temperatures, and corresponds to the off-center shift expected for a d<sup>0</sup> cation like W<sup>6+</sup>. These are followed by the emergence of an  $R_4^+$  tilt (i.e. rotation) of the WO<sub>6/2</sub> octahedra around the tetragonal (**d**<sub>3</sub>) axis below 900°C. These two features persist in all of the lower-symmetry distortions. Below 790°C, a monoclinic distortion with unique axis parallel to **d**<sub>1</sub>+**d**<sub>2</sub> emerges, which involves a low-amplitude  $X_5^-$  mode of tungsten-displacements along the same direction, and a second  $R_4^+$  octahedral tilt around **d**<sub>1</sub>-**d**<sub>2</sub>. Below 760°C, the  $R_4^+$  octahedral tilt around **d**<sub>1</sub>-**d**<sub>2</sub> disappears, giving rise to an orthorhombic structure that includes  $X_5^-$  tungsten displacements along **d**<sub>2</sub> and an  $M_3^+$  octahedral tilt around this same axis. Below 400°C, a second  $R_4^+$  octahedral tilt appears, but around **d**<sub>1</sub> this time, giving rise to a different monoclinic structure (same space group as above, but different lattice orientation) with special axis

parallel to  $\mathbf{d}_2$ . A third  $R_4^+$  octahedral tilt then develops around  $\mathbf{d}_2$  below 17°C to form a triclinic structure. Below -40°C, yet another monoclinic phase emerges, with lattice orientation and displacive modes very similar to those of the 760-790°C phase, except for the new appearance of ferroelectric  $\Gamma_4^-$  oxygen displacements parallel to  $\mathbf{d}_3$ .

The group-subgroup relationships that exist among the distortion symmetries in Table 1 are as follows.

$$Pm\bar{3}m \rightarrow P4/nmm \rightarrow P4/nnc \rightarrow Pbcn \rightarrow P2_1/n \rightarrow P\bar{1}$$

$$\searrow P2_1/c \rightarrow Pc$$

For any pair of structures that have a group-subgroup symmetry relationship, it is possible to decompose the lower-symmetry structure into distortion-modes of the higher-symmetry structure. For two adjacent phases in the diagram, such a decomposition can reveal the primary and secondary order parameters responsible for the phase transition that separates them. In Table 1, we instead prefer to decompose all of the low-symmetry structures into the modes of the hypothetical high-temperature cubic structure, which is not actually observed in nature. We do this because we can, and because it provides a more meaningful picture of the entire phase diagram. The cubic structure proves to be a natural reference point for each of the low-symmetry phases.

In summary, the relatively small number of large-amplitude distortion modes for each phase emphasizes the importance of the distortion-mode basis. Especially for the lowest-symmetry phases, the number of large distortion-mode amplitudes is far smaller than the total number. We find it interesting that most of the active order parameter branches in Table 1 give rise to only one large-amplitude distortion mode.

## 4.0 Distortion-mode analysis of the $P2_1/n$ phase of $WO_3$

### 4.1 Mode decomposition

$WO_3$  has a monoclinic phase that exists between 17°C and 400°C. The structural parameters of this phase at room temperature are listed in Table 2. We will use the ISODISPLACE software tool<sup>2</sup> here to transform the  $P2_1/n$  structure of  $WO_3$  onto the distortion-mode basis in order to visualize and quantify the displacive modes that give rise to this distortion. ISODISPLACE provides a variety of intuitive methods for exploring distortion symmetries and distortion modes. We invite the reader to treat this section as a tutorial by accessing the ISODISPLACE website and following along.

To enter the cubic parent structure, follow the "Enter structure manually" link on the main page, and then type the space group ( $Pm\bar{3}m$ ), lattice parameter ( $a = 3.81 \text{ \AA}$ ) and atom coordinates,  $W(0,0,0)$  and  $O(\frac{1}{2},0,0)$ , into the web forms provided. The "View Structure" button on the next page will open a Java applet window that allows you to interactively view the parent structure that you have created. If the structure looks good, close the applet window and use the "Make CIF file" button to save the structure to a file named `wo3_cubic.cif`. Then go back to the ISODISPLACE home page and repeat the structure-entry process for the monoclinic  $P2_1/n$  structure in Table 2, following the same procedure as before except that you need to choose "Monoclinic cell choice 2" in the section called "Space group preferences". After visually checking the structure in the viewer applet, save it to a file called `wo3_300k.cif`. Alternatively, you can download the monoclinic structure from ISODISPLACE website via the following link: [http://stokes.byu.edu/wo3\\_300k.cif](http://stokes.byu.edu/wo3_300k.cif).

**Table 2:** The  $P2_1/n$  structure of  $WO_3$  at room temperature from Woodward et al.<sup>8</sup>:  $a = 7.30084(7)$ ,  $b = 7.53889(7)$ ,  $c = 7.68962(8)$ ,  $\alpha = 90$ ,  $\beta = 90.892(1)$ ,  $\gamma = 90$ .

W1	0.2513(6)	0.0277(7)	0.2865(5)	O3	0.2821(4)	0.2602(7)	0.2870(4)
W2	0.2481(6)	0.0342(6)	0.7815(5)	O4	0.2107(4)	0.2602(8)	0.7310(4)
O1	0.0008(6)	0.0366(8)	0.2116(5)	O5	0.2859(6)	0.0390(6)	0.0065(5)
O2	0.9973(6)	0.4632(8)	0.2164(5)	O6	0.2849(6)	0.4850(5)	0.9922(4)

ISODISPLACE provides four methods of generating distortions. We will start with the mode-decomposition tool (Method 4), which assumes that you already have .cif files containing the parent and distorted structures, and are ready to perform an automatic distortion-mode analysis. Go back to the main page, select "Upload parent structure from a CIF file", browse to your cubic parent structure (wo3\_cubic.cif file) and upload it. Choose the "Monoclinic cell choice 2" option, a setting that will still be in effect later when you need it. This brings you to the "search" page (Figure 1). Scroll down to "Method 4" and upload your distorted structure file (wo3\_300k.cif).

Because the distorted structure has a  $2 \times 2 \times 2$  supercell relative to the parent cell, enter  $((2,0,0), (0,2,0), (0,0,2))$  as the relative supercell basis. This transformation matrix is defined according to  $\bar{a}_i^s = \sum b_{ij} \bar{a}_j^p$ , where  $\bar{a}^p$  and  $\bar{a}^s$  are the absolute parent and supercell bases. When the decomposition calculation is finished, which may take a few seconds, the "distortion" page (Figure 2a) should open in a new window, which contains a summary of the parent structure at the top, followed by a description of the distortion symmetry. The basis, which you entered manually, and the space group type, which comes from the structure file, should be as expected. The supercell origin turns out to be at  $(\frac{1}{2}, 0, \frac{1}{2})$  in parent-cell coordinates. The size of the primitive unit cell (relative to that of the cubic parent) is indicated as "s=8". The index of the isotropy subgroup is indicated as "i=96", which means that parent structure has 96

## ISODISPLACE: search

Space Group: 221 Pm-3m Oh-1, Lattice parameters: a=3.81000, b=3.81000, c=3.81000, alpha=90.00000, beta=90.00000, gamma=90.00000  
 Space-group preferences: monoclinic axes a(b)c, monoclinic cell choice 2, orthorhombic axes abc, origin choice 2, hexagonal axes  
 W 1a (0,0,0), O 3d (1/2,0,0)  
 Nearest neighbor distances: W-W= 3.81000, W-O= 1.90500, O-O= 2.69408

[\(help\)](#)

[\(help\)](#) Atomic radius (Angstroms):  Maximum bond length (Angstroms):  Applet width (pixels):

### Method 1: Search over all special $k$ points

Crystal system(s): triclinic  monoclinic  orthorhombic  tetragonal  trigonal  hexagonal  cubic   
 Space-group symmetry:  Conventional lattice:  Primitive lattice:  Maximal

### Method 2: General method

Specify  $k$  point:  a= b= c= incommensurate:  [\(help\)](#)

Specify number of IRs if coupled IRs are needed: [\(help\)](#)

### Method 3: Search over arbitrary $k$ points for specified space-group and basis

Space-group:    
 Conventional or primitive real-space supercell shape -- choose a representative basis:  
 Primitive reciprocal-space superlattice -- choose a representative basis:  
 b11= b12= b13= b21= b22= b23= b31= b32= b33=  
 [\(help\)](#)

### Method 4: Mode decomposition

Upload distorted structure from CIF file. [\(help\)](#)

Option 1: Upload CIF file

**Figure 1:** The ISODISPLACE search page, which contains a description of the parent structure and a starting point for generating structural distortions.

symmetry elements for every symmetry element in the distorted structure – a very substantial lowering of the symmetry.

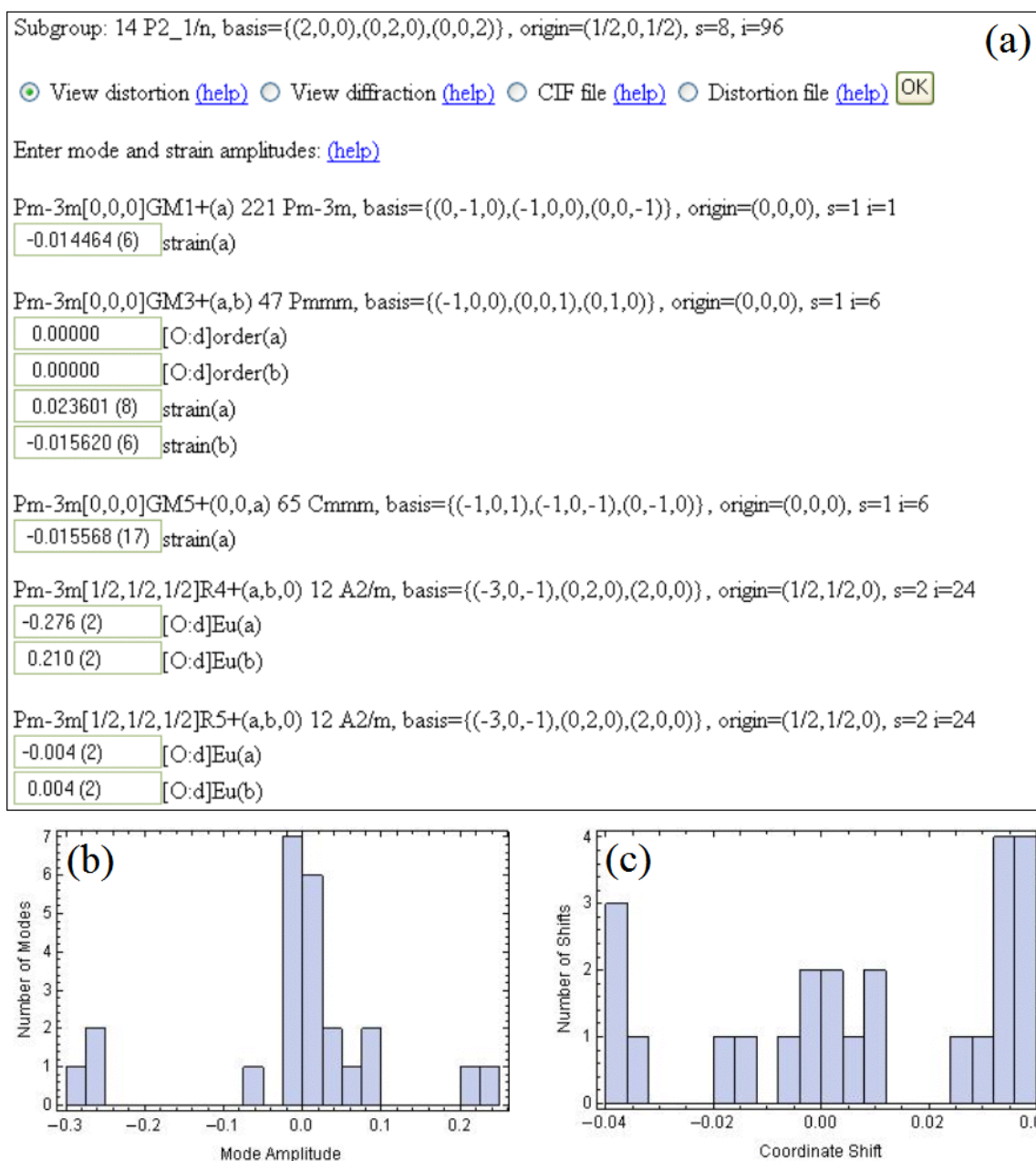


**Figure 2:** (a) Excerpt from the ISODISPLACE **distortion** page, which contains a description of the distortion symmetry, and a list of the distortion modes and their amplitudes. (b) Histogram of displacement-mode amplitudes (in Å) from the distortion page of P2<sub>1</sub>/n WO<sub>3</sub>. (c) Histogram of the corresponding fractional atomic-coordinate shifts.

The **distortion** page (Figure 2a) contains a list of all of the irreps capable of contributing to the specified distortion symmetry, along with the individual distortion modes induced by each irrep. Note that ISODISPLACE only computes distortion modes associated with three types of order parameters: strains, atomic displacements, and occupancy-related orderings. Irreps that don't induce these order parameter types (but might induce some other kind of order parameter) are grouped together at the bottom of the list. When multiple irreps contribute to a distortion, we say that the irreps are *coupled*, or that their order parameters are coupled. Coupled irreps tend to result in lower symmetry and greater structural complexity than individual irreps. To the right of each irrep/OPD in the list, there is a description of the distortion symmetry that would result if that irrep/OPD were to act alone without any coupling.

Most importantly, you can now see exactly how much of each mode couples into the total distortion. ISODISPLACE defines the amplitude of a displacive mode to be the magnitude (in Å) of the largest atomic displacement that it produces. Individual distortion modes are identified with unique labels of the form  $Pm\bar{3}m [\frac{1}{2}, \frac{1}{2}, \frac{1}{2}] R_4^+ (a, b, 0)[O:d]Eu(b)$ , which indicates the parent space group ( $Pm\bar{3}m$ ), the  $k$ -point  $[\frac{1}{2}, \frac{1}{2}, \frac{1}{2}]$ , the irrep ( $R_4^+$ ), the OPD (a,b,0), the parent atom [O] and Wyckoff site [d], the point-group irrep (Eu) that breaks the local site symmetry, and the branch of the OPD (b) involved. Compared to intuitive atomic-coordinate labels like  $O(\frac{1}{4}, \frac{1}{4}, \frac{1}{2}+z)$ , this scheme takes some getting used to. But ISODISPLACE mode labels (described in more detail in Ref. [2]) do provide a very concise description of any distortion mode. Observe that, in agreement with Table 1, five of the 24 distortion-mode amplitudes in Figure 2b are clearly much larger than the others. In contrast, the 24 atomic-coordinate shifts (relative to their ideal undistorted parent positions) in Figure 2c exhibit a much more random distribution. These histograms illustrate that structural information tends to be highly concentrated in the distortion-mode basis.

A series of radio buttons near the top of the **distortion** page provide several avenues of exploration. First, select "Distortion file" and click "OK" to save the **distortion** page. You then have the option of quitting and later returning directly to this **distortion** page via the "Upload distortion file" link on the main page.

Next, select "View distortion" and click the "OK" button, which opens an interactive Java applet in a separate window (Figure 3). The applet has one interactive slider per distortion mode that allows you to visualize an individual mode's effect on the structure. Try clicking the "Animate" checkbox to graphically animate the entire distortion. Displacements and strains are represented in the obvious way. Occupancy-related orderings are represented by a variable atomic radius. Other types of order parameters (e.g. anisotropic thermal parameters, etc.) might be accommodated in the future. Abbreviated mode labels save space by omitting information that can be inferred from the **distortion** page.

From the **distortion** page, select "CIF file" and click "OK" to export the distorted  $P2_1/n$  structure to

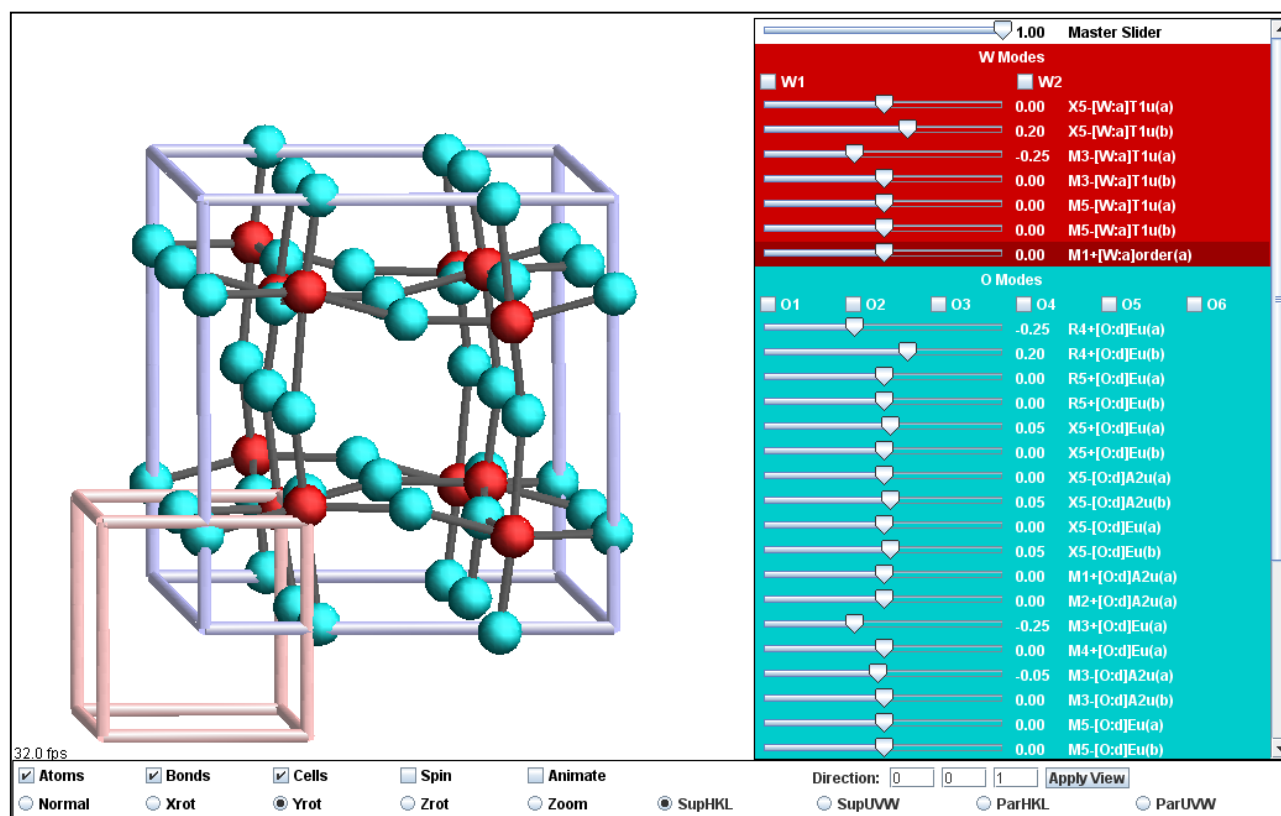


**Figure 3:** *The ISODISPLACE View Distortion applet. Interactive sliders control individual distortion mode amplitudes with a resolution 0.05 Å. Master slider value scales all distortion modes. Click-and-drag structure rotation. Toggle-controls for animation and viewing controls.*

another file named wo3\_iso.cif. Then open this file in a text editor (see Appendix). In addition to the traditional atomic-coordinate description of the distorted structure, the file contains the complete distortion-mode description. A quick check verifies that there are 24 variable atomic coordinates and 24 distortion modes. This file also includes other information that structure-refinement packages like TOPAS will need in order to directly refine the distortion-mode amplitudes. These are (1) the atomic-coordinate shifts, which all equal zero in the undistorted parent phase, (2) the formula relationships between the distorted atomic coordinates, undistorted coordinates and coordinate shifts, and (3) the 24×24 matrix (in sparse form) that transforms the distortion-mode amplitudes into the coordinate shifts.

## 4.2 Search restricted by space-group and basis

Now return to the main ISODISPLACE page and assume that we don't yet know the details of the distorted structure, but see evidence from the diffraction data for a 2×2×2 supercell with space group  $P2_1/n$ . Upload your previously saved parent-structure file (wo3\_cubic.cif), select "Monoclinic cell choice 2" again, scroll down to "Method 3" within the **search** page, and choose space group #14. Select the "conventional or primitive real-space supercell shape" button and use ((2,0,0),(0,2,0),(0,0,2)) for the supercell basis. Clicking the "OK" button (immediately below the basis fields) leads to a new page (which may take a minute to generate) containing a pull-down list of distortion symmetries that match your choice of space-group type and basis. You should find that there are no less than 6 different origin choices for this basis, each of which results in very different distortion modes! Which one is correct? In general, one needs to explore each possibility, unless there are prior expectations regarding the irreps/OPDs involved. In our case, we already know from the mode-decomposition example above that the correct supercell origin is  $(\frac{1}{2}, 0, \frac{1}{2})$ . Making this selection then takes us on to the **distortion** page, which looks much the same as before, except that the mode amplitudes are all zero. Given this example, we hope that you will never again place too much faith in a supercell description that doesn't specify the origin!

## 4.3 The general method: search for specific k-points, irreps, and OPDs

Return again to the main ISODISPLACE page and assume that you already know which  $k$ -points, irreps and OPDs are required to generate the desired distortion symmetry. As in the previous example, upload the cubic parent structure and move on to the **search** page. Method 2 allows us to directly couple an arbitrary selection of commensurate  $k$ -point irreps, so almost any physically-realizable distortion involving strains, occupancies and atomic displacements can be accessed. From Table 1, we see that the  $P2_1/n$  structure of  $WO_3$  can be generated by coupling  $M_3^-(a,b,0)$ ,  $R_4^+(a,b,0)$  and  $X_5^-(0,0,a,a,b,-b)$ . First indicate that you wish to couple 3 irreps and click the corresponding "OK" button, which brings up three pull-down menus containing  $k$ -point choices. Select M, R, and X. On the next page, choose the correct irrep for each  $k$ -point. The following page contains a list of distortion symmetries (also called isotropy subgroups). If the pull-down menu only contains one item, there will be a "Generate isotropy subgroups" button -- click it and wait a minute or two while the menu is loaded. The result is a bewildering list of 46 different distortion symmetries that includes all of the acceptable ways to couple the OPDs available to each irrep. The coupled OPD that we are looking for is just an aggregate of the three OPDs above:  $(a,b,0) \oplus (a,b,0) \oplus (0,0,a,a,b,-b) \rightarrow (a,b,0;c,d,0;0,0,e,e,f,-f)$ . This choice appears about 1/3 of the way down the list, and yields the expected space-group type and origin. The basis, however, is an equivalent monoclinic cell with a different shape. The resulting **distortion** page is similar to that obtained in the previous examples, except that  $M_3^-$ ,  $R_4^+$  and  $X_5^-$  have been moved to the top of the irrep list.

## 4.4 Filtered search over special k-points

Method 1 on the **search** page allows one to conveniently explore the database of all distortion symmetries that can be generated by a single irrep at a special  $k$ -point of symmetry. Because the  $P2_1/n$  structure of  $WO_3$  requires coupled irreps, Method 1 cannot be applied to this example.



In summary, ISODISPLACE provides several different methods of generating distortion symmetries: (1) a filtered search over special  $k$ -points, (2) a general selection of coupled  $k$ -points/irreps/OPDs, (3) a search restricted by space-group type and basis, and (4) the automated decomposition of a known structure into distortion-mode amplitudes. Regardless of which technique is used, the resulting distortion can be saved into a .cif file that contains computer-friendly instructions for refining distortion-mode amplitudes. Such a refinement is the topic of the next section.

## 5.0 Distortion-mode refinements

We now proceed to illustrate a distortion-mode refinement using laboratory X-ray data collected on a sample of predominantly monoclinic  $\text{WO}_3$  ( $P2_1/n$ ) which was cooled slowly from 1000 °C as described by Woodward *et al.*<sup>8</sup> Data were recorded at 300 K using a Bruker d8 diffractometer equipped with a LynxEye position sensitive detector. A conventional Rietveld refinement used a total of 50 parameters: 24  $xyz$  fractional coordinates, 1 isotropic displacement parameter per atom type, 4 cell parameters, a scale factor, a height correction, 6 parameters of an asymmetric pseudo-Voigt peak shape function and the terms of a 12<sup>th</sup> order polynomial background function. A final profile weighted R-factor of  $R_{wp} = 14.1$  and  $R_{Bragg} = 3.1$  % was achieved. Though the structure also has 24 displacive mode amplitudes, we observe that most of the structural information is concentrated within a mere handful (i.e. 5) of these modes.

Distortion-mode refinements can be performed in a straightforward fashion using the menus/macros incorporated in the jEdit TOPAS interface and the wo3\_300K.cif file described in Section 4.1 above. See [http://www.dur.ac.uk/john.evans/topas\\_academic/jedit\\_main.htm](http://www.dur.ac.uk/john.evans/topas_academic/jedit_main.htm) for more information about this interface. As shown in Figure 4, a series of menu items lets you create an input file for distortion-mode refinements with just four mouse clicks:

- **Select Data File:** allows you to browse for one of a number of TOPAS-supported data file formats (.raw files, .xy, .xye, .rd, etc) and writes corresponding lines to the .inp file.
- **Instrument/Corrections:** introduces lines describing the diffractometer wavelength and geometry. Common laboratory setups are included as choices, or the diffractometer can be described from scratch.
- [http://www.dur.ac.uk/john.evans/topas\\_academic/jedit\\_main.htm](http://www.dur.ac.uk/john.evans/topas_academic/jedit_main.htm): allows one to import a .cif file created by ISODISPLACE or else read in a previously prepared .str distortion-mode file (TOPAS format). With the former choice, the macro runs a small executable (isociftotopas.exe) which sits in the main TOPAS directory to convert the .cif to .str format, and then imports the results.
- **→TA:** saves the file with an automatically-generated logical name and sets this as the file that TOPAS Academic (TA) will read from.

These “four clicks” will set up a command file containing everything needed for a sensible default Rietveld refinement. With one more click on the “TA” icon, one can launch TOPAS and perform the distortion-mode refinement. One can, of course, further modify the .inp file, either manually or by using the other built-in TOPAS-related menus. If one already has a .inp file set up for the system in question, isociftotopas.exe can be used independently to create distortion-mode-specific instructions. See [http://www.dur.ac.uk/john.evans/topas\\_academic/jedit\\_setup.htm](http://www.dur.ac.uk/john.evans/topas_academic/jedit_setup.htm) for a full description of how to prepare jEdit for use with TOPAS and how to obtain menus which create .inp files for most common procedures (Rietveld refinement, Pawley refinement, Indexing, time of flight refinements, distortion-mode refinements, etc) is available on line. A tutorial with example data sets for a simple distortion-mode refinement of  $\text{LaMnO}_3$  ([http://www.dur.ac.uk/john.evans/topas\\_workshop/tutorial\\_isoriet.htm](http://www.dur.ac.uk/john.evans/topas_workshop/tutorial_isoriet.htm)) is also available. The jEdit menus contain “help” links which direct the user to these sites.

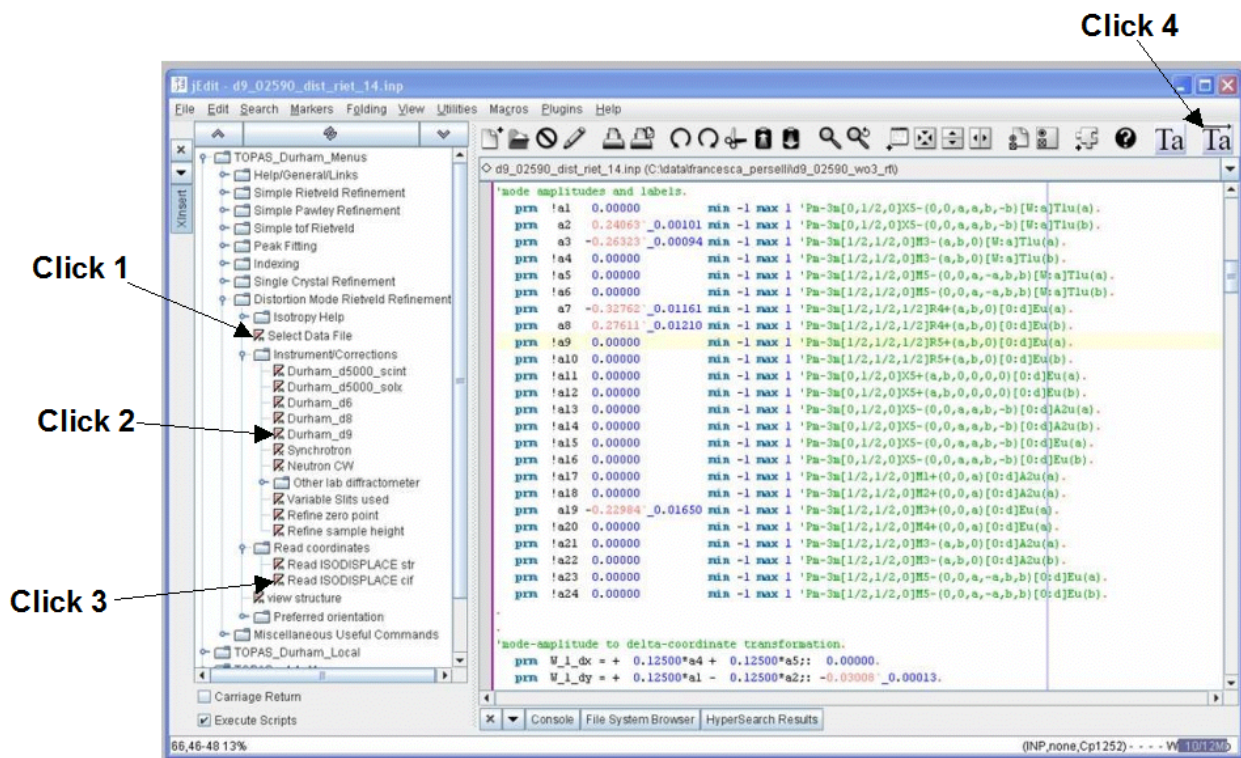


**Figure 4:** Screen shot of distortion-mode refinement menus in jEdit. The minimum “four clicks” required to prepare and perform a distortion-mode refinement are annotated. The colour-coded .inp file on the right shows the amplitudes of each of the 24 displacive distortion modes of the monoclinic structure of  $WO_3$  at 300 K.

This straightforward process produces a .inp file in which each mode amplitude is set up as a refinable parameter labelled  $a1 - a_n$  for brevity (though the full mode label is listed alongside). Atomic-coordinate shifts (e.g.  $dy$ ) are expressed in TOPAS syntax using equations of the form:

$$\text{prm } W\_1\_dy = + 0.125*a1 - 0.125*a2;: -0.00308$$

where the number after the colon indicates the derived value and is updated on refinement. Atomic coordinates are then expressed in the form:

$$\text{site } W1 \text{ } Y = \text{ideal\_}W\_1\_y + W\_1\_dy;$$

where  $\text{ideal\_}W1\_y$  is the fractional coordinate of W1 in the current cell setting appropriate for the high-symmetry structure.

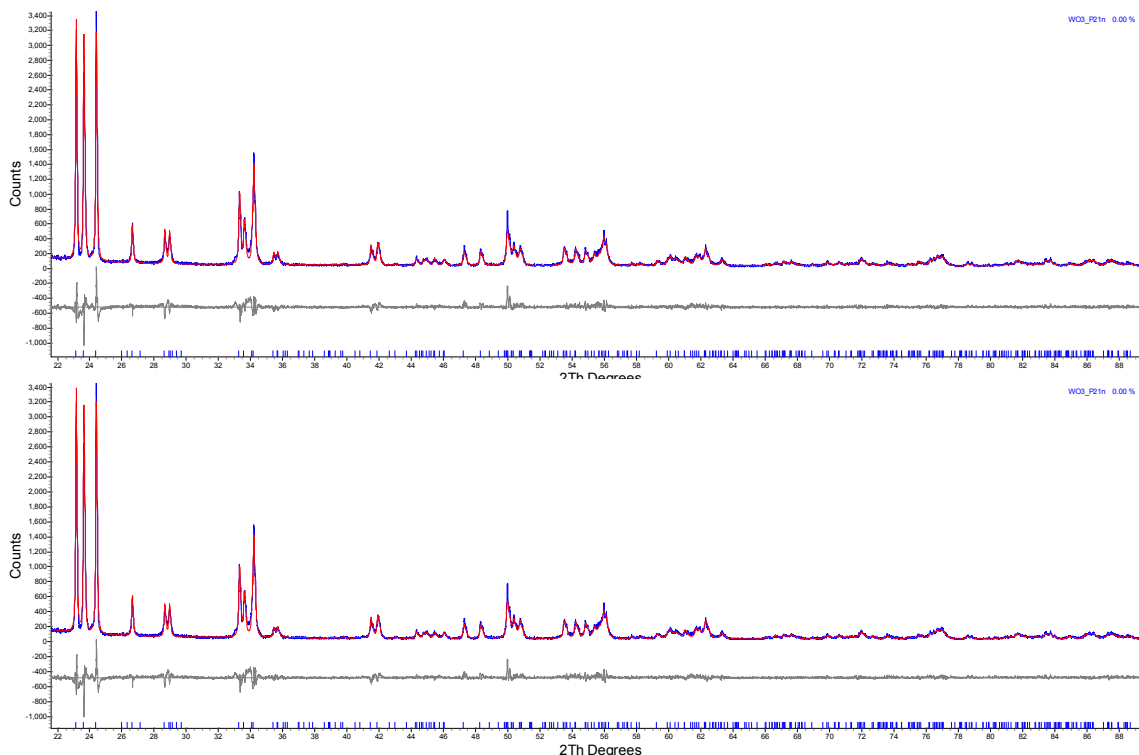


**Figure 5:** Top: Rietveld fit from a refinement of the 5 most important distortion-mode amplitudes of  $P2_1/n$   $WO_3$  against 300 K lab X-ray data. Bottom: The refinement of the full set of 24 mode amplitudes (bottom) does not noticeably improve the fit. The observed and calculated intensities are colored blue and red, respectively. Allowed peak positions are indicated by vertical tick marks.

As an example, Figure 5 shows a Rietveld refinement in which only 5 key distortion-mode amplitudes are allowed to refine (i.e. modes  $a_2$ ,  $a_3$ ,  $a_7$ ,  $a_8$  and  $a_{19}$  from the .inp file visible in Figure 4; also see the  $P2_1/n$  entry in Table 1). Thus we achieved  $R_{wp} = 14.3\%$  and  $R_{Bragg} = 3.6\%$  using just 5 structural degrees of freedom rather than the 24 parameters of a conventional refinement. Note that these 5 parameters contribute to shifts in 16 of the 24  $xyz$  coordinates. The need to use at least 5 modes is illustrated in Figure 6, which shows the closest fit to the published  $P2_1/n$  coordinates one can obtain using modes  $a_1$ ,  $a_2$ ,  $a_3$  and  $a_4$ , with and without mode  $a_{19}$ . With only 5 modes, all atoms are placed within 0.1 Å of the published positions determined from high-resolution neutron data.

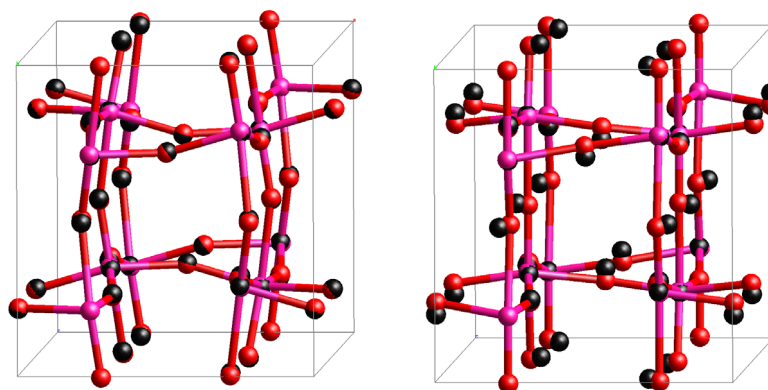


**Figure 6:** Comparison of published  $P2_1/n$  structure of  $WO_3$  and a structure described by modes ( $a_2$ ,  $a_2$ ,  $a_7$  and  $a_8$ ) with (left) and without (right) mode  $a_{19}$ . Published coordinates shown in black. Distortion-mode structure in pink (W) and red (O).

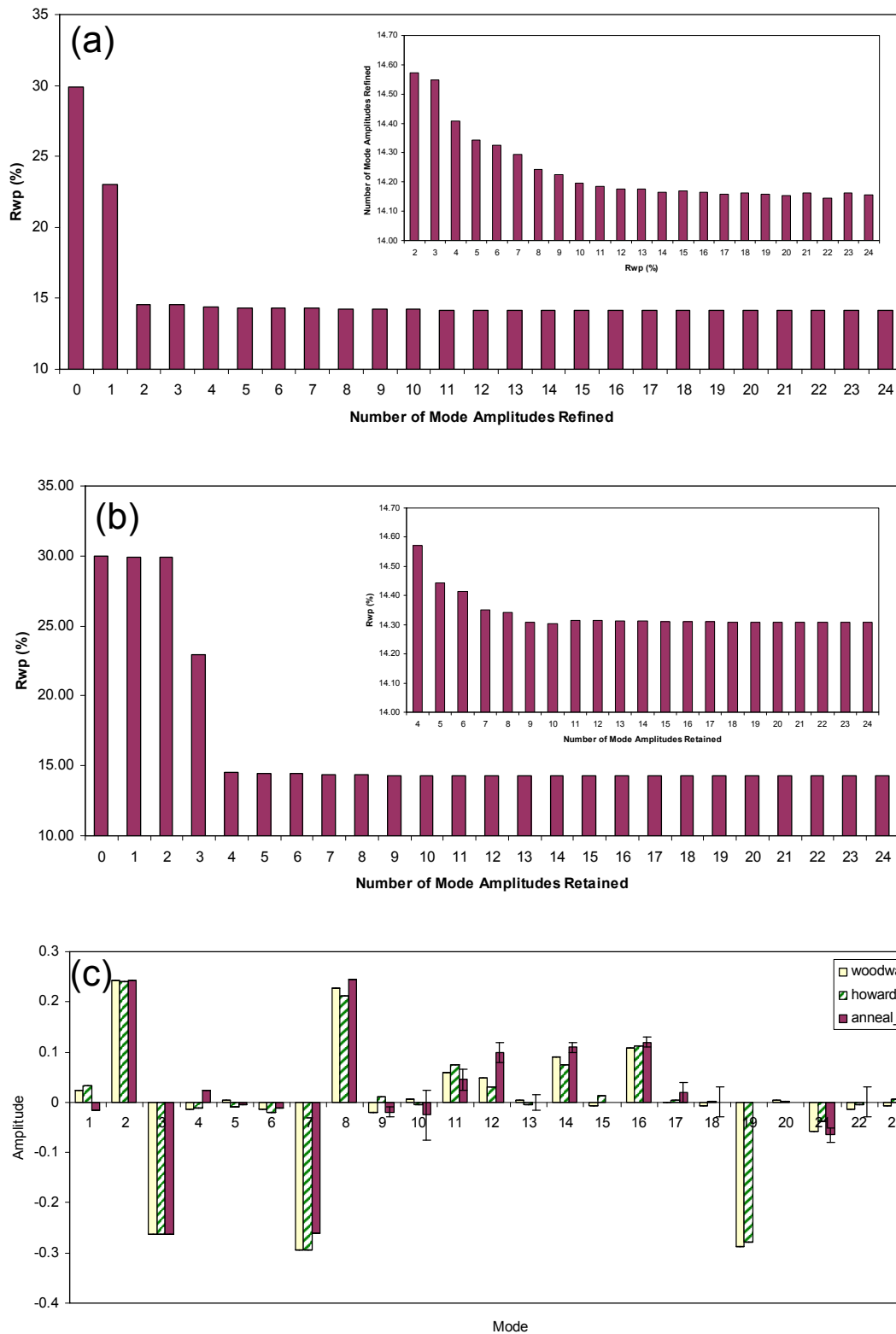


Figure 7: (a) Dependence of  $R_{wp}$  on the number of non-zero distortion-modes refined (see text for explanation). (b) Dependence of  $R_{wp}$  on the number of distortion-modes retained from the structure of Woodward et al.<sup>8</sup> (c) Mode amplitudes refined from X-ray data compared to values for structures from Woodward et al.<sup>8</sup> and Howard et al.<sup>6</sup> The insets in panels (a) and (b) are enlargements that eliminate the first few data points.

The sensitivity of the data to the number of distortion-mode amplitudes retained is shown quantitatively in the histograms of Figure 7a and 7b. Figure 7a shows how the value of  $R_{wp}$  depends on the number of distortion-mode amplitudes used in the refinement. To obtain these graphs, a series of refinements were performed in which only the  $n$  modes with the highest ratios of amplitude/esd in a refinement using  $n+1$  modes were retained. A good fit can be achieved with 5 mode-amplitudes, whereas beyond about 9 mode-amplitudes,  $R_{wp}$  is approximately constant. The  $R_{wp}$  factors plotted in Figure 7b show the influence of sequentially adding distortion-modes derived from the published structure of Woodward,<sup>8</sup> with the largest-magnitude distortions being added first. The  $R_{wp}$  obtained with just 8 distortion modes included is essentially as good as that obtained with 24. It's interesting to note that  $R_{wp}$  actually increases very slightly in this plot on moving from 10 to 11 distortion-modes. The distortion-mode included at this point ( $X_5^-$ ) involves W motion. The neutron-derived amplitude actually leads to a worse fit to the X-ray data. Histograms in 4a and 4b differ in shape due to the different sensitivities of neutron and X-ray data to distortions involving W and O.

Figure 7c gives an indication of how sensitive laboratory X-ray data are to the distortion modes involving oxygen – note that the W:O ratio of scattering powers is  $83^2:8^2 \sim 108$  for X-rays, and that previous structural studies have relied primarily on neutron data. The histogram compares mode-amplitudes from the two neutron refinements with the present X-ray refinement involving the full set of 24 mode amplitudes. The amplitudes of the most important O modes ( $a7$ ,  $a8$  and  $a19$ ) refine to values quite close to those determined from neutron diffraction data.

## 6.0 Conclusions

The internet-based ISODISPLACE software tool allows one to generate and interactively visualize almost any superstructural distortion, and to save the result in a .cif file that contains two complete structural descriptions: traditional atomic coordinates and symmetry-motivated distortion modes, together with the linear transformation between these two bases. With the use of enhanced jEdit macros, TOPAS Academic can now read ISODISPLACE .cif files, allowing one to refine distortion-mode amplitudes directly using standard optimization algorithms. These tools eliminate the need for manual structure transforms and most structural constraints, and also greatly simplify the process of exploring and testing candidate models. By identifying the important distortion modes, one can successfully perform what might otherwise be a highly underdetermined refinement. As an example, we have demonstrated a distortion-mode Rietveld refinement that captures the primary structural features of the 300 K monoclinic phase of  $WO_3$  and shows excellent agreement to laboratory X-ray data using just 5 variable mode amplitudes.

## Acknowledgements

We acknowledge Alan Coelho for the development of the TOPAS Academic software package. BJC acknowledges supported from an award from Research Corporation. Lars Peters and Anne Soleilhavoup are thanked for help with data collection.

## References

- [1] L. D. Landau and E. M. Lifshitz, *Statistical Physics*, 3rd ed., (Pergamon Press, 1980).
- [2] B. J. Campbell, H. T. Stokes, D. E. Tanner and D. M. Hatch, *ISODISPLACE: a web-based tool for exploring structural distortions*, *J. Appl. Cryst.* **39**, 607-14 (2006).
- [3] H. T. Stokes and D. M. Hatch, *Isotropy subgroups of the 230 crystallographic space groups*, (World Scientific, Singapore, 1987).
- [4] C. J. Bradley and A. P. Cracknell, *The mathematical theory of symmetry in solids*, (Oxford, Clarendon Press, 1972).
- [5] H. T. Stokes, D. M. Hatch and J. D. Wells, *Group-theoretical methods for obtaining distortions in crystals - applications to vibrational-modes and phase-transitions*, *Phys. Rev. B* **43**, 11010-8 (1991).
- [6] C. J. Howard, V. Luca and K. S. Knight, *High-temperature phase transitions in tungsten trioxide - the last word?*, *J. Phys. Cond. Matter* **14**, 377-87 (2002).
- [7] T. Vogt, P. M. Woodward and B. A. Hunter, *The high-temperature phases of WO<sub>3</sub>*, *J. Solid State Chem.* **144**, 209-15 (1999).
- [8] P. M. Woodward, A. W. Sleight and T. Vogt, *Structure refinement of triclinic tungsten trioxide*, *J. Phys. Chem. Solids* **56**, 1305-15 (1995).
- [9] R. Diehl, G. Brandt and E. Salje, *Crystal-Structure of Triclinic WO<sub>3</sub>*, *Acta Cryst. B* **34**, 1105-11 (1978).
- [10] E. K. H. Salje, S. Rehmman, F. Pobell, D. Morris, K. S. Knight, T. Herrmannsdorfer and M. T. Dove, *Crystal structure and paramagnetic behaviour of epsilon WO<sub>3-x</sub>*, *J. Phys. Cond. Matter* **9**, 6563-77 (1997).
- [11] A. M. Glazer, *The classification of tilted octahedra in perovskites*, *Acta Cryst. B* **28**, 3384-92 (1972).
- [12] C. J. Howard and H. T. Stokes, *Group-theoretical analysis of octahedral tilting in perovskites*, *Acta Cryst. B* **54**, 782-9 (1998).

## Appendix: CIF output from the mode decomposition of the $P2_1/n$ phase of WO<sub>3</sub>

```
# This file was generated by ISODISPLACE, version 4.0.5
# Harold T. Stokes, Branton J. Campbell, David Tanner, Dorian M.
# Hatch
# Brigham Young University, Provo, Utah, USA
#
# Space Group: 221 Pm-3m      Oh-1
# Space-group preferences: monoclinic axes a(b)c, monoclinic cell
# choice 2, orthorhombic axes abc, origin choice 2, hexagonal axes
# Lattice parameters: a=3.81000, b=3.81000, c=3.81000, al-
# pha=90.00000, beta=90.00000, gamma=90.00000
# W 1a (0,0,0)
# O 3d (1/2,0,0)
# Subgroup: 14 P2_1/n, basis={(2,0,0),(0,2,0),(0,0,2)}, ori-
# gin=(1/2,0,1/2), s=8, i=96
# Order parameter values:
# Pm-3m[0,0,0]GM1+(a) 221 Pm-3m s=1 i=1
#   strain(a): -0.01446
# Pm-3m[0,0,0]GM3+(a,b) 47 Pm-3m s=1 i=6
#   strain(a): 0.02360
#   strain(b): -0.01562
# Pm-3m[0,0,0]GM5+(0,0,a) 65 Cm-3m s=1 i=6
#   strain(a): -0.01557
# Pm-3m[1/2,1/2,1/2]R4+(a,b,0) 12 A2/m s=2 i=24
# [O:d]Eu(a): -0.27600
# [O:d]Eu(b): 0.21000
# Pm-3m[1/2,1/2,1/2]R5+(a,b,0) 12 A2/m s=2 i=24
# [O:d]Eu(a): -0.00400
# [O:d]Eu(b): 0.00400
# Pm-3m[0,1/2,0]X5+(a,b,0,0,0) 11 P2_1/m s=2 i=24
# [O:d]Eu(a): 0.06800
# [O:d]Eu(b): 0.02900
# Pm-3m[0,1/2,0]X5-(0,0,a,a,b,-b) 59 Pm-3m s=4 i=24
# [W:a]T1u(a): 0.02500
# [W:a]T1u(b): 0.23600
# [O:d]A2u(a): 0.00000
# [O:d]A2u(b): 0.07800
# [O:d]Eu(a): 0.00100
# [O:d]Eu(b): 0.09100
# Pm-3m[1/2,1/2,0]M1+(0,0,a) 123 P4/m-3m s=2 i=6
# [O:d]A2u(a): 0.00600
# Pm-3m[1/2,1/2,0]M2+(0,0,a) 127 P4/m-3m s=2 i=6
# [O:d]A2u(a): -0.00100
# Pm-3m[1/2,1/2,0]M3+(0,0,a) 127 P4/m-3m s=2 i=6
# [O:d]Eu(a): -0.27200
# Pm-3m[1/2,1/2,0]M4+(0,0,a) 123 P4/m-3m s=2 i=6
# [O:d]Eu(a): 0.00200
# Pm-3m[1/2,1/2,0]M3-(a,b,0) 72 I-3m s=4 i=24
# [W:a]T1u(a): -0.25900
# [W:a]T1u(b): -0.01200
# [O:d]A2u(a): -0.05400
# [O:d]A2u(b): -0.01300
# Pm-3m[1/2,1/2,0]M5-(0,0,a,-a,b,b) 71 I-3m s=4 i=24
# [W:a]T1u(a): 0.00200
# [W:a]T1u(b): -0.01900
# [O:d]Eu(a): 0.00400
# [O:d]Eu(b): -0.01800

data_isodisplace-output
_symmetry_space_group_name_H-M "P 1 21/n 1"
_symmetry_Int_Tables_number 14
_cell_length_a 7.30084(7)
_cell_length_b 7.53889(7)
_cell_length_c 7.68962(8)
_cell_angle_alpha 90.00000
_cell_angle_beta 90.8920(10)
_cell_angle_gamma 90.00000

loop_
_symmetry_equiv_pos_as_xyz
x,y,z
-x-1/2,y+1/2,-z-1/2
-x,-y,-z
x-1/2,-y+1/2,z-1/2

loop_
_atom_site_label
_atom_site_type_symbol
```

```

_atom_site_fract_x
_atom_site_fract_y
_atom_site_fract_z
W1 W 0.2513 (6) 0.0277 (7) 0.2865 (5)
W2 W 0.2482 (6) 0.0343 (6) 0.7815 (5)
O1 O 0.0008 (6) 0.0366 (8) 0.2117 (5)
O2 O -0.0026 (6) 0.4631 (8) 0.2164 (5)
O3 O 0.2821 (4) 0.2602 (7) 0.2871 (4)
O4 O 0.2107 (4) 0.2602 (8) 0.7309 (4)
O5 O 0.2860 (6) 0.0390 (6) 0.0064 (5)
O6 O 0.2849 (6) 0.4849 (5) -0.0077 (4)

```

```

O3_y "1/4 + O3_dy"
O3_z "1/4 + O3_dz"
O4_x "1/4 + O4_dx"
O4_y "1/4 + O4_dy"
O4_z "3/4 + O4_dz"
O5_x "1/4 + O5_dx"
O5_y "0 + O5_dy"
O5_z "0 + O5_dz"
O6_x "1/4 + O6_dx"
O6_y "1/2 + O6_dy"
O6_z "0 + O6_dz"

```

```
_iso_displacivemode_number 24
```

```
# matrix conversion: deltaxcoords = matrix * modeamplitudes
# Square matrix with _iso_displacivemode_number rows and columns
```

```

loop_
_iso_displacivemode_ID
_iso_displacivemode_label
_iso_displacivemode_value
1 Pm-3m[0,1/2,0]X5-(0,0,a,a,b,-b)[W:a]Tlu(a) 0.02500
2 Pm-3m[0,1/2,0]X5-(0,0,a,a,b,-b)[W:a]Tlu(b) 0.23600
3 Pm-3m[1/2,1/2,0]M3-(a,b,0)[W:a]Tlu(a) -0.25900
4 Pm-3m[1/2,1/2,0]M3-(a,b,0)[W:a]Tlu(b) -0.01200
5 Pm-3m[1/2,1/2,0]M5-(0,0,a,-a,b,b)[W:a]Tlu(a) 0.00200
6 Pm-3m[1/2,1/2,0]M5-(0,0,a,-a,b,b)[W:a]Tlu(b) -0.01900
7 Pm-3m[1/2,1/2,1/2]R4+(a,b,0)[O:d]Eu(a) -0.27600
8 Pm-3m[1/2,1/2,1/2]R4+(a,b,0)[O:d]Eu(b) 0.21000
9 Pm-3m[1/2,1/2,1/2]R5+(a,b,0)[O:d]Eu(a) -0.00400
10 Pm-3m[1/2,1/2,1/2]R5+(a,b,0)[O:d]Eu(b) 0.00400
11 Pm-3m[0,1/2,0]X5+(a,b,0,0,0,0)[O:d]Eu(a) 0.06800
12 Pm-3m[0,1/2,0]X5+(a,b,0,0,0,0)[O:d]Eu(b) 0.02900
13 Pm-3m[0,1/2,0]X5-(0,0,a,a,b,-b)[O:d]A2u(a) 0.00000
14 Pm-3m[0,1/2,0]X5-(0,0,a,a,b,-b)[O:d]A2u(b) 0.07800
15 Pm-3m[0,1/2,0]X5-(0,0,a,a,b,-b)[O:d]Eu(a) 0.00100
16 Pm-3m[0,1/2,0]X5-(0,0,a,a,b,-b)[O:d]Eu(b) 0.09100
17 Pm-3m[1/2,1/2,0]M1+(0,0,a)[O:d]A2u(a) 0.00600
18 Pm-3m[1/2,1/2,0]M2+(0,0,a)[O:d]A2u(a) -0.00100
19 Pm-3m[1/2,1/2,0]M3+(0,0,a)[O:d]Eu(a) -0.27200
20 Pm-3m[1/2,1/2,0]M4+(0,0,a)[O:d]Eu(a) 0.00200
21 Pm-3m[1/2,1/2,0]M3-(a,b,0)[O:d]A2u(a) -0.05400
22 Pm-3m[1/2,1/2,0]M3-(a,b,0)[O:d]A2u(b) -0.01300
23 Pm-3m[1/2,1/2,0]M5-(0,0,a,-a,b,b)[O:d]Eu(a) 0.00400
24 Pm-3m[1/2,1/2,0]M5-(0,0,a,-a,b,b)[O:d]Eu(b) -0.01800

```

```

loop_
_iso_displacivodematrix_row
_iso_displacivodematrix_col
_iso_displacivodematrix_value

```

```

1 4 -0.13123
1 5 -0.13123
2 1 -0.13123
2 2 0.13123
3 3 -0.13123
3 6 -0.13123
4 4 0.13123
4 5 -0.13123
5 1 0.13123
5 2 0.13123
6 3 -0.13123
6 6 0.13123
7 17 -0.13123
7 18 0.13123
7 22 -0.13123
8 7 -0.13123
8 9 -0.13123
8 15 -0.13123
9 19 0.13123
9 20 -0.13123
9 24 0.13123
10 17 -0.13123
10 18 0.13123
10 22 0.13123
11 7 0.13123
11 9 0.13123
11 15 -0.13123
12 19 0.13123
12 20 -0.13123
12 24 -0.13123
13 7 -0.13123
13 9 0.13123
13 11 -0.09280
13 12 0.09280
14 13 -0.13123
14 14 0.13123
15 8 0.13123
15 10 0.13123
15 11 0.09280
15 12 0.09280
16 7 0.13123
16 9 -0.13123
16 11 -0.09280
16 12 0.09280
17 13 0.13123
17 14 0.13123
18 8 -0.13123
18 10 -0.13123
18 11 0.09280
18 12 0.09280
19 19 -0.13123
19 20 -0.13123
19 23 0.13123
20 8 0.13123
20 10 -0.13123
20 16 0.13123
21 17 -0.13123
21 18 -0.13123
21 21 -0.13123
22 19 -0.13123
22 20 -0.13123
22 23 -0.13123
23 8 -0.13123
23 10 0.13123
23 16 0.13123
24 17 -0.13123
24 18 -0.13123
24 21 0.13123

```

```

loop_
_iso_deltacoordinate_ID
_iso_deltacoordinate_label
_iso_deltacoordinate_value
1 W1_dx 0.00131
2 W1_dy 0.02769
3 W1_dz 0.03648
4 W2_dx -0.00184
5 W2_dy 0.03425
6 W2_dz 0.03150
7 O1_dx 0.00079
8 O1_dy 0.03661
9 O1_dz -0.03832
10 O2_dx -0.00262
11 O2_dy -0.03688
12 O2_dz -0.03360
13 O3_dx 0.03208
14 O3_dy 0.01024
15 O3_dz 0.03709
16 O4_dx -0.03931
17 O4_dy 0.01024
18 O4_dz -0.01908
19 O5_dx 0.03596
20 O5_dy 0.03898
21 O5_dz 0.00643
22 O6_dx 0.03491
23 O6_dy -0.01509
24 O6_dz -0.00774

```

```

loop_
_iso_coordinate_label
_iso_coordinate_formula
W1_x "1/4 + W1_dx"
W1_y "0 + W1_dy"
W1_z "1/4 + W1_dz"
W2_x "1/4 + W2_dx"
W2_y "0 + W2_dy"
W2_z "3/4 + W2_dz"
O1_x "0 + O1_dx"
O1_y "0 + O1_dy"
O1_z "1/4 + O1_dz"
O2_x "0 + O2_dx"
O2_y "1/2 + O2_dy"
O2_z "1/4 + O2_dz"
O3_x "1/4 + O3_dx"

```

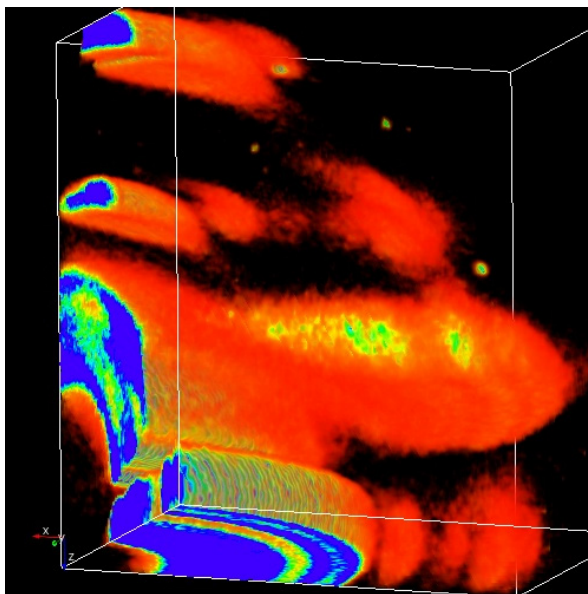
```
# end of structure file
```

---

## MAX3D - Visualization of Reciprocal Space Volumes

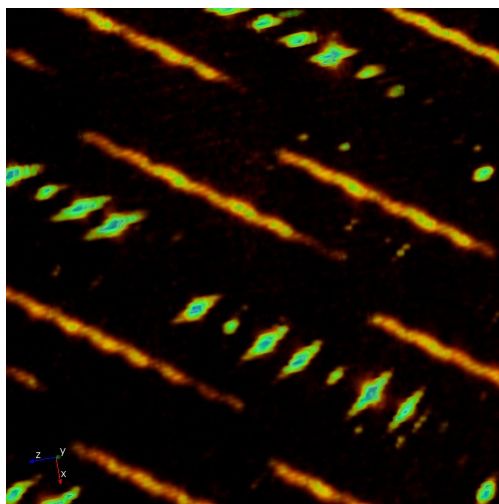
**Jim Britten<sup>a</sup> and Weiguang Guan<sup>b</sup>**

<sup>a</sup>McMaster Analytical X-ray Diffraction Facility, McMaster University, Hamilton, Ontario, L8S 4L7, Canada. <sup>b</sup>Research and High Performance Computing Support, McMaster University, Hamilton, Ontario, L8S 4L7, Canada. Email: [britten@mcmaster.ca](mailto:britten@mcmaster.ca) ;  
WWW: <http://www.chemistry.mcmaster.ca/facilities/xray/MAX3D.htm> ;  
<http://www.rhpcs.mcmaster.ca/~guanw/>



### Introduction

Crystallographers have been rotating samples in front of 2D electronic detectors and collecting 3D diffraction data for several years. We have learned to interpret the detector images and recognize good and bad samples, 1D and 2D diffuse scattering, supercells, incommensurate scattering, texture in polycrystalline solids, and crystallite orientation in polymers. We have commercial and academic software to process this data and solve crystal structures, deal with twinned data, integrate and model incommensurate scattering, model diffuse scattering from short range ordering, as well as generate pole figures and orientation distribution functions. Oriented slices through reciprocal space can be calculated and displayed. What we have not been able to do, until recently, is to visualize and manipulate the complete reciprocal space volume all at once.





This article describes a simple software tool, MAX3D, which can be used to quickly load CCD or image plate scans and allow you to see the amazing diffraction features you have stored in your archives or collecting on your diffractometer. We will also present several examples of how useful the visualization of complete reciprocal space can be in characterizing materials.

## MAX3D

### Platforms

The MAX3D reciprocal space volume visualizer is an offshoot of WG's general 3D viewing software SciVis, used for medical scanning data, astronomical data, PDB files, etc.. The program was adapted and streamlined for 3D diffraction data, with the addition of readers for various types of frame data and specialized tools for studying reciprocal space.

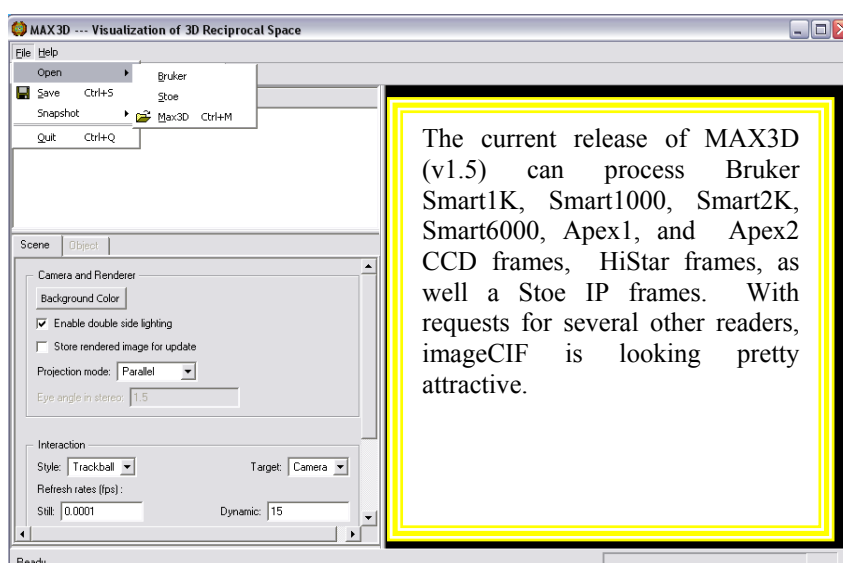
The program is built on Visual C++ using VTK and QT libraries. It has been developed and compiled for Linux and MS Windows. MacOS is also a possibility.

The speed and success of building a large volume object for visualization depends on the hardware available. 1Gb RAM is recommended as a minimum. The reciprocal space volumes represented in this article were generated on a laptop with 1Gb RAM, usually with the help of paging. Load times ranged from ~ 1 minute to 10 minutes, depending on frame size, number of frames, and requested voxel density. Real-time rotation and zooming in reciprocal space require a decent video card with at least 256 Mb RAM, e.g. nVIDIA GeForce Go 6200.



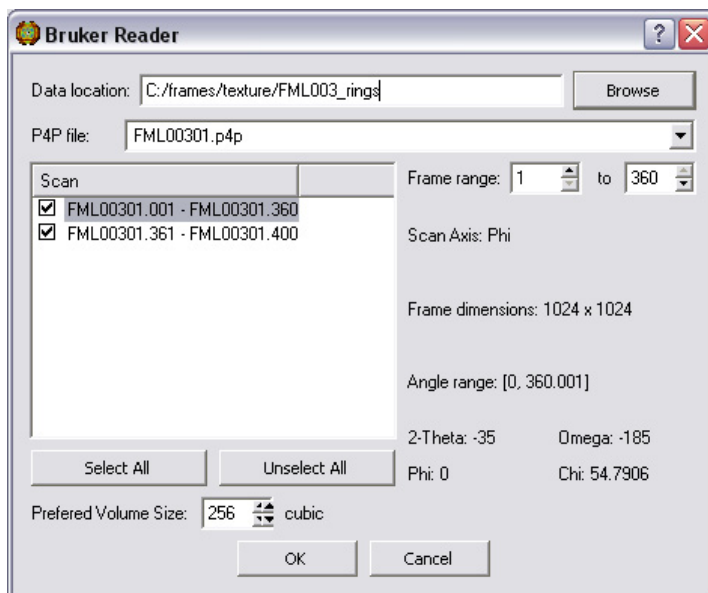
### Input

One or more  $\omega$ - or  $\phi$ -scans can be chosen as input. For Bruker CCD data, a '.p4p' file with orientation information can be selected from the scan directory. A volume size can be chosen to suit the reciprocal space detail required, with consideration for hardware constraints. It is best not to overtax the system, since subsections of the volume can be, and most often are, reloaded later at higher voxel density.

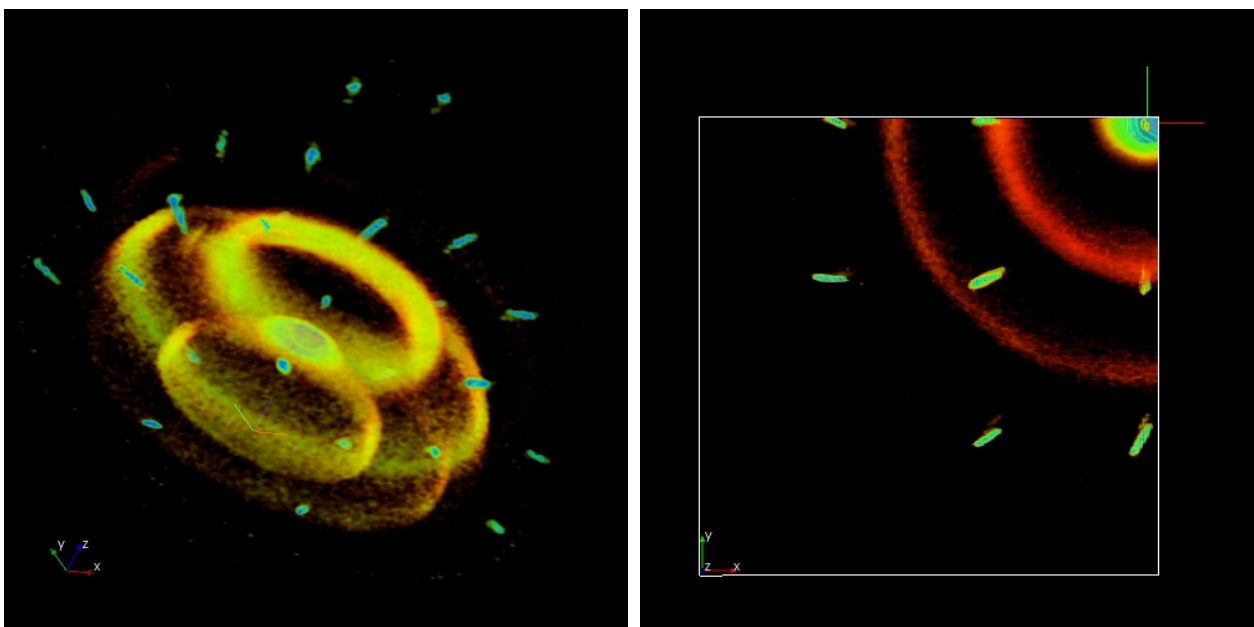


Once rendered, reciprocal space volumes can be saved as '.m3d' files for faster loading later. These files are in vti format and can also be loaded into programs such as Paraview (<http://www.paraview.org>).

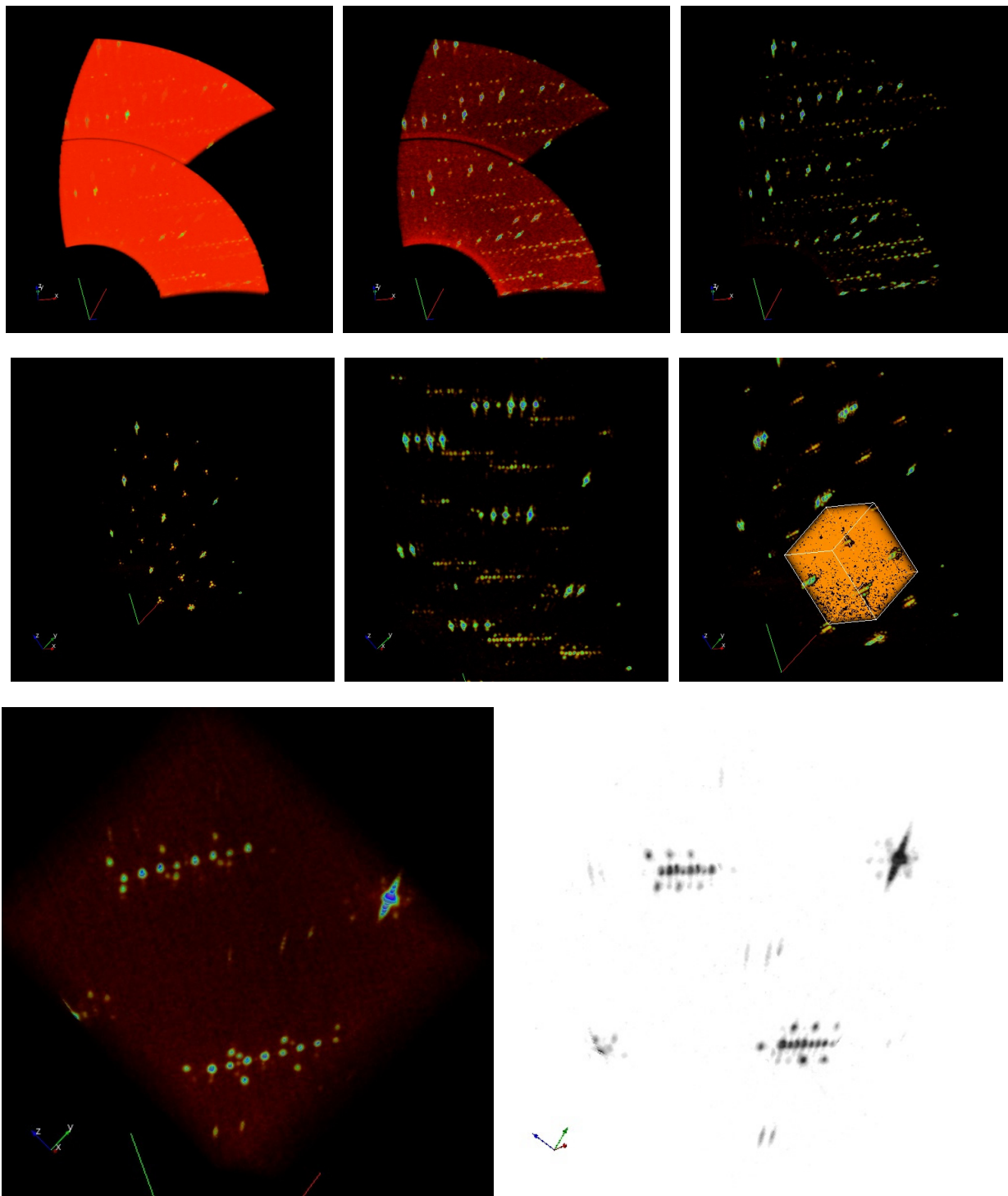
The mapping of overlapping pixels into voxels is done simply and quickly. Scattering details can be missed if the collected data is mapped into a low density space. Reloading to detector resolution is the best way to get a good night's sleep. If very accurate reciprocal space volumes are required, with all refined (Bruker) detector corrections applied, Branton Campbell at Brigham Young University's Physics Dept. (<http://www.physics.byu.edu/faculty/campbell/>) has written the program you need.



**Example 1:** CdTe film deposited on YSZ and annealed. The CdTe (111) axis is normal to the substrate, but the in-plane epitaxy is lost. ([Peter Mascher, Eng. Physics, McMaster University](#))

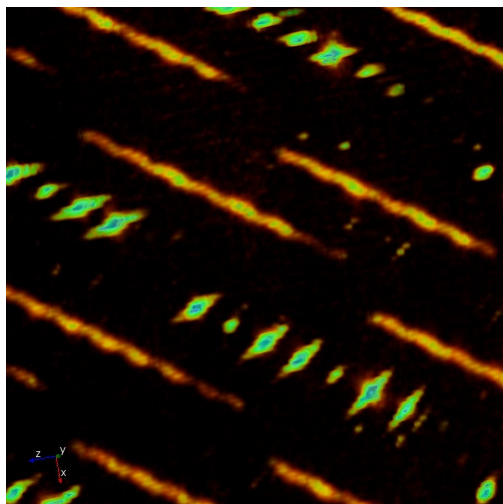


**Example 2:** Load a couple of  $\phi$ -scans, adjust the opacity, rotate and zoom, reload a subsection at 3 times the density, zoom, adjust colour, be amazed at nature ( $\text{LuFe}_2\text{O}_4$ , [Young June Kim, Physics Department, University of Toronto](#))

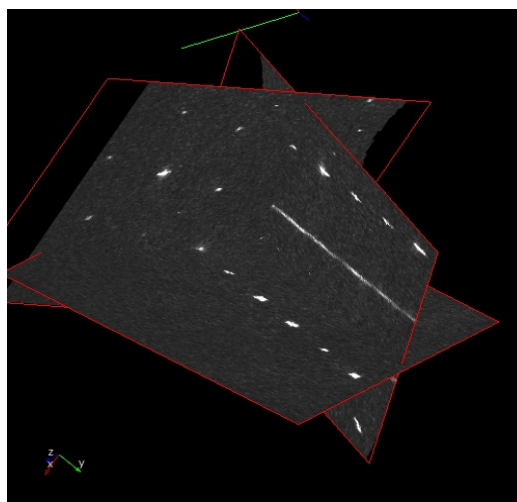


## Tools

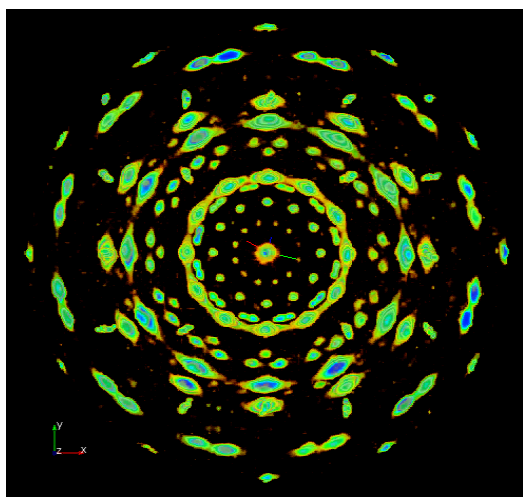
MAX3D includes the usual VTK tools for manipulation of 3D solid objects: rotate, zoom, mouse response options, saving snapshots and videos, colour mapping, multiple object handling, slicing, view control, etc. We have written some crystallography specific tools to help the user interpret what he/she is staring at. In slice mode, rolling the cursor over the planes with the left mouse button pressed reads out the fractional  $h,k,l$  and voxel intensity values.  $a^*$ ,  $b^*$ , and  $c^*$  are displayed, and buttons are available to snap the view along each of them. There is a  $2\theta$  sphere probe, with  $2\theta$  and  $h,k,l$  readout. Multiple r.s. volumes can be displayed at the same scale and oriented relative to the lab frame.



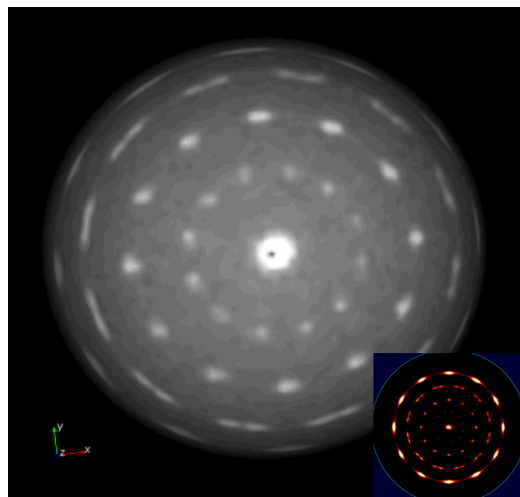
LuFe<sub>2</sub>O<sub>4</sub> at 80C.



2D slices



CdTe film + substrate



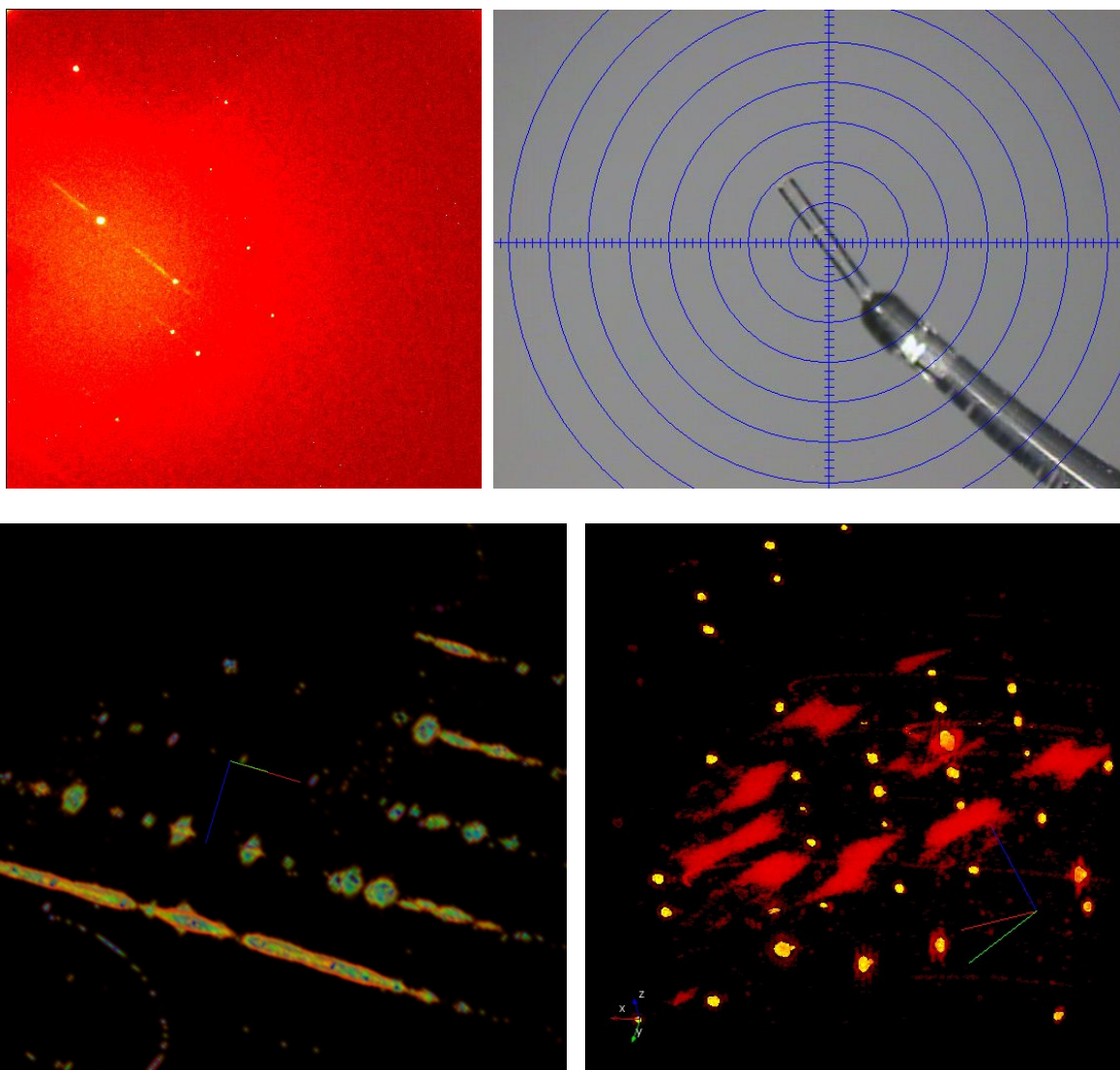
(111) sphere (with pole figure: [GADDS](#))

## Single crystal applications

The examples presented in this article are from routine datasets collected on single crystal CCD and IP diffractometers in the MAX Diffraction Facility. In some cases, diffuse or incommensurate scattering was expected, in others it was not. Even when looking for non-Bragg features in the scattering, we have been surprised by the variety and temperature variation of the features observed. More often than not, this evidence of short or intermediate range correlations in atomic or molecular displacement or substitution is simply used as an excuse for poor single crystal refinement, or a reason to search for another crystal. Fortunately, within a few years we will all have the tools to interpret and model diffuse scattering, as seen in the [American Crystallographic Association's](#) 2007 Transactions session 'Diffuse scattering for the masses: the characterization of local structural correlations in molecular, macromolecular, and inorganic crystals'. The tools for modeling incommensurate scattering (e.g. [Jana2000](#)) are available, although most of us (especially in North America) are in need of a workshop or two.

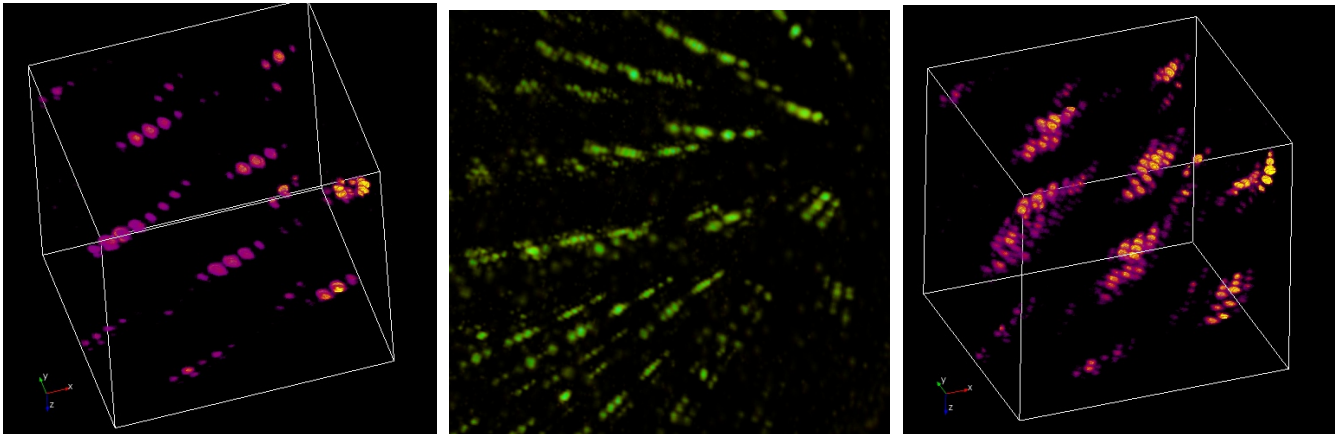
## Diffuse Scattering

**Example 3:** Hexanaphthylbenzene packs in columns in P6/mcc with 1D ordering along the stack, and 2D disorder stack to stack. Streaks were observed in the frames. We expected planes of diffuse scattering perpendicular to the c-axis, but were surprised to see a lot of structure to the r.s. layer – a lot of order in the disorder. Paper to be published ([McGlinchey](#), [Harrington](#), Britten).

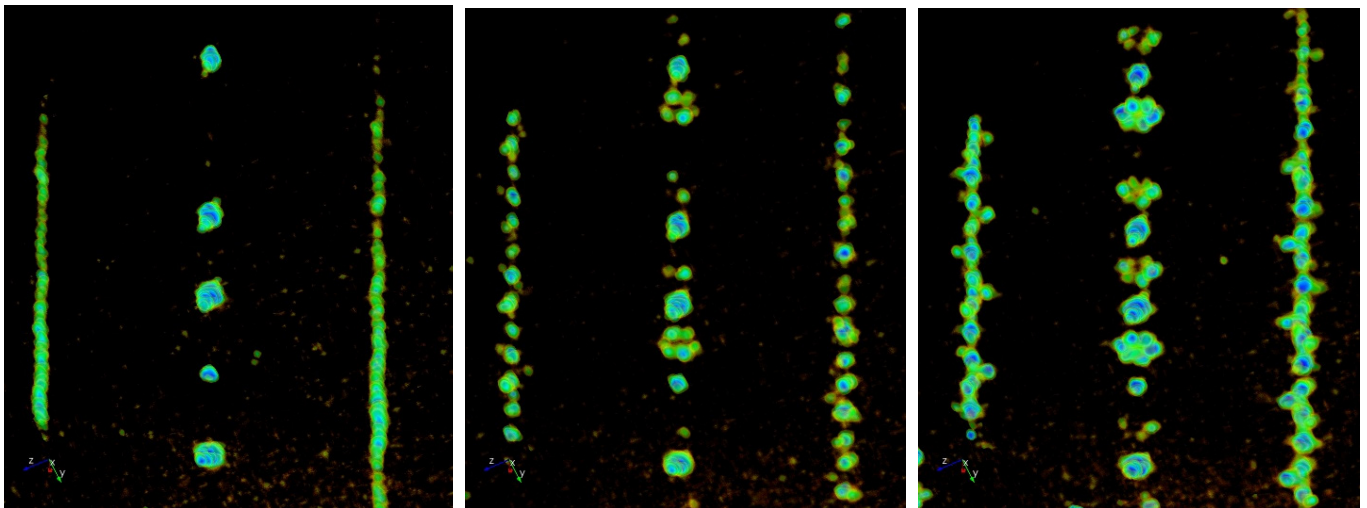


## Incommensurate Scattering

**Example 4:**  $\text{Bi}_2\text{Sr}_2\text{CaCu}_2\text{O}_8$  is a high  $T_c$  superconductor that shows incommensurate scattering. The first sample was twinned, but the second was good. ([Gaulin](#), [Dabkowska](#), McMaster University)



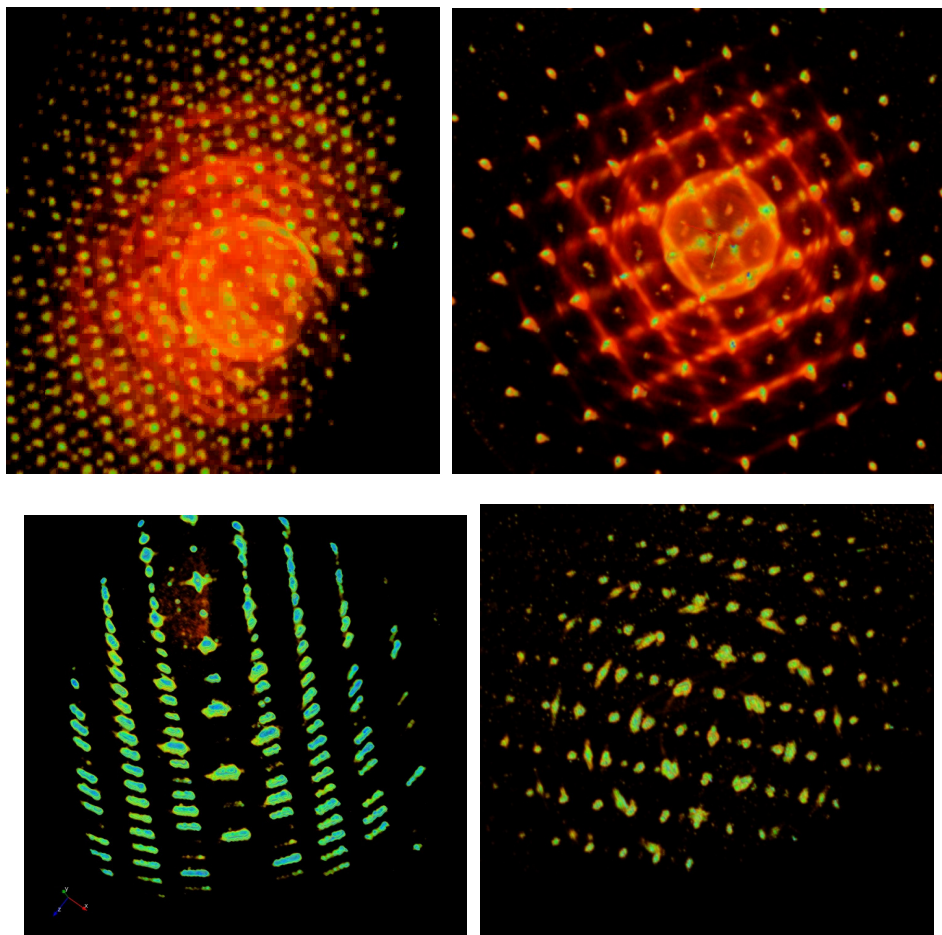
**Example 5:** The  $\text{LuFe}_2\text{O}_4$  example shown above demonstrates both diffuse scattering and satellite peaks. Bilayers of  $\text{Fe}^{\text{II}}/\text{Fe}^{\text{III}}$  oxide are separated by a layer of  $\text{Lu}^{\text{III}}$  oxide. At temperatures above 500C there is a simple trigonal structure with disordered (spin and charge frustrated) Fe atoms. The left image is from 80C data, where short range 2D ordering in the iron layers shows 1D lines of diffuse scattering. Cooling the crystal results in 3D charge density waves (ordering across the Lu layers) and the diffuse scattering becomes structured. Other satellite peaks appear between the original Bragg peaks parallel to the 3-fold axis. ([Young June Kim](#), Physics Department, University of Toronto)



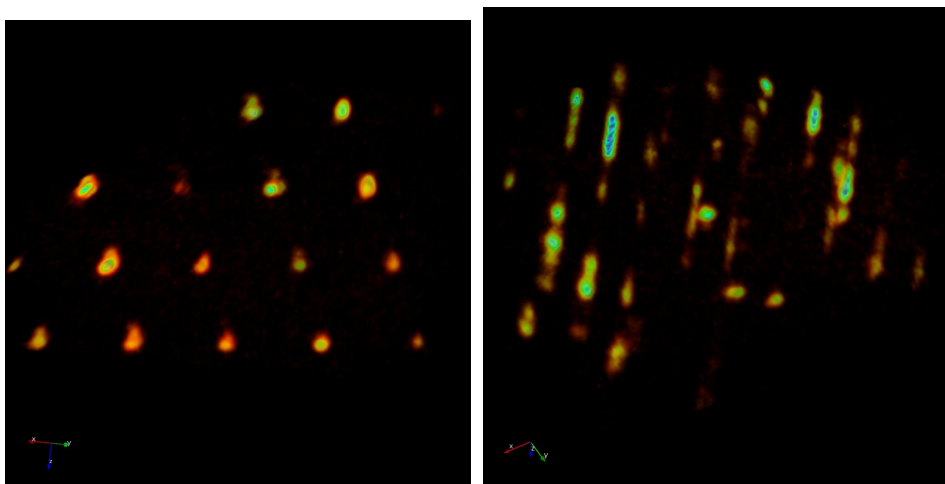
## Crystal Screening

Why do refinements give problems? When do you toss the crystal? A complete picture of the diffraction can help you decide when enough is enough.

**Example 6:** Loss of acetonitrile gives powder spheres at 100K, and shows a very interesting association with the single crystal. A cluster of needles show a rotational spread (and a glide plane). A monoclinic and a cubic phase co-crystallize. The spot shapes of the two phases are noticeably different. ([Schrobligen, McMaster University](#))



**Example 7:** This compound forms plate-like crystals. It appears that there is 2D ordering at the molecular level, but the third dimension shows a loss of order. ([Valliant, McMaster University](#))

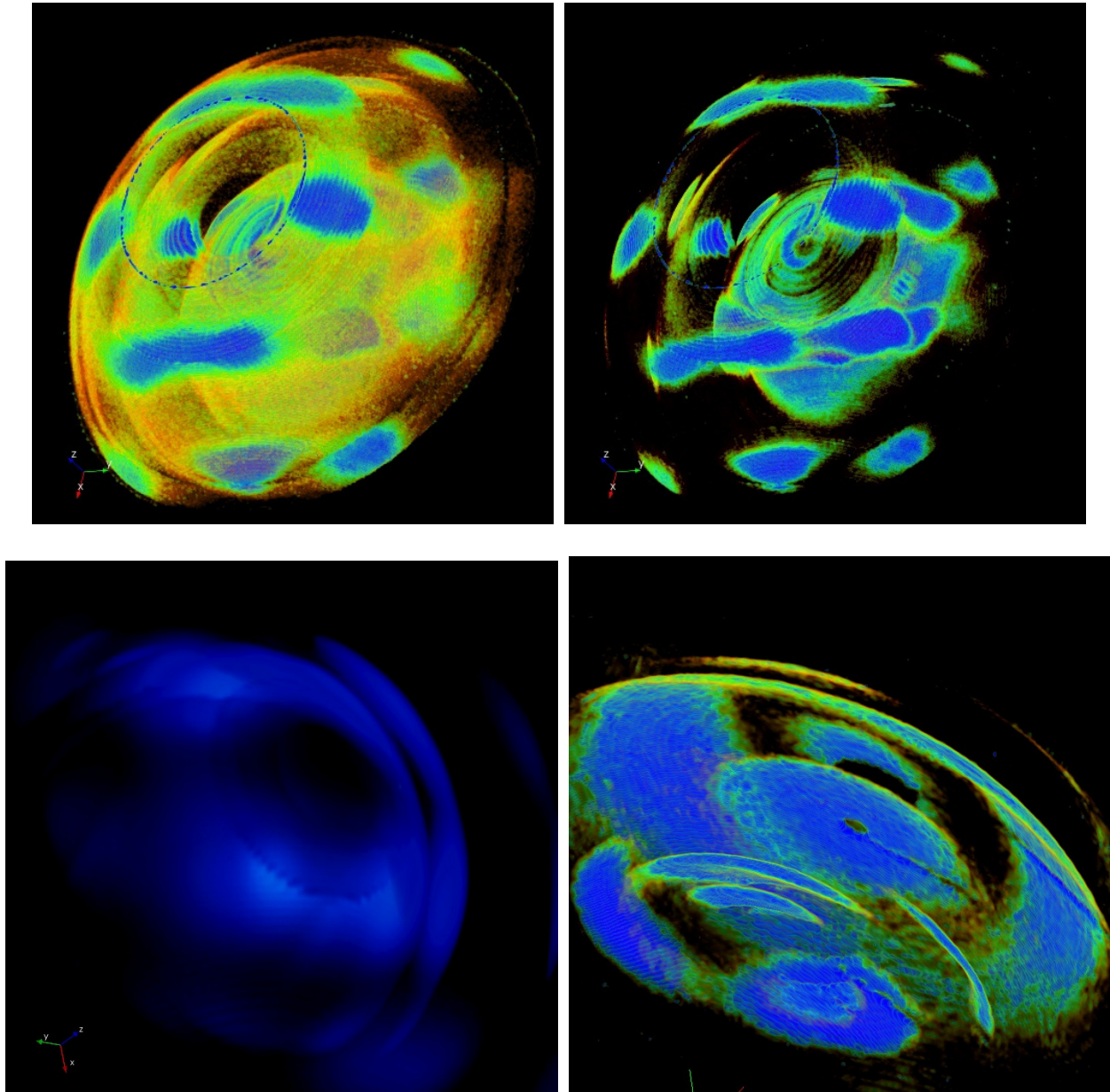


## XRD<sup>3</sup> Applications

The diffraction of polycrystalline solids is studied in 3D to characterize the orientation distribution of the crystallites. Some materials can have almost random grain structure as in a powder, while others can scatter like a single crystal. In all cases, the 3D reciprocal space volume contains information on the preparation, treatment, or damage of the material.

### Texture Analyses

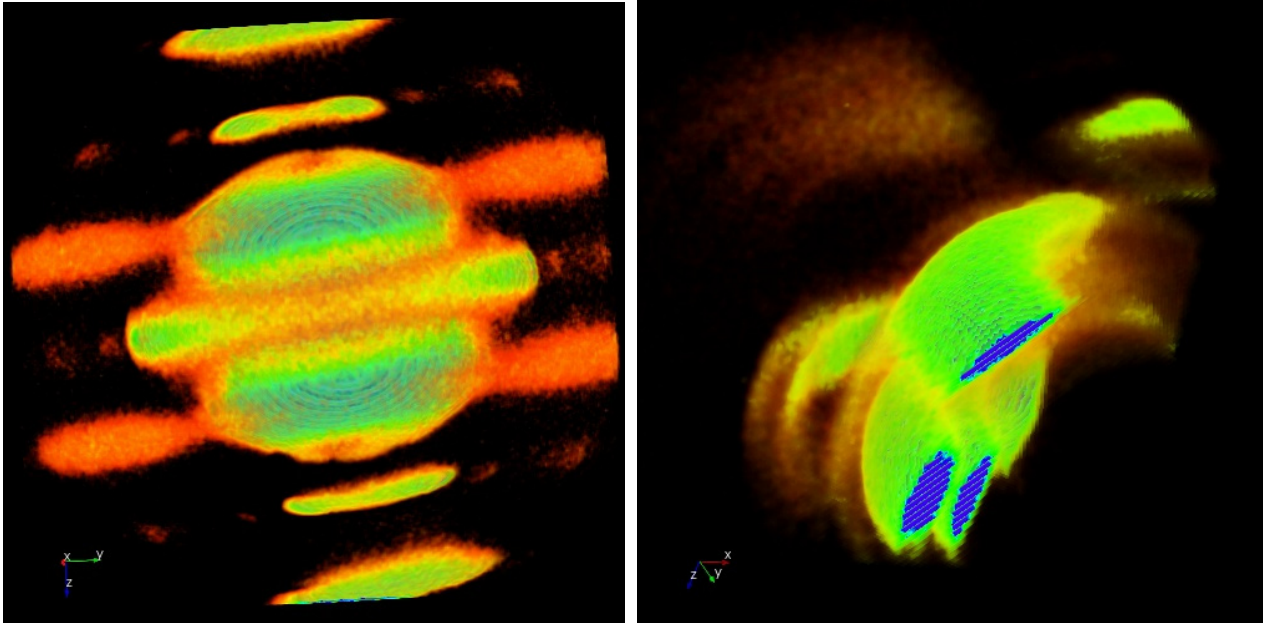
**Example 8:** Various representations of Au/Pt nanolayered rolled sheets. All pole figures are observed at once. Each shell corresponds to a different d-spacing, and the preferred orientation of the metal grains gives rise to the intensity variation on each hemisphere. ([Purdy, McMaster University](#))





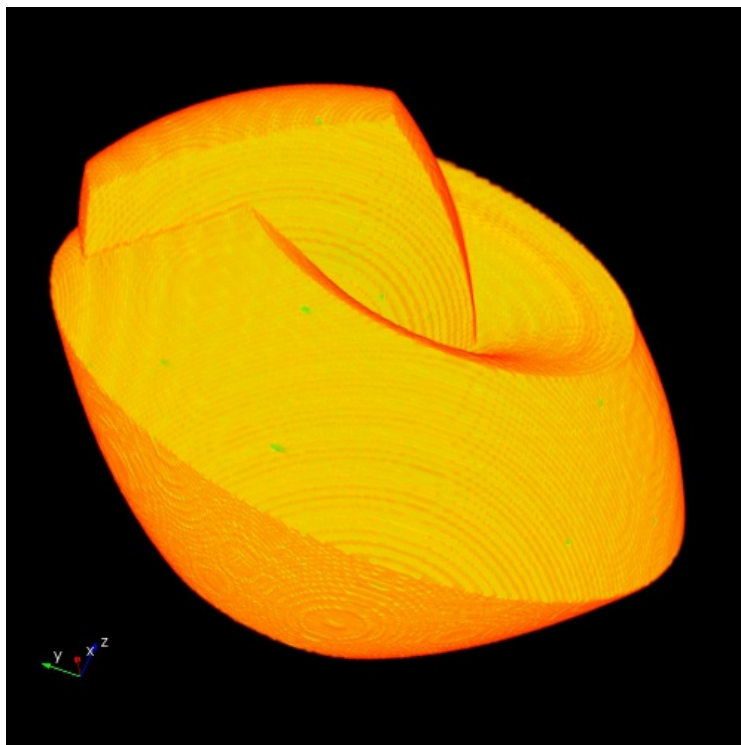
## Polymer diffraction

**Example 9:** Extruded polypropylene shows a high degree of orientation. This type of polymer shows Bragg scattering from the crystalline phase, diffuse scattering from the amorphous phase, and diffuse scattering from the partially oriented fibrous phase between the two. Modifications to the polymer result in a redistribution of the intensities observed in reciprocal space. ([Jain, McMaster University](#))

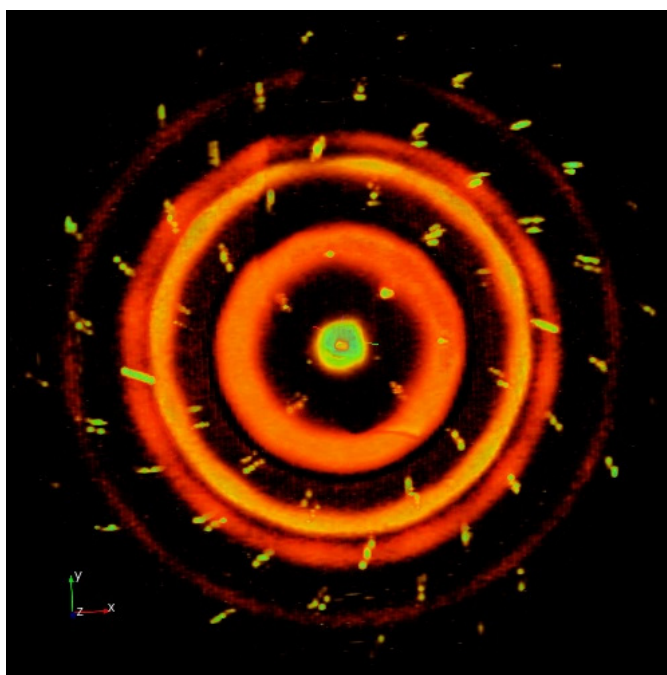


## Thin Film Characterization

**Example 10a:** The ‘mortar and pestle’  $\phi$ - and  $\omega$ -scans for texture analysis.

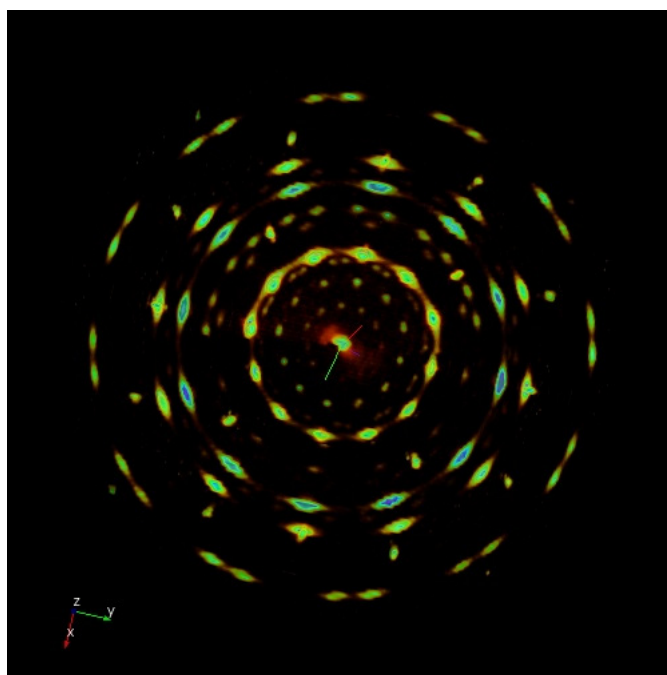


**Example 10b:** CdTe film showing almost random in-plane orientation. The orientation of the substrate can easily be determined



**Example 11:** CdTe deposited with (111) direction normal to the substrate surface. Four major in-plane orientations are observed. The data is collected in 400 2s 1° frames, as shown in Example 10.

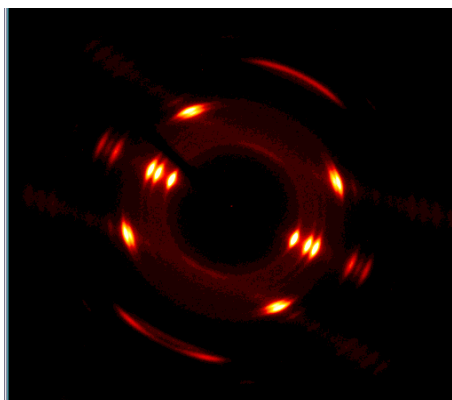
Neretina, S.; Zhang, Q.; Hughes, R. A.; Britten, J. F.; Sochinskii, N. V.; Preston, J. S.; Mascher, P. The role of lattice mismatch in the deposition of CdTe thin films. *Journal of Electronic Materials* (2006), 35(6), 1224-1230.



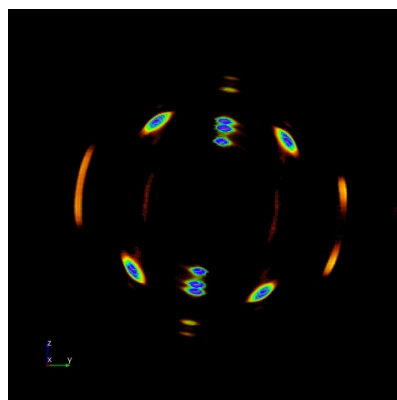
## Teaching

There are an infinite number of ways you can use full reciprocal space volume visualization as a teaching aid for crystallography. Any of the examples given above can be used. Even more powerful are real time videos in Powerpoint presentations, on web pages, or in live demonstrations. Simply *defining* reciprocal space for single crystals or polycrystalline materials can benefit from visualization. Viewing opaque data sets can show the coverage of reciprocal space for single crystal, texture, or residual stress experiments. Etc. etc. etc. . . .

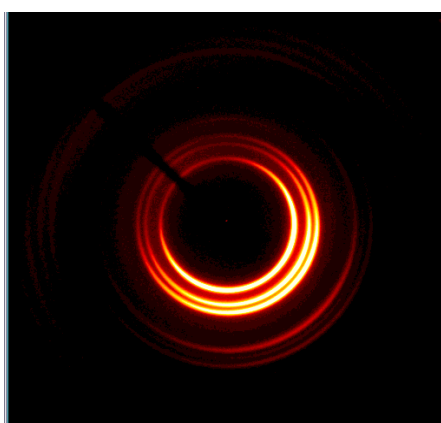
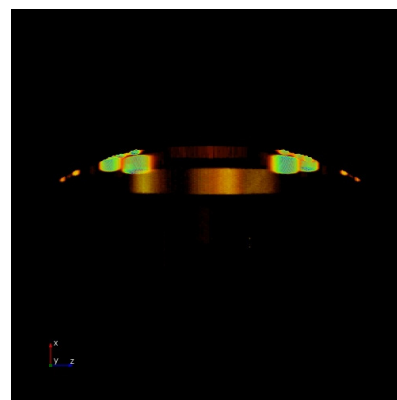
**Example 12:** The following images relate the 2D frames observed for a polymer transmission experiment to full picture in reciprocal space.



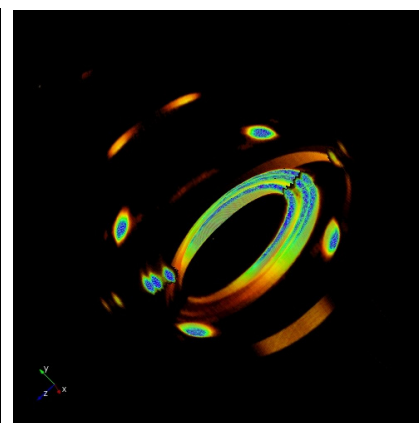
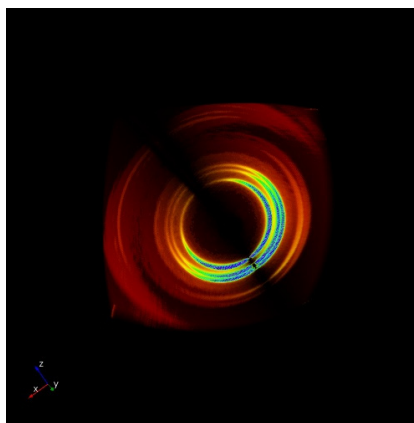
2D frame at  $\varphi=0$



Same frame mapped into reciprocal space.



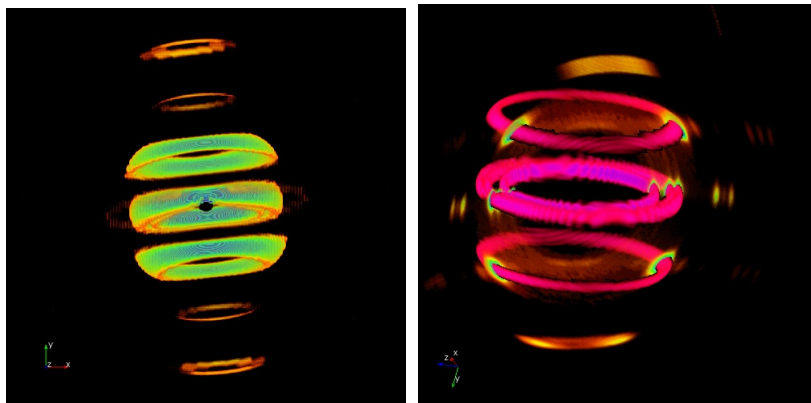
Frame at  $\varphi=90$



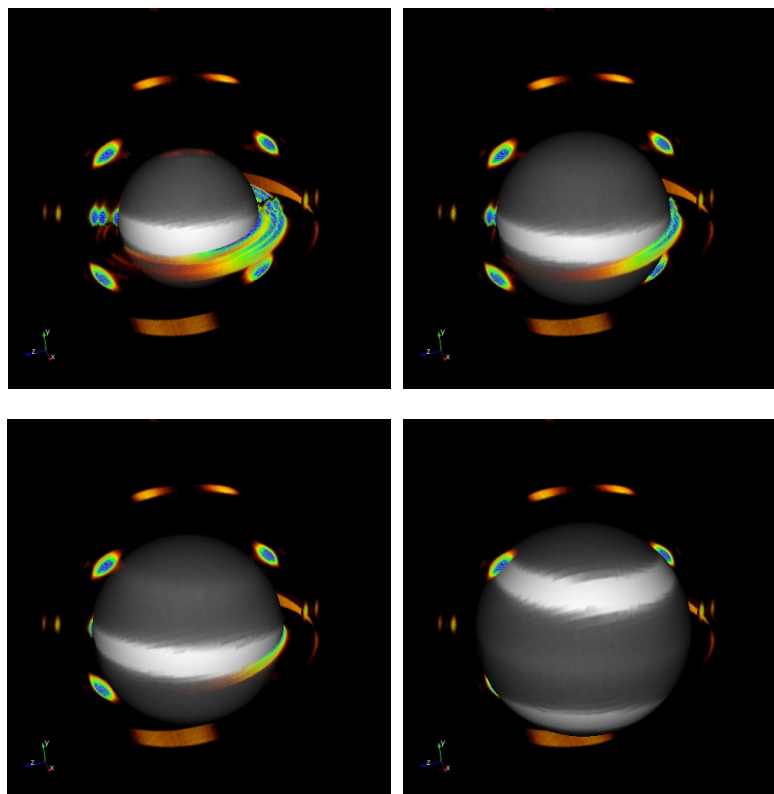
2 frames combined

### Example 12 (cont.):

Full reciprocal space volume for polymer on left, and overlay with  $\phi=0$  r.s. map on right. The sample rotation was around an axis approximately perpendicular to the extrusion axis.



The  $2\theta$  sphere sampling of the full scan volume object can be scanned to show the relationship of the various d-spacings (or pole figures) to the individual frames. You can see how the tilt of the polymer fibers relative to the rotation axis affects the pair of observed 2D frames.



### More Information

Instrument vendors are finally recognizing the advantages of 3D visualization of reciprocal space. Bruker-AXS has announced a viewing module for their software packages, and Rigaku will soon release one of their own.

MAX3D is currently available through [Flintbox](#). It is an unfunded project, and is owned by McMaster University. McMaster has an academic and a commercial price for the software, to help fund its development. For those of you not inclined to purchase MAX3D, it is possible to send interesting data sets to the authors if you would like to see a video or snapshots of reciprocal space. Have fun exploring!

---

## Call for Contributions to the Next CompComm Newsletter

The ninth issue of the Compcomm Newsletter is expected to appear around August of 2009 (2008 being an IUCr congress year) with the primary theme to be determined. If no-one is else is co-opted, the newsletter will be edited by Lachlan Cranswick.

Contributions would be also greatly appreciated on matters of general interest to the crystallographic computing community, e.g. meeting reports, future meetings, developments in software, algorithms, coding, historical articles, programming languages, techniques and other news.

Please send articles and suggestions directly to the editor.

### ***Lachlan M. D. Cranswick***

Canadian Neutron Beam Centre (CNBC),  
National Research Council of Canada (NRC),  
Building 459, Station 18, Chalk River Laboratories,  
Chalk River, Ontario, Canada, K0J 1J0

Tel: (613) 584-8811 ext: 3719

Fax: (613) 584-4040

E-mail: [lachlan.cranswick@nrc.gc.ca](mailto:lachlan.cranswick@nrc.gc.ca)

WWW: [http://neutron.nrc-cnrc.gc.ca/peep\\_e.html#cranswick](http://neutron.nrc-cnrc.gc.ca/peep_e.html#cranswick)